RESEARCH ARTICLE

OPT3 Transports Copper to the Phloem, Mediates Shoot-to-Root Copper Signaling and Crosstalk Between Copper and Iron Homeostasis in *A. thaliana*.

Ju-Chen Chia[a], Jiapei Yan[a], Maryam Rahmati Ishka[a,e], Marta Marie Faulkner[a], Eli Simons[a], Rong Huang[c], Louisa Smieska[c], Arthur Woll[c], Ryan Tappero[d], Andrew Kiss[d], Chen Jiao[e], Zhangjun Fei[e,f], Leon V. Kochian[f†], Elsbeth Walker[g], Miguel Piñeros[b,e,f] Olena K. Vatamaniuk[a,b,h]

[a]Soil and Crop Sciences Section, School of Integrative Plant Science, Cornell University, NY, USA

[b]Plant Biology Section, School of Integrative Plant Science, Cornell University, NY, USA

[c]Cornell High Energy Synchrotron Source (CHESS), Cornell University, NY, USA

[d]National Light Source II, Brookhaven National Laboratory, USA

[e]Boyce Thompson Institute for Plant Research, Ithaca, NY, USA

[f]Robert W. Holley Center for Agriculture and Health, USDA-ARS, NY, USA

[g]University of Massachusetts, MA, USA

[†]Current address: Global Institute for Food Security, University of Saskatchewan, Saskatoon, Canada.

[h]Corresponding Author:

Olena K. Vatamaniuk

Email: okv2@cornell.edu

Short title: AtOPT3 mediates systemic copper and iron signaling

One-sentence summary: AtOPT3 loads copper and iron into the phloem companion cells, for subsequent distribution to sink tissues and systemic signaling of copper and iron deficiency.

The author responsible for distribution of material integral to the findings presented in this article in accordance with the policy described in the Instructions for Authors (www.plantcell.org) is Olena Vatamaniuk (okv2@cornell.edu)

Abstract

Copper and iron are essential micronutrients but are toxic when accumulating in cells in excess. Thus, their uptake by roots is tightly regulated. While plants sense and respond to local copper availability, the systemic regulation of copper uptake has not been documented. By contrast, both local and systemic control for iron uptake has been reported. Iron abundance in the phloem has been suggested to act systemically, regulating the expression of iron uptake genes in the root. Consistently, shoot-to-root iron signaling is disrupted in *A. thaliana* mutants lacking the phloem companion cell-localized iron transporter, AtOPT3: *opt3* mutants overaccumulate iron in leaves while constitutively upregulating iron deficiency-responsive genes in roots. We report that AtOPT3 transports copper and mediates its delivery from source leaves to sinks including young leaves and developing embryos. Consequently, the *opt3* mutant accumulates less copper in the phloem, is sensitive to copper deficiency, and mounts transcriptional copper deficiency response in roots. Copper rescues these defects. Notably, feeding the *opt3* mutant with copper or iron *via* the phloem in leaves downregulates the expression of both copper and iron-deficiency marker genes in roots, suggesting that copper and iron can substitute each other's function in the phloem in shoot-to-root communication.

Introduction

Iron and copper are essential elements, required in trace amounts to complete the life cycle of all organisms, including plants and humans. However, these elements are toxic to cells if they accumulate in ionic form (Broadley et al., 2012; Ravet and Pilon, 2013). The essential yet toxic nature of iron and copper is attributed to the ease with which they accept and donate electrons (Broadley et al., 2012; Ravet and Pilon, 2013). This ability has been capitalized by nature, and so copper and iron-containing enzymes are required for vital physiological processes, including photosynthesis, respiration and scavenging of reactive oxygen species (Broadley et al., 2012; Ravet and Pilon, 2013). In addition to these processes, copper is required for cell wall lignification and reproduction (Epstein and Bloom, 2005; Broadley et al., 2012; Chen et al., 2020; Rahmati Ishka and Vatamaniuk, 2020; Sheng et al., 2021; Rahmati Ishka et al., 2022). Recent studies implicate copper in light-dependent seed germination (Jiang et al., 2020), shaping the shoot architecture, transition to flowering, stigmatic papillae development and senescence (Rahmati Ishka and Vatamaniuk, 2020; Sheng et al., 2021) and reviewed in (Rahmati Ishka et al., 2022). Mounting evidence from studies in animal species suggests that in addition to a static function as a cofactor of cellular enzymes, copper is involved in cell signaling (Turski and Thiele, 2009; Turski et al., 2012; Chang, 2015; Tsang et al., 2020). In plants, copper participates in hormone signaling and accumulation. Specifically, Cu(I) presence in the transmembrane sensor domain of the ethylene receptor, ETR1, is essential for ethylene binding and receptor function in ethylene signaling in *A. thaliana* (Rodríguez et al., 1999; Schott-Verdugo et al., 2019). Likewise, the binding of the plant defense hormone salicylic acid to its receptor NPR1 occurs *via* copper and copper deficiency increases the accumulation of jasmonic acid in leaves of *A. thaliana* (Wu et al., 2012; Yan et al., 2017; Rahmati Ishka et al., 2022). Iron-containing enzymes are also involved in nitrate and sulfate assimilation and chlorophyll synthesis, as well as ethylene and jasmonic acid accumulation (Broadley et al., 2012; Li and Lan, 2017; Cui et al., 2018).

Copper and iron uptake by plant roots and their internal transport and storage are rigorously regulated at transcriptional and posttranscriptional levels in response to the availability of these elements in a local environment and the demands of the developing shoot (Burkhead et al., 2009; Ravet and Pilon, 2013; Kobayashi, 2019; Pottier et al., 2019; Spielmann and Vert, 2020). To maintain copper homeostasis, plants regulate cellular copper uptake and

economize on copper by prioritizing it during deficiency from non-essential to essential copper enzymes (Rahmati Ishka et al., 2022). In *A. thaliana*, both processes are controlled by a conserved transcription factor, SPL7 (**S**quamosa **P**romoter Binding Protein–**l**ike7 (Yamasaki et al., 2009; Bernal et al., 2012). In addition to SPL7, a member of the basic helix-loop-helix (bHLH) family, CITF1 (**C**opper Deficiency-**i**nduced **T**ranscription **F**actor 1, *alias* bHLH160) regulates copper uptake into roots, delivery to leaves, flowers and anthers (Yan et al., 2017). CITF1 acts together with SPL7, and the function of both is required for copper delivery to reproductive organs and fertility (Yan et al., 2017). The SPL7-dependent regulon includes Iron (**F**e)/Cu **r**eductase **o**xidases, *FRO4* and *FRO5*, and several copper transporters, including *COPT1, COPT2* and, in part, *COPT6*, that are members of the CTR/COPT/SLC31 (**C**opper **T**ransporter/**Cop**per **T**ransporter/**Sol**ute **C**arrier **31**) family (Yamasaki et al., 2009; Bernal et al., 2012; Jung et al., 2012; Gayomba et al., 2013; Jain et al., 2014; Araki et al., 2018; Alexander et al., 2019). *FRO4/5* and *COPT2* are also downstream targets of CITF1 (Yan et al., 2017). Altered expression of SPL7- and CITF1-regulated genes and the increased expression of *CITF1* constitute a signature of the copper deficiency response. Recent studies have shown that SPL7 is expressed mainly in the vasculature of *A. thaliana* and locally regulates root and shoot responses to copper deficiency (Araki et al., 2018). The existence of long-distance copper signaling has not been yet reported.

Regulation of iron homeostasis in *A. thaliana* involves a network of transcription factors from the bHLH family (Jeong et al., 2017; Kim et al., 2019). Specifically, a member of the IVb subgroup of the bHLH family, URI (Upstream Regulator of IRT1, bHLH121), acts upstream as an iron-dependent switch (Kim et al., 2019; Gao et al., 2020). It heterodimerizes with a subgroup IVc bHLH members to regulate the expression of the master regulator of iron homeostasis FIT (**F**ER-like iron deficiency-induced **t**ranscription factor, alias bHLH29) (Kim et al., 2019; Gao et al., 2020). FIT forms heterodimers with the Ib subgroup of bHLH transcription factors to regulate the expression of multiple genes in *A. thaliana* roots, among which are some components of the iron uptake system, *IRT1* (**I**ron-**R**egulated **T**ransporter **1**), *FRO2* and *AHA2* (Plasma Membrane Proton ATPase) (reviewed in (Jeong et al., 2017; Schwarz and Bauer, 2020). The upregulated expression of *Ib bHLH* genes, *FIT*, *AHA2*, *FRO2* and *IRT1*, and the newly discovered *IMA/FEP* iron-sensing peptides (**I**ron **Ma**n [IMA]/**Fe** Uptake-Inducing **P**eptide [FEP]) is a hallmark of root iron-deficiency response (Jeong et al., 2017; Grillet et al., 2018; Hirayama

111 et al., 2018; Schwarz and Bauer, 2020). These and other iron-responsive genes are upregulated in
112 response to local and systemic iron status signals (Gayomba et al., 2015; Jeong et al., 2017;
113 Grillet et al., 2018; Hirayama et al., 2018; Schwarz and Bauer, 2020).

114 Several mutants with disrupted shoot-to-root iron deficiency signaling have been
115 identified in *A. thaliana* and other plant species, and all exhibit constitutive activation of iron-
116 acquisition genes even when grown under iron-sufficient conditions (Kumar et al., 2017) and
117 reviewed in (Gayomba et al., 2015). Of these, a member of the OPT (**O**ligo **P**eptide **T**ransporter)
118 clade of the OPT transporter family, *A. thaliana* OPT3, is considered a key player in the systemic
119 signaling of iron deficiency (Stacey et al., 2002; Stacey et al., 2008; Mendoza-Cózatl et al., 2014;
120 Zhai et al., 2014). While the *opt3-1* knockout allele is embryo-lethal, the *opt3-2* and *opt3-3*
121 alleles that possess residual levels of *OPT3* expression, overaccumulate iron in roots and leaves
122 because they cannot appropriately downregulate the expression of *AHA2*, *IRT1* and *FRO2* and
123 other iron deficiency-responsive genes (Stacey et al., 2002; Stacey et al., 2008; Mendoza-Cózatl
124 et al., 2014; Zhai et al., 2014). AtOPT3 mediates iron ions uptake into *Xenopus laevis* oocytes
125 and *Saccharomyces cerevisiae*, localizes to companion cells of the phloem, mediates iron loading
126 to the phloem, and facilitates iron delivery from sources (mature leaves) to sinks (roots and seeds)
127 (Zhai et al., 2014). Based on these findings it is suggested that by loading iron into the phloem in
128 leaves, OPT3 communicates iron sufficiency status to the root. Consistent with this suggestion,
129 the loss of the iron transport function in the *opt3-3* mutant and the decreased iron accumulation
130 in its phloem sap not only leads to a decreased iron accumulation in seeds but also is perceived
131 as the iron deficiency signal by the root (Zhai et al., 2014). Local sensing of high iron status in
132 the shoot seems not to be disrupted in the *opt3* mutant, as evidenced by the increased expression
133 of genes encoding iron-storage proteins *FER3* and *FER4* (Khan et al., 2018).

134 Iron abundance or a lack thereof in plant tissues is tightly linked to the accumulation of
135 other transition metals (Baxter et al., 2008). In this regard, crosstalk between iron and copper is
136 now well documented. The hallmark of this crosstalk is the overaccumulation of copper under
137 iron deficiency and overaccumulation of iron under copper deficiency (Bernal et al., 2012;
138 Waters and Armbrust, 2013; Kastoori Ramamurthy et al., 2018; Rai et al., 2021; Sheng et al.,
139 2021). Consistent with the increased copper uptake under iron deficiency, iron deficiency
140 downregulates the expression of copper-deficiency-regulated genes (Waters et al., 2012; Waters
141 et al., 2014; Yan et al., 2017). On the other hand, iron overaccumulation can also reduce copper

142 uptake in *A. thaliana* and animal systems (Klevay, 2001; Waters and Armbrust, 2013; Ha et al.,
143 2016). Together, these studies suggest that copper and iron homeostasis are interconnected and
144 deficiency for one of the metals or both can interfere with their local and/or long-distance status
145 signaling

146 Here we provide evidence that in addition to iron, AtOPT3 mediates copper uptake into
147 *Xenopus* oocytes and *S. cerevisiae* cells. Loss of this function in the *opt3-3* mutant results in a
148 decreased copper accumulation in the phloem and reduced copper recirculation from sources
149 (mature leaves) to sinks (roots, young leaves, siliques and developing embryos) compared to
150 wild type. In addition, the *opt3-3* mutant experiences copper deficiency as evidenced by low
151 copper accumulation in roots and young leaves, and increased expression of copper deficiency
152 marker genes. These defects are rescued by copper application. Furthermore, copper feeding *via*
153 the phloem in the shoot rescued molecular symptoms of copper deficiency in the root of wild
154 type and the mutant, highlighting the existence of long-distance shoot-to-root copper signaling.
155 Interestingly, phloem feeding with copper in the shoot also rescued molecular symptoms of iron
156 deficiency in the root of the *opt3-3* mutant and decreased the transcript abundance of molecular
157 markers of iron deficiency in the root of wild type. Likewise, phloem feeding with iron in the
158 shoot downregulated the expression of both iron and copper-deficiency marker genes in the root
159 of the *opt3-3* mutant. These data assign new transport capabilities to AtOPT3, provide evidence
160 for the existence of shoot-to-root signaling of copper status, and increase understanding of the
161 crosstalk between copper and iron in long-distance signaling.
162

163 ## Results

164

165 **The *opt3-3* Mutant Accumulates Less Copper in the Phloem.**

166 AtOPT3 localizes to the phloem (**Figure 1A** and Zhai et al., 2014), resides in companion cells
167 (Mustroph et al., 2009), and facilitates iron accumulation in the phloem perhaps *via* xylem to
168 phloem transfer (Zhai et al., 2014). As a result of this function, iron concentration in the phloem
169 sap is significantly lower, while it is significantly higher in the xylem sap in the *opt3-3* mutant
170 compared to wild type (Zhai et al., 2014). This finding suggested that the distribution of iron in
171 the vascular tissue of the mutant *vs.* wild type might be altered. To test this hypothesis, we used
172 synchrotron x-ray fluorescence (XRF) microscopy to compare the spatial distribution of iron and

173 other elements in the vasculature of the *opt3-3* mutant (from here on referred to as *opt3*) *vs.* wild
174 type. We first evaluated mineral distribution in mature leaves that serve as photosynthetic
175 sources of nutrients for developing leaves at the vegetative stage. Consistent with our past
176 findings (Zhai et al., 2014), the *opt3* mutant accumulated more iron throughout the leaf blade,
177 with the bulk of iron located in minor veins compared to wild type (**Figure 1B** and
178 **Supplemental Figure 1 online A to D**). We also found that in addition to iron, mature leaves of
179 the *opt3* mutant accumulated more copper (**Figure 1C** and **Supplemental Figure 1 online A to**
180 **D**), manganese and zinc (**Figure 1C** to **E**). The spatial distribution of manganese and zinc was
181 not altered in the *opt3* mutant compared to wild type: manganese was spread throughout the leaf
182 blade with the highest accumulation in basal cells of trichomes, while zinc was also noticeable in
183 the vasculature (**Figure 1D, E and K**). Copper also overaccumulated in the vasculature of the
184 *opt3* mutant, and its distribution pattern in minor veins resembled the distribution of iron (**Figure**
185 **1B, C and K,** and **Supplemental Figure 1 online A to D**).

186 We then used 2D-XRF in a confocal mode (2D-CXRF) with a specialized x-ray
187 collection optic to obtain a micron-scale resolution; this enabled analyses of mineral localization
188 in the phloem *vs.* xylem in the *opt3* mutant *vs.* wild type. For the current study, this technique is
189 preferable to traditional XRF methods (both 2D XRF and 3D micro-XRF tomography) because it
190 allows quantitative comparisons of metal distributions among different samples without the need
191 to control or limit the sample thickness or lateral size (Mantouvalou et al., 2012). Using 2D-
192 CXRF, we found that the spatial distribution of iron and copper but not of manganese or zinc
193 was altered in the *opt3* mutant compared to wild type (**Figure 1 F** to **I**). This was further
194 confirmed by comparing the distribution of fluorescence from calcium (used to visualize cell
195 boundaries, [**Figure 1J**]) overlayed with the fluorescence from iron or copper, zinc or
196 manganese (**Figure 1K**). Specifically, while iron was evenly distributed between the xylem and
197 the phloem regions in the wild type, the bulk of iron was found in the xylem and fascicular
198 cambium region and to a lesser extent in the phloem region in the *opt3* mutant. (**Figure 1F and**
199 **K**). Copper was mainly located in the fascicular cambium and phloem regions and, to a lesser
200 extent, the xylem in the wild type (**Figure 1G and K**). By contrast, the bulk of copper was
201 associated with the xylem and fascicular cambium and to a lesser extent, the phloem tissues in
202 the *opt3* mutant (**Figure 1G and K**). The loss of OPT3 function led to a significant increase in

203 the concentration of manganese and zinc in both the xylem and the phloem of the mutant
204 compared to wild type (**Figure 1H, I and K**).
205 Consistent with 2D-CXRF results, the concentration of copper in the phloem was
206 significantly lower in the *opt3* mutant compared to the wild type (**Figure 2A**). The decreased
207 accumulation of copper in the phloem of the *opt3* mutant *vs.* wild type was independently found
208 by the Walker lab (**Supplemental Fig. S1E online**).
209

210 **Roots, Young Leaves and Developing Embryos of the *opt3* Mutant Accumulate Less**
211 **Copper.**

212 Past studies have shown that mutant alleles of *OPT3* over accumulate iron, manganese and zinc
213 in roots and leaves (Stacey et al., 2008; Mendoza-Cózatl et al., 2014; Zhai et al., 2014). Since the
214 2D-CXRF analysis of mineral distribution in the vasculature has also pointed to the role of OPT3
215 in copper homeostasis, we refined our past analysis of total internal metal accumulation to
216 include copper. Consistent with past findings, roots and both mature and young leaves of the
217 *opt3* mutant accumulated significantly more iron, manganese and zinc compared to the
218 corresponding organs of wild type (**Supplemental Fig. S2 online**). By contrast, the
219 concentration of copper in the roots of the *opt3* mutant was reduced to less than 1/3 of the wild
220 type level (**Figure 2A**). We also found that the copper concentration was higher in mature leaves
221 (sources) and lower in young leaves (sinks) in the *opt3* mutant *vs.* wild type (**Figure 2A**). Similar
222 results were obtained using a different, *opt3-2* allele (**Supplemental Fig. S3 online**).
223 We then analyzed copper and also the accumulation and distribution of iron, manganese
224 and zinc in other source tissues such as silique valves and their sinks, developing embryos and
225 seeds. ICP-MS analysis disclosed that silique valves of the *opt3* mutant overaccumulated copper,
226 iron, manganese and zinc compared to wild type (**Figure 2B**). Using 2D-XRF we found that
227 developing embryos of the mutant accumulated less copper and iron (**Figure 2C and**
228 **Supplemental Figure 4A online**) but more manganese and zinc (**Figure 2C**), suggesting that
229 copper and iron delivery from sources to sinks is reduced in the mutant *vs.* wild type. It was
230 noticeable that the 2D-XRF detectable spatial distribution of copper in developing embryos of
231 both wild type and the *opt3* mutant was distinct from iron. Specifically, copper was associated
232 primarily with the developing seed coat, while iron was mostly localized in the embryo
233 vasculature.

234 We then used high-resolution 2D computed tomography XRF (CT-XRF) to visualize
235 minerals in mature seeds. Similar to embryos, copper was associated mainly with the seed coat
236 and was detected throughout the seed and the vasculature (**Supplemental Figure 4B online)**. In
237 some areas of the seed coat, copper concentration was lower in the wild type than in the mutant,
238 while the level of copper in the vasculature was lower in the mutant than in the same areas of
239 wild type (**Supplemental Figure 4B online)**. This subtle difference in copper distribution in
240 mutant *vs.* wild type seeds translated to the overall similar internal seed copper concentration in
241 both genotypes (**Supplemental Figure 4C online)**. As was shown previously, iron was
242 associated with the vascular parenchyma cells in mature wild type seeds (**Supplemental Figure**
243 **4B online** and (Kim et al., 2006)). Iron distribution did not change in the mutant, although iron
244 accumulation in the *opt3* vascular parenchyma cells was significantly lower than in wild type.
245 Consistently, the total internal iron concentration was lower in the *opt3* mutant seeds *vs.* wild
246 type (**Supplemental Figure 4C online)**. While the distribution of manganese and zinc did not
247 change in the mutant *vs.* wild type, the *opt3* mutant seeds accumulated significantly more zinc
248 (**Supplemental Figure 4B, C online)**. Together, our data suggest that OPT3 contributes to the
249 phloem-based redistribution of copper from mature leaves to young leaves and from silique
250 valves to developing embryos, and thus, in addition to iron, may also transport copper.
251

252 **OPT3 Mediates Copper Uptake in *Xenopus* oocytes and *S. cerevisiae*.**

253 The ability of OPT3 to transport copper was studied in *Xenopus laevis* oocytes as we have
254 previously shown that in this expression system, OPT3 localizes to the plasma membrane and
255 mediated iron and cadmium ions uptake into oocytes (Zhai et al., 2014). As potential transport
256 substrates, we tested Cu^{2+} (provided as $CuSO_4$) and copper complexed with its biological ligand,
257 nicotianamine (Cu-NA). We found that OPT3 transported both free copper ions as well as copper
258 provided as Cu-NA complex into oocytes (**Figure 3A**). Furthermore, OPT3-expressing oocytes
259 accumulated 4.2 times more copper when it was provided as a free ion than when complexed
260 with NA. This finding suggested that free copper ions are a preferred OPT3 substrate, at least in
261 this heterologous system. Visual examination and membrane potential measurements allowed us
262 to assess the cellular integrity of mock and *OPT3* expressing oocytes throughout the uptake
263 experiments to rule out the possibility that the observed fluxes were the product of membrane
264 leakiness due to cellular toxicity rather than specific OPT3-mediated uptake (**Supplemental**

265 **Figure 5 online)**. Under control conditions, the cells expressing OPT3 had less negative
266 membrane potential than mock cells, consistent with our earlier reports (Zhai et al., 2014). The
267 appearance and survival rates of mock and OPT3-expressing oocytes remained the same within
268 the three hours of the experiment, and only a minor reduction in resting potential (7 and 14 mV
269 in mock and OPT3-expressing cells, respectively) was recorded, suggesting the cells-maintained
270 membrane integrity throughout the uptake time (**Supplemental Figure 5A online)**. After
271 transferring cells into the copper-free solution, the survival rates and resting potentials of OPT3-
272 expressing cells, but not of mock-treated cells, were dramatically reduced over the next 21 h of
273 incubation in the copper-free medium (**Supplemental Figure 5B online**). We concluded that the
274 drop in the survival rates of OPT3-expressing cells resulted from the OPT3-mediated copper-
275 accumulation, leading to cellular toxicity, which was manifested as a loss in the cell's ability to
276 maintain their resting potential, and eventual death.

277 The ability of OPT3 to transport copper was further validated by functional
278 complementation assays in the *S. cerevisiae*, which lack the capability to synthesize NA. We
279 used a copper-deficient *S. cerevisiae ctr1Δctr2Δctr3Δ* mutant lacking the high-affinity plasma
280 membrane copper uptake transporters Ctr1p and Ctr3p and the vacuolar membrane copper efflux
281 transporter, Ctr2p (Dancis et al., 1994; Rees et al., 2004). Due to low internal copper, the
282 *ctr1Δctr2Δctr3Δ* mutant cells manifest a respiratory defect because of the altered activity of the
283 copper-dependent cytochrome *c* oxidase complex of the mitochondrial respiratory chain. This
284 defect can be visualized by the failure of the *ctr1Δctr2Δctr3Δ* mutant to grow on non-
285 fermentable carbon sources such as ethanol and glycerol (YPEG medium) unless copper is
286 supplied exogenously (Dancis et al., 1994). As expected, the *ctr1Δctr2Δctr3Δ* cells expressing
287 the empty YES3-Gate vector accumulated 10-fold less copper than the vector-expressing wild
288 type (**Figure 3B**). The expression of *OPT3* in mutant cells increased their copper accumulation
289 by 5-fold compared to the vector expressing cells, although it did not bring it to the level of the
290 vector-expressing wild type cells (**Figure 3B**).

291 Growth of *ctr1*Δ*ctr2*Δ*ctr3*Δ mutant and wild type strains expressing the empty *YES3-*
292 *Gate* vector and the *ctr1*Δ*ctr2*Δ*ctr3*Δ mutant transformed with *YES3-Gate* with the *OPT3* cDNA
293 insert was also compared on a medium containing the non-fermentable carbon sources, ethanol
294 and glycerol (YPEG). The *ctr1*Δ*ctr2*Δ*ctr3*Δ mutant transformed with the *A. thaliana* copper
295 transporter, *COPT2*, was used as an additional positive control (Gayomba et al., 2013). As

296 shown previously, the vector-expressing *ctr1*Δ*ctr2*Δ*ctr3*Δ cells did not grow in YPEG medium
297 even when the medium was supplemented with low (10 and 20 μM) concentrations of copper but
298 grew well on YPEG supplemented with 100 μM $CuSO_4$ (**Figure 3C** and (Gayomba et al., 2013)).
299 Unlike *COPT2* expressing cells, *OPT3* expressing mutant cells did not grow on YPEG medium
300 without supplemental copper. However, in contrast to vector expressing *ctr1*Δ*ctr2*Δ*ctr3*Δ cells,
301 *OPT3* expressing cells were able to grow when 10 or 20 μM $CuSO_4$ was added to the medium
302 (**Figure 3C**). These results are consistent with the role of OPT3 in copper uptake and suggest
303 that, unlike CTR/COPTs, OPT3 might be a low-affinity copper transporter at least when
304 expressed in *S. cerevisiae*. Together, our results show that OPT3 mainly contributes to the
305 transport of copper ions in heterologous systems.
306
307 **The *opt3* Mutant is Sensitive to Copper Deficiency.**
308 We next tested the sensitivity of the *opt3* mutant to copper deficiency by comparing its growth
309 and development to the wild type, both grown hydroponically with or without copper
310 supplementation (**Figure 4)**. As we observed previously, the rosette size of the *opt3* mutant was
311 smaller than that in wild type even under control conditions (**Figure 4A** and (Zhai et al., 2014))
312 and decreased further under copper deficiency *vs.* control conditions; by contrast, copper
313 deficiency did not affect the rosette size of the wild type (**Figure 4A**) early in the vegetative
314 stage of the development. A different *opt3-2*, allele exhibited similar sensitivity to copper
315 deficiency in the medium (**Supplemental Figure S6A**). As evidenced by the shorter root length
316 and lower fresh weight of the *opt3* mutant, the increased sensitivity of the *opt3-3* mutant *vs.* wild
317 type to copper deficiency was also observed in seedlings grown on a solid medium supplemented
318 with the copper chelator bathocuproine disulfonate (BCS) (**Supplemental Figure S6B, C** and **D**
319 **online**). Consistent with the increased sensitivity of the *opt3* mutant to copper deficiency and our
320 finding that it experiences copper deficiency, cupric reductase activity was significantly higher in
321 roots of the *opt3* mutant *vs.* wild type (**Supplemental Figure S6E online**).
322 We then tested whether the transition to flowering is delayed in the *opt3* mutant under
323 control conditions and/or under copper deficiency because we recently found that copper is
324 involved in this process (Rahmati Ishka and Vatamaniuk, 2020). Consistent with our recent
325 findings, wild type plants flowered significantly later and developed more rosette leaves when
326 grown without *vs.* with copper (**Figure 4B** to **D** and **Table 1**). The *opt3* mutant failed to flower

327 within the time frame of the experiment (8 weeks) and developed 30%- and 90% more rosette
328 leaves than wild type in the medium without or with $CuSO_4$, respectively (**Figure 4C, D** and
329 **Table 1**). Leaves of the *opt3* mutant were significantly shorter and were extensively chlorotic
330 compared to wild type, both grown without added copper (**Figure 4E, F**). Although the length of
331 the rosette leaves of mutant and wild type plants was comparable to control copper (125 nM
332 $CuSO_4$), the leaves of the mutant possessed characteristic chlorotic spots (**Figure 4F**). The
333 delayed transition to flowering, the increased number, and the length of rosette leaves of the
334 mutant were rescued by transferring the mutant to the medium with high (500 nM) $CuSO_4$
335 (**Figure 4C to E, Table 1** and **Supplemental Figure 7A online**). Transferring the mutant to a
336 lower (250 nM) copper also rescued the small size of the mutant, although to a lesser extent
337 compared to the higher copper concentration (500 nM) (**Supplemental Figure 7B online**).
338

339 **The *opt3* Mutant Mounts Transcriptional Iron-Deficiency Responses in Roots but not in**
340 **Shoots.**

341 We next used deep transcriptome sequencing to test whether the expression of copper
342 deficiency-responsive genes is altered in roots, mature and young leaves of the *opt3* mutant
343 compared to wild type. Using Illumina sequencing, we obtained 54, 79 and 59 million clean
344 reads from roots, mature and young leaves, respectively (**Supplemental data set 1**). Of these,
345 86% of reads from roots and mature leaves and 93% of reads from young leaves were mapped to
346 the *A. thaliana* genome and employed to estimate the transcript abundance and differential
347 expression. Compared to wild type, 376, 673 and 1,942 genes were differentially expressed in
348 the *opt3-3* mutant roots, young leaves and mature leaves, respectively (ratio ≥ 1.5 or ≤ 0.67,
349 false-discovery rate [FDR] < 0.05; **Fig. 5A to C**). As expected, the expression of canonical iron
350 deficiency-responsive genes, known to positively regulate iron-deficiency responses to facilitate
351 iron uptake (*e.g., FIT*, *IRT1*, *FRO2*, *bHLH38*, *bHLH39*, *bHLH100*, *bHLH101, MYB10, MYB72),*
352 iron-sensing peptide *FEP2/IMA2*, coumarin synthesis and transport (*CYP82C4*, *S8H* and
353 *PDR9/ABCG37*) was highly up-regulated in roots of the *opt3* mutant (**Figure 5B** and
354 **Supplemental Data Set 2**). In addition, IRT1 polypeptide was detected in roots of the *opt3*
355 mutant grown under control conditions and roots of wild type grown under iron deficiency but
356 not in roots of wild type or the *fit-2* mutant grown under control conditions (**Supplemental**
357 **Figure S8 online**). Of other iron deficiency-regulated genes, the chloroplast-localized *FRO3* and

358 iron exporter *IREG3/FPN3*, which is dual-targeted to mitochondria and chloroplast, were also
359 upregulated in roots of the *opt3* mutant compared to the wild type (**Figure 5B** and **Supplemental**
360 **Data Set 2)**. Of 237 genes upregulated in roots of the *opt3* mutant, 32 (13.5%) were among the
361 robust FIT targets and 6 (0.025%) were among PYE targets (**Supplemental data set 2** and (Mai
362 et al., 2015)), suggesting that the *opt3* mutant mounts primarily FIT-regulated iron deficiency
363 response under iron sufficiency.

364 Notably, the expression of a negative FIT regulator, *ZAT12*, was upregulated in roots of
365 the *opt3* mutant *vs.* wild type as well (**Figure 5B** and **Supplemental Data Set 2**). In addition, the
366 expression of genes mediating cellular response to iron overload was upregulated. Specifically,
367 the expression of *FER1* encoding a chloroplast-localized iron-sequestering protein, whose
368 expression is upregulated by iron overload to protect chloroplasts from iron toxicity, was
369 upregulated in roots of the *opt3* mutant *vs.* wild type (**Figure 5B** and **Supplemental Data Set 2)**.
370 The expression of *IREG2/FPN2, VTL1, 2, 5* mediating iron sequestration into the vacuole was
371 upregulated too (**Figure 5B** and **Supplemental Data Set 2)**. These data suggest that despite the
372 upregulated FIT-transcriptional network, root cells also perceived the iron-sufficiency/overload
373 signal and responded by increasing the expression of FIT negative regulators and genes involved
374 in the mitigation of iron-overload toxicity. It is noteworthy that while roots of the *opt3* mutant
375 constitutively overexpressed genes encoding iron uptake system even when grown in iron
376 sufficient conditions, the magnitude of the response was significantly larger when mutant was
377 grown under iron deficiency (**Figure 5D**). This is consistent with the important role of OPT3 in
378 mitigating and controlling the basal response of the root to iron deficiency.

379 We then compared the expression of iron-deficiency responsive genes in young and
380 mature leaves of the *opt3* mutant *vs.* wild type. Unlike roots, both mature and young leaves of the
381 *opt3* mutant did not show transcriptional iron deficiency response. Specifically, none of the
382 canonical iron-deficiency upregulated genes were upregulated in young or mature leaves of the
383 *opt3* mutant (**Figure 5B** and **Supplemental Data Set 3 and 4**). Moreover, *FEP1/IMA3*, shown
384 to be involved in iron sensing and typically upregulated in leaves and roots under iron deficiency
385 (Grillet et al., 2018), was downregulated in mature leaves of the *opt3* mutant *vs.* wild type;
386 *At5g05250*, encoding a protein with unknown function, was upregulated by iron deficiency in
387 leaves of different *A. thaliana* ecotypes (Waters et al., 2012) was downregulated in both young
388 and mature leaves of the *opt3* mutant *vs.* wild type. Iron deficiency downregulated genes *NAS3*,

389 *YSL1* and *YSL3* were highly upregulated in mature leaves in the *opt3* mutant, and *YSL1* was also
390 upregulated in young leaves of the *opt3* mutant compared to wild type (**Figure 5B** and
391 **Supplemental Data Set 3 and 4**). The chloroplast-localized ferric chelate reductase *FRO7* and
392 plasma membrane-localized *FRO6*, although not regulated by iron deficiency in shoots of *A.*
393 *thaliana* (Mukherjee et al., 2006), were highly upregulated in mature leaves of the *opt3* mutant *vs.*
394 wild type (**Figure 5B** and **Supplemental Data Set 3**). At the same time, iron-sufficiency
395 markers, *FER1, FER3* and *FER4*, were highly upregulated in both mature and young leaves of
396 the *opt3* mutant compared to wild type (**Figure 5B** and **Supplemental Data Set 3 and 4**).
397 Together, our RNA-seq data are helping to unravel the details of contrasting responses of the
398 iron-regulon in roots, young and mature leaves of the *opt3-3* mutant and supported the past
399 observation that leaves of the *opt3* mutants sensed iron overload (Khan et al., 2018).
400

401 **The *opt3* Mutant Mounts Transcriptional Copper Deficiency Response.**

402 Roots of the *opt3* mutant accumulated significantly less copper than roots of wild type plants,
403 albeit the total internal concentration in roots was at the sufficiency level (Fig. 2A and (Broadley
404 et al., 2012)). We thus, anticipated that the expression of genes belonging to copper-deficiency
405 regulon in roots would not be altered in the *opt3* mutant. However, we found that the expression
406 of canonical copper-deficiency induced genes, responsible for copper uptake (*CITF1*, *COPT2*,
407 *FRO4* and *FRO5*) was up-regulated in roots of the *opt3* mutant compared to wild type (**Table 2,**
408 **Figure 5B** and **Supplemental Data Set 2**). Since small RNAs were not included in the RNA-seq
409 analysis, we tested the expression of canonical copper miRNAs expression in roots of the *opt3*
410 mutants *vs.* wild type plants by RT-qPCR (Pilon, 2017). We found that the expression of copper
411 deficiency regulated micro RNAs, *miR397a/b*, *miR857a*, *miR389b/c* and *miR408* was
412 upregulated in roots of the *opt3* mutant vs. wild type (**Figure 6A**). Also, copper deficiency-
413 repressed genes, contributing to copper economy/metal switch, *CSD1*, *CSD2* and *BCB*, encoding
414 Cu/Zn superoxide dismutases 1 and 2 and blue-copper-binding protein, respectively, were
415 downregulated by more than 2-fold. Consistently, the expression of *FSD1* (Fe-containing
416 superoxide dismutase) was upregulated by 2.7-fold in roots of the *opt3* mutant *vs.* wild type
417 (**Table 2, Figure 5C** and **Supplemental Data Set 2**). In addition, several other canonical
418 copper-deficiency upregulated genes (*bHLH23, ZIP2*, *YSL2, TCH4, AT2G47010, AT4G10500***,**
419 *AT1G31710*) were upregulated in roots of the *opt3* mutant compared to wild type (**Table 2,**

420 **Figure 5B** and **Supplemental Data Set 2)**. Of 16 copper-deficiency regulated genes in the *opt3*
421 mutant, 10 are regarded as SPL7-dependent (**Supplemental Data Set 2)**. These results show that
422 roots of the *opt3* mutant manifest molecular symptoms of copper deficiency even though plants
423 were grown under copper-sufficient conditions and the internal concentration of copper in roots
424 was at the level of sufficiency (**Figure 2A** and **Supplemental Figure online 3**).
425 We also found that young leaves of the *opt3* mutant manifested molecular symptoms of
426 copper deficiency as evident by the increased expression of *YSL1* and *YSL2*, typically
427 upregulated under copper deficiency and involved in lateral movement of minerals, including
428 copper (**Figure 5B, C** and **Table 2, Supplemental Data Set 3**). Genes associated with either
429 copper buffering *(MT1A* and *MT2A*) or copper economy (*CSD1*, *CSD2*, *CCS1*, *ARPN, UCC2)*
430 were downregulated, while *FSD1* was upregulated (**Figure 5B, C** and **Supplemental Data Set**
431 **3**).
432 Regarding mature leaves, a different set of genes was differentially expressed in the *opt3*
433 mutant *vs.* wild type, and the pattern of the regulation (up or down) of canonical copper-
434 deficiency-regulated genes was not symptomatic for either deficiency or sufficiency
435 (**Supplemental Data Set 4)**. Specifically, as would be expected under copper deficiency, the
436 expression of genes associated with copper uptake and lateral movement, *COPT1*, *YSL1* and
437 *YSL3,* was upregulated in the *opt3-3* mutant *vs.* wild type. Other *A. thaliana* copper-deficiency
438 upregulated genes, including *AT1G32350* and *AT5G02670*, were also upregulated in mature
439 leaves of the *opt3* mutant. Of genes typically downregulated by copper deficiency, *AT4G15660*
440 was also downregulated in the *opt3* mutant *vs.* wild type as well as *PETE2*, associated with
441 copper sparing and *MT1B*, associated with copper buffering. By contrast, the expression of
442 another copper sink, *UCC2*, typically downregulated by copper deficiency, was upregulated in
443 mature leaves of the *opt3* mutant *vs.* wild type while *NRT2.7*, typically upregulated by copper
444 deficiency in *A. thaliana*, was downregulated in the *opt3* mutant *vs.* wild type.
445 To conclude, our RNA-Seq data show that both roots and young leaves of the *opt3*
446 mutant mounted transcriptional copper deficiency response while only roots of the mutant
447 manifested transcriptional iron deficiency response. In addition, our finding of the distinct
448 transcriptional response and metal accumulation in mature *vs.* young leaves of the mutant
449 emphasizes the need to separate these leaves in analyses of mutant phenotypes.
450

451 ***OPT3* is Transcriptionally Upregulated by the Short-term Copper Deficiency.**

452 While *OPT3* is robustly upregulated in roots and leaves by iron deficiency, it was not found
453 among copper-deficiency-responsive genes in the existing RNA-seq data. In these RNA-seq
454 analyses, plants were exposed to copper deficiency for a minimum of three days. Since *OPT3*
455 responds to iron deficiency within 24 h (Khan et al., 2018), we hypothesized that *OPT3* might
456 also be transcriptionally upregulated by short-term exposure to copper deficiency. Thus, we
457 compared the *OPT3* expression in *A. thaliana* subjected to copper deficiency for 24 or 96 h. We
458 also examined the expression of a copper-deficiency marker, *CITF1,* to validate the efficiency of
459 treatments. *CITF1* was up-regulated in roots by 16-fold after 24 h of copper deficiency and
460 remained highly upregulated after 96 h. The expression of *OPT3* was also upregulated, although
461 to a lesser extent, after 24 h of copper deficiency, but unlike *CITF1*, the transcript abundance of
462 *OPT3* decreased after 96 h of treatment (**Figure 6B**). The expression of *IRT1* was not
463 upregulated by copper deficiency (**Figure 6B**).

464

465 **The Molecular Symptoms of Copper Deficiency in the *opt3* Mutant are Rescued by**
466 **Supplemental Copper.**

467 Since transferring the *opt3* mutant to higher copper concentrations decreased its time to
468 flowering to the level of wild type and rescued the length of rosette leaves (**Figure 4** and
469 **Supplemental Fig. 7A online**), we predicted that supplemental copper would also decrease the
470 expression of copper-deficiency responsive genes. To test this hypothesis, we compared the
471 transcript abundance of copper deficiency markers, *CITF1*, *COPT2*, *FRO4* and *FRO5* in roots of
472 the *opt3* vs. wild type. In parallel, we also tested the expression of key iron deficiency markers,
473 *IRT1* and *FRO2*. Consistent with RNA-seq data (**Table 2**), the expression of *CITF1*, *COPT2*,
474 *FRO4* and *FRO5* was upregulated in roots of the *opt3* mutant *vs.* wild type, both grown under
475 control conditions (**Figure 7)**. The transcript abundance of copper deficiency markers decreased
476 in roots of the *opt3* mutant after transfer to higher concentrations of copper (**Figure 7A** to **H**).
477 We note that transferring wild type plants to higher copper also decreased the expression of
478 *CITF1, COPT2*, *FRO4* and *FRO5,* suggesting that 125 nM $CuSO_4$ was somewhat copper limiting
479 even though the growth and development of wild type plants were not affected. Supplemental
480 copper in both concentrations also decreased the expression of *IRT1* and *FRO2* in roots of the
481 *opt3* mutant compared to their expression levels under control conditions (**Figure 7 J to M**). It is

482 noteworthy that the higher copper concentration (500 nM) increased the expression of both *IRT1*
483 and *FRO2* in roots of wild type, reinforcing the existence of interactions between copper and iron
484 homeostasis.
485
486 **Copper Deficiency Response in Roots of the *opt3* Mutant is Regulated by the Shoot.**
487 We next tested whether the increased expression of copper deficiency markers in roots of the
488 *opt3* mutant is due to its altered shoot-to-root signaling. To do so, we used reciprocal grafting
489 with wild type and *opt3* plants and examined the transcript abundance of copper deficiency
490 markers *CITF1*, *COPT2*, *FRO4*, *FRO5* in roots (**Figure 8)**. The expression of these genes was
491 up-regulated in roots of grafted *opt3*/*opt3* (*opt3* scions grafted to *opt3* rootstocks) compared to
492 the grafted WT/WT (wild type scions grafted to wild type rootstocks [control grafts], **Figure 8A**).
493 The expression of *CITF1*, *COPT2*, *FRO4* and *FRO5* was also elevated in roots of grafts with
494 *opt3* scions and wild type rootstock (**Figure 8A**). In contrast, grafting of the wild type shoots
495 onto the *opt3* rootstocks downregulated *CITF1*, *COPT2*, *FRO4* and *FRO5* expression relative to
496 control grafts (**Figure 8A**). These data show that the OPT3 function in the shoot is sufficient to
497 regulate the transcriptional copper deficiency responses in the root.
498 Grafted plants performed as expected, as evidenced by the expression of the iron-
499 deficiency markers, *IRT1* and *FRO2* in different graft combinations (**Figure 8B** and (Zhai et al.,
500 2014)). As we showed previously, *IRT1* and *FRO2* were up-regulated in roots of *opt3*/*opt3*
501 compared to WT/WT grafts (**Figure 8B** and (Zhai et al., 2014)). Grafting wild type shoots onto
502 *opt3* mutant roots downregulated *IRT1* and *FRO2* expression relative to their expression in
503 control grafts (**Figure 8B**). In contrast, grafting of *opt3* shoots onto wild type roots increased the
504 expression of iron deficiency markers (**Figure 8B**). Together, these data show that OPT3
505 function in the shoot regulates both iron and copper deficiency responses of the root. These data
506 also suggested the existence of the systemic shoot-to-root copper status signaling.
507
508 **Copper Movement *via* the Phloem from the Shoot to the Root Regulates the Expression of**
509 **Copper-deficiency Responsive Genes.**
510
511 To test whether copper status of the shoot can be communicated to the root, and whether copper
512 movement *via* the phloem from the shoot to the root influences the expression of copper

513 acquisition genes, we performed phloem feeding experiments *via* the abrasion of the leaf
514 vasculature. We first tested this approach by using the phloem symplastic tracer 5,6
515 carboxyfluorescein-diacetate (CFDA) (Grignon et al., 1989; Oparka et al., 1994). After diffusing
516 into plant cells, CFDA is cleaved by cellular esterases to yield a membrane-impermeable form of
517 the dye, carboxyfluorescein (CF). As expected, we detected CF accumulation in roots of wild-
518 type plants after CFDA solution feeding *via* the incision in the leaf vasculature (**Supplemental**
519 **Figure 9A, B online**).

520 Since systemic signaling of iron deficiency has already been established, we first exposed
521 *Arabidopsis* wild type to iron deficiency and tested whether iron feeding to the phloem in the
522 shoot would rescue the expression of iron deficiency markers *FIT* and *IRT1.* Since *COPT2* is
523 also upregulated by iron deficiency *via FIT*, we also used *COPT2* as a marker for iron as well as
524 copper deficiency. Consistent with the role of iron in the phloem in systemic signaling, feeding
525 iron directly to the phloem of iron deficient plants decreased the expression of *FIT*, *IRT1* and
526 *COPT2* (**Figure 9A**). We also noticed that iron but not mock-feeding, rescued the chlorosis of
527 young leaves of iron-deficient plants (**Supplemental Figure 9D online**).

528 We then exposed wild type to copper deficiency, fed copper to the phloem in the shoot
529 and found that the expression of the copper deficiency markers, *CITF1*, *COPT2* and copper
530 miRNAs, *miR397a/b*, *miR857a, miR389a/b* and *miR408* was significantly downregulated in the
531 root (**Figure 9B**). These data show the existence of systemic signaling of copper deficiency in *A.*
532 *thaliana* and the important role of copper movement *via* the phloem from the shoot to the root in
533 the regulation of copper-responsive genes in the root. Our data also provide evidence that iron in
534 the leaf phloem plays a repressive role in regulating iron deficiency-responsive genes.
535

536 **Feeding Copper or Iron to the Phloem in the Shoot of the *opt3* Mutant Attenuates the**
537 **Expression of both Iron- and Copper-deficiency Responsive Genes in the *opt3* Mutant**
538 **Roots.**
539

540 Past studies of foliar iron application by iron spraying did not rescue the expression of iron
541 acquisition genes, constitutively overexpressed in roots of the *opt3* mutant (Garcia et al., 2013).
542 This finding is not surprising considering the *opt3* mutant's defect in iron and copper loading to
543 the phloem in leaves (**Figures. 1F, G, K** and **5B** and (Zhai et al., 2014). We, thus, asked whether

544 feeding with iron *via* the vasculature in the shoot would rescue the expression of iron deficiency
545 markers, *FIT* and *IRT1* in the root. Consistent with the suggested repressive role of iron
546 movement *via* the phloem from the shoot to the root, the expression of *FIT* and *IRT1* was
547 downregulated in roots of iron- *vs.* mock-fed plants (**Figure 9C**). Unexpectedly, we also found
548 that the expression of copper deficiency markers, *CITF1* and *COPT2* was downregulated in the
549 root of iron *vs.* mock-fed mutant (**Figure 9C**). Interestingly, the expression of copper miRNAs,
550 *miR397a/b*, *miR857a, miR389a/b* and *miR408* in the root of the *opt3* mutant did not respond to
551 the phloem feeding with iron in the shoot (**Figure 9C**).
552 Next, we fed copper to the phloem in the shoot to test whether it would have a similar
553 repressive effect on the expression of iron and copper-deficiency regulated genes in roots of the
554 *opt3* mutant. The expression of copper-deficiency markers including *CITF1*, *COPT2* and copper
555 miRNAs, *miR397a/b*, *miR857a, miR389a/b* and *miR408* was significantly downregulated in the
556 roots of copper *vs.* mock-fed mutant (**Figure 9D**). The expression of iron deficiency marker
557 genes, *FIT* and *IRT1*, constitutively upregulated in the *opt3* mutant, was also downregulated in
558 roots of the *opt3* mutant, fed with copper *via* the phloem in the shoot (**Figure 9D**). Together,
559 these data suggest the existence of crosstalk between iron and copper in systemic signaling
560 directed on the regulation of copper and iron uptake system.
561
562 **Phloem Copper or Iron Feeding Downregulates the Autonomously Upregulated Expression**
563 **of *CITF1, copper miRNAs* and *FIT* in Roots of *A. thaliana* Under Simultaneous Copper and**
564 **Iron Deficiency.**
565
566 We showed that copper and iron accumulation in the phloem was lower in the *opt3* mutant than
567 in wild type and that OPT3 function is important for regulating copper and iron deficiency
568 responses in the root (**Figures 1, 8** and **9**). To mimic the effect of simultaneous copper and iron
569 deficiency in the phloem of the *opt3* mutant and its effect on the expression of corresponding
570 deficiency markers in roots, we subjected *A. thaliana* wild type to deficiency of these metals
571 applied concurrently. We tested the expression of *CITF1*, *miR397a/b*, *miR857a, miR389a/b* and
572 *miR408* because these genes are highly regulated by copper deficiency and are downregulated by
573 iron deficiency (Waters et al., 2012; Yan et al., 2017). We also tested the expression of *FIT* as it
574 is responsive to iron but not copper deficiency (Colangelo and Guerinot, 2004; Bernal et al.,

575 2012). As expected, copper and iron deficiency applied individually had an opposite effect on the
576 expression of *CITF1, miR397a/b*, *miR857a, miR389a/b* and *miR408* (**Figure 10A**); *FIT*
577 expression was upregulated under iron but not copper deficiency (**Figure 10A**). In contrast, all
578 tested genes were highly upregulated when iron and copper deficiencies were applied
579 simultaneously (**Figure 10A**). This result suggested that iron and copper deficiency applied
580 simultaneously act in parallel/autonomously on the expression of copper and iron-responsive
581 genes in the root.

582 Copper feeding *via* the phloem in the shoot downregulated the expression of not only
583 *copper-miRNAs* and *CITF1* but also *FIT* in the root of plants grown under simultaneous copper
584 and iron deficiency (**Figure 10B**). Feeding with iron also downregulated not only the expression
585 of *FIT* but also *CITF1*; of copper miRNAs, the expression of all, but not *miR857a,* was
586 downregulated in roots of wild type grown under simultaneous copper and iron deficiencies
587 (**Figure 10C**). Together, these data suggest that copper and iron in the phloem can mimic each
588 other's function in long-distance signaling function.
589

590 **Copper and Iron Deficiencies Applied Simultaneously Increase Root Iron Uptake and**
591 **Delivery to Shoots While High Iron Reduces Copper Uptake**

592 Because copper deficiency stimulates iron uptake, we hypothesized that copper deficiency in the
593 *opt3* mutant and its lower copper and iron accumulation in the phloem compared to wild type,
594 contributes to increased iron accumulation in its roots and leaves. To test this hypothesis, we
595 exposed wild type to copper and iron deficiency individually and concurrently. We then analyzed
596 iron accumulation in roots and leaves of wild type plants. As was found previously, copper
597 deficiency increased iron accumulation in both roots and leaves of *A. thaliana* wild type
598 compared to control conditions (**Figure 11A** and (Bernal et al., 2012; Waters et al., 2012;
599 Kastoori Ramamurthy et al., 2018; Sheng et al., 2021)). As expected, iron accumulation was
600 reduced in both roots and shoots under iron deficiency. Interestingly, the simultaneous
601 application of copper and iron deficiency increased iron accumulation in both roots and shoots
602 compared to iron deficiency applied individually (**Figure 11A**). We note that plants were
603 subjected to iron deficiency for one week and prior to that they were grown under iron replete
604 conditions. Thus, it is possible that root apoplastic iron reserves were absorbed and accounted for
605 iron accumulation in shoots under simultaneous iron and copper deficiencies. It is also possible

606 that simultaneous application of both copper and iron deficiency stimulated alternative high-
607 affinity iron uptake pathways that contributed to the root absorption of residual iron in medium.
608 Here, we also asked whether increased accumulation of iron in roots of the *opt3* mutant
609 contributed to the reduced copper accumulation in its roots (**Figure 2A**). To mimic high iron
610 conditions, we grew wild type plants under control (10 μM) or high (50 μM) iron in the medium
611 and evaluated the accumulation of copper in its tissues. As expected, due to the toxic nature of
612 iron, high iron in the medium reduced the root growth while increasing root iron level in the wild
613 type compared to controls (**Supplemental Figure 10A, B online**). Iron accumulation in the root
614 was accompanied with significantly reduced copper accumulation in roots and shoots (**Figure**
615 **11B**).
616 We recognize that these experiments do not perfectly match the scenario in the *opt3*
617 mutant that experiences the internal copper and iron deficiency under control conditions.
618 Nevertheless, our results favor the intriguing suggestion that decreased copper accumulation in
619 roots and leaves and the reduced iron and copper accumulation in the phloem contribute to iron
620 overaccumulation in the *opt3* mutant. We also propose that high iron in roots of the *opt3* mutant
621 negatively effects copper accumulation in roots of the mutant compared to wild type.
622

623 ## Discussion

624

625 Iron and copper are essential micronutrients and yet if their accumulation is not highly regulated,
626 they are toxic for the growth and development of all organisms, including plants, and
627 homeostasis of these elements is intricately related. The hallmark of this relationship is the
628 increased accumulation of copper in plant tissues under iron deficiency and the
629 overaccumulation of iron under copper deficiency (**Figure 11** and (Bernal et al., 2012; Waters
630 and Armbrust, 2013; Kastoori Ramamurthy et al., 2018; Rai et al., 2021; Sheng et al., 2021). The
631 toxicity of both metals is avoided by the ability of plants to regulate copper and iron transport
632 systems in response to the fluctuation of copper and iron availability in the immediate root
633 environment and the demands of the developing shoot. The *A. thaliana* phloem companion cells-
634 specific iron transporter, OPT3, is involved in both signaling iron demand from shoots to roots
635 and in transporting iron to developing tissues such as the seed. The systemic control of copper
636 uptake into roots and its relationship to the systemic control of iron uptake in plants has not yet

637 been documented. In this manuscript, we show the existence of systemic signaling of copper
638 status, its relationship with systemic iron signaling, and the central role of AtOPT3 in these
639 processes (**Figure 12**).
640

641 **AtOPT3 Transports Copper and the Copper-NA Complex, but Free Copper Ions are**
642 **Preferred Substrates in Heterologous Systems.**
643

644 The nature of the transport substrate of OPT3 has been under scrutiny and a matter of
645 debate in the literature. OPT3 belongs to the OPT family that is phylogenetically divided into
646 two groups: the Yellow Stripe-Like (YSL) and Oligopeptide Transporter (PT) clades (Lubkowitz,
647 2011). Analyses of the transport capabilities of some members of *A. thaliana* and *Oryza sativa*
648 OPT family have disclosed their capacity to transport synthetic tetra- and pentapeptides in
649 heterologous systems (Osawa et al., 2006), while members of the YSL clade are expected to
650 transport metal-chelate complexes (Osawa et al., 2006). Given the role of OPT3 in iron
651 homeostasis and signaling, it was expected to transport either peptides that can serve as metal
652 ligands (*e.g.,* glutathione [GSH]) or metal-ligand complexes (*e.g.,* metal-nicotianamine [metal-
653 NA]) (Stacey et al., 2008; Lubkowitz, 2011). Thus, our past finding that OPT3 transports free
654 ions, iron and cadmium when expressed in *Xenopus* oocytes or the yeast iron uptake mutant, *fet3*
655 *fet4* was unexpected (Zhai et al., 2014). However, consistent with the proton-coupled nature of
656 OPT-mediated transport, our past studies have shown that the acidification of uptake medium
657 stimulated the OPT3-mediated inward currents (Osawa et al., 2006; Zhai et al., 2014). Past
658 studies of the AtOPT3-GFP, heterologously expressed in *S. cerevisiae* showed that in this system,
659 the GFP-tagged OPT3 mislocalizes to internal vesicles rather than residing at the plasma
660 membrane (Mendoza-Cózatl et al., 2014). To prevent AtOPT3-GFP processing/folding
661 challenges and its retention at the endoplasmic reticulum, that may occur with heterologously-
662 overexpressed integral plasma membrane proteins that, in addition, are also fused to a relatively
663 large epitope tag (*e.g.* GFP (Emmerstorfer et al., 2014)), we used an untagged AtOPT3 for
664 functional complementation assays in yeast, reported in Zhai et al 2014, and this manuscript.
665 Here, we show that OPT3, in addition to iron and cadmium ions, also transported copper
666 ions when expressed in *Xenopus* oocytes or the *S. cerevisiae* copper transport mutant (**Figure 3**).
667 We also found that OPT3 was able to transport both free copper ions as well as the copper

provided as Cu-NA complex (**Figure 3A**). However, it is noteworthy that OPT3-expressing oocytes accumulated 4.2 times more copper when it was provided as a free ion rather than complexed with nicotianamine, suggesting that free copper ions are the preferred OPT3 substrate in this heterologous system. Consistent with the proton-coupled nature of OPT-mediated transport, our past studies have shown that the acidification of uptake medium stimulated the OPT3-mediated inward currents (Osawa et al., 2006; Zhai et al., 2014). A recent report has shown that members of the YSL clade of the OPT transporter family, *Brachypodium distachyon* YSL3 and maize YS1 also transport copper ions in *Xenopus* oocytes (Sheng et al., 2021). Unlike AtOPT3, copper uptake by BdYSL3 was not detected when the Cu-NA complex was provided as a substrate (Sheng et al., 2021). Similar to AtOPT3, ZmYS1 was capable of transporting copper provided as free ions as well as the Cu-NA complex; similar to AtOPT3, copper ions were the preferred transport substrates of ZmYS1 in the *Xenopus* oocyte heterologous system (Sheng et al., 2021). Vascular tissue-localized NA transporters, NAET1 and NAET2, have been identified recently (Chao et al., 2021). These transporters localize to the synaptic-like vesicles in the vasculature and control iron and copper delivery to seeds. Therefore, as suggested by Chao et al 2021, OPT3 and NAET1/NAET2 may act in concert in copper/iron and NA delivery, respectively, to the phloem. In the phloem, copper and iron would then form a complex with NA to facilitate mineral delivery to the sink tissues. Similar scenario occurs with iron and citrate transport to the xylem *via* IREG1/FPN1 (**I**ron **Reg**ulated1/**F**erro**p**orti**n** 1) and FRD3 (**M**ultidrug **a**nd **T**oxin **E**fflux) transporters, respectively (Rogers and Guerinot, 2002; Green and Rogers, 2004; Morrissey et al., 2009). In the xylem, the tri-iron(III), tri-citrate complex is formed to facilitate iron delivery to shoots (Rellán-Álvarez et al., 2009).

Recent *in silico* analysis using protein secondary and tertiary structure simulation and binding affinity results of the docking analyses suggested that AtOPT3 and its counterpart from maize, ZmOPT3 may transport iron complexed with GSH (Kurt, 2021)). Despite this prediction, AtOPT3 does not transport GSH when expressed in the GSH transport mutant, *hgt1*Δ, and the addition of GSH to the *Xenopu*s oocytes bathing medium reduces cadmium transport (Zhai et al., 2014). Our finding that AtOPT3 does not transport GSH in yeast has been recently validated by (Zhang et al., 2016). AtOPT3 counterpart from rice, OsOPT7 is essential for iron homeostasis and sources to sink partitioning but does not transport Fe-NA, Fe-DMA complexes, or GSH in oocytes as well (Bashir et al., 2015). It is noteworthy that unlike AtOPT3, other OPT family

699 members in *A. thaliana*, AtOPT4 and AtOPT6 and the closest OPT3 homolog from *Brassica*
700 *juncae*, BjGt1 transport GSH (Bogs et al., 2003; Cagnac et al., 2004; Zhang et al., 2016). Recent
701 analyses of the *Arabidopsis opt6* mutant implicated AtOPT6 in GSH long-distance transport and
702 delivery to sink organs, especially flowers (Wongkaew et al., 2018). It is noteworthy that similar
703 to the *opt3* mutant, the loss-of-function of At*OPT6* delays the transition from the vegetative to
704 reproductive stage of the development (Wongkaew et al., 2018). It would be interesting to test
705 whether mineral nutrient homeostasis is disrupted in the *opt6* mutant.
706
707 **AtOPT3 Mediates Copper (and Iron) Loading to the Phloem Companion Cells for the**
708 **Delivery to Sink Tissues.**
709
710 The role of AtOPT3 in iron and copper loading to the phloem companion cells for subsequent
711 partitioning from source to sink tissues is evidenced by the decreased accumulation of these
712 metals in the phloem of the *opt3* mutant (**Figures 1F, G, K** and **Supplemental Figure S1E**
713 **online** and (Zhai et al., 2014)). At the whole plant level, this function of AtOPT3 is important for
714 the phloem-based delivery of copper and iron from sources to sinks, including roots and young
715 leaves (**Figure 2A**, **Supplemental Figure 3 online** and (Zhai et al., 2014), respectively). Here
716 we also show that AtOPT3 is important for copper and iron delivery to developing embryos and,
717 in addition to leaves, silique valves might act as sources of these minerals for developing seeds
718 (**Figure 2B** and **C**, and **Supplemental Figure 4A online**). This suggestion is based on our
719 findings that silique valves of the mutant overaccumulated iron and copper while developing
720 embryos accumulated less iron and copper compared to wild type (**Figure 2B** and **C**). We note
721 that unlike copper and iron, manganese and zinc were overaccumulated in the vasculature and
722 both silique valves and embryos, while zinc was also overaccumulated in seeds of the *opt3*
723 mutant compared to corresponding tissues in wild type (**Figure 1H, I** and **2B**). Together, these
724 data suggest that AtOPT3 functions in copper and iron but not manganese and zinc loading to the
725 phloem and the phloem-based delivery to sink tissues.
726 We note that while the role of AtOPT3 and OsOPT7 in iron delivery to seeds is
727 evidenced by the lower iron concentration in mature seeds (**Supplemental Figure 4B, C online**
728 and (Stacey et al., 2008; Mendoza-Cózatl et al., 2014; Zhai et al., 2014; Bashir et al., 2015),
729 copper accumulation in mature seeds was not affected in the *opt3* mutant in our assays using

730 ICP-MS analysis (**Supplemental Figure 4C online** and (Stacey et al., 2008)). However, we
731 noted a subtle difference in copper distribution in the mature seed of the *opt3* mutant *vs.* wild
732 type using CT-XRF. Specifically, less copper was associated with the vasculature of the *opt3*
733 mutant *vs.* wild type, and somewhat more copper was associated with the seed coat of the mutant
734 (**Supplemental Figure 4B online**). However, this subtle difference in copper distribution was
735 not sufficient to account for total seed concentration.
736
737 **AtOPT3 Mediates Copper Homeostasis and Systemic Copper Signaling.**
738
739 Our finding that OPT3 transports copper in heterologous systems and that both *opt3-2* and *opt3-3*
740 mutant alleles accumulate less copper in roots and young leaves compared to wild type (**Figure**
741 **2A** and **Supplemental Figure 3 online**) suggested that the mutant might be more sensitive to
742 copper deficiency and/or manifest molecular symptoms of copper deficiency. Indeed, the size of
743 rosette leaves of both *opt3-2* and *opt3-3* mutants grown under copper deficiency was
744 significantly smaller compared to control conditions, and their leaves were extensively chlorotic
745 compared to wild type also grown without added copper (**Figure 4** and **F Supplemental Figure**
746 **6 online)**. Furthermore, consistent with our recent findings of the role of copper in transition to
747 flowering (Rahmati Ishka and Vatamaniuk, 2020), the *opt3* mutant failed to flower within the
748 time frame of the experiment and developed more rosette leaves than the wild type when grown
749 in the medium without and even with copper (**Figure 4C, D**). Copper deficiency-associated
750 phenotypes were rescued by transferring the mutant to a medium with higher copper
751 concentrations (**Figure 4C** to **E** and **Supplemental Figure 7 online**).
752 In addition, the *opt3* mutant mounted molecular copper-deficiency responses even when
753 it was grown under control conditions. This was evidenced by the increased activity of cupric
754 reductase in roots and the upregulated expression of the copper-deficiency regulon in roots and
755 young leaves of the *opt3* mutant *vs.* wild type (**Figure 4** and **Supplemental Datasets 2 to 4**).
756 Changes in the transcriptome of mature leaves of the *opt3* mutant were indicative of neither
757 deficiency nor sufficiency. The transcriptional copper deficiency responses of young leaves and
758 an unspecific response of mature leaves in the *opt3* mutant are consistent with their respective
759 copper concentrations (**Figure 2A, Supplemental Figure 3 online** and **Supplemental Datasets**
760 **2 to 4**). By contrast, copper accumulation in roots of the *opt3* mutant, although was lower than in

761 wild type, was still at the level of sufficiency (**Figure 2A** and (Broadley et al., 2012));
762 nevertheless roots of the *opt3* mutant mounted the transcriptional copper deficiency response.
763 Using reciprocal grafting with wild type and the *opt3* mutant, we showed that OPT3
764 function in the shoot regulates not only iron but also copper deficiency responses of the root
765 (**Figure 4**) suggesting the existence of shoot-to-root copper status signaling and the contribution
766 of OPT3 to this process. Our finding that copper feeding *via* the phloem in the shoot
767 downregulates the expression of the copper deficiency markers, *CITF1*, *COPT2* and *copper*
768 *miRNAs* in the root of copper-deficient wild type and the *opt3* mutant that constitutively
769 overexpresses copper deficiency marker genes even when it is grown under control conditions,
770 favors the existence of OPT3-mediated systemic copper signaling (**Figure 9B** and **D**).
771 Furthermore, our data suggest that similar to iron, phloem copper act as a repressor of copper-
772 deficiency responsive genes in the root.
773 An upstream regulator of *CITF1*, *COPT2* and *copper miRNAs*, SPL7, is expressed in the
774 vascular tissues of both shoot and roots, locally senses copper availability, and transmits it to
775 surrounding cells (Araki et al., 2018). In the root, *SPL7* is detected in the pericycle (Long et al.,
776 2010). Considering that phloem pole pericycle plays a major role in regulating symplastic
777 phloem unloading in the root (Ross-Elliott et al., 2017), it is possible that SPL7 senses the
778 availability of the phloem-arrived copper in the pericycle to regulate the expression of *CITF1*,
779 *COPT2*, *copper miRNAs*, and, perhaps, other SPL7 targets in the root.
780
781 **Copper and Iron Can, in Part, Substitute Each Other's Signaling Function in the Phloem.**
782
783 One of the unexpected outcomes from the phloem feeding experiments was finding that feeding
784 with copper *via* the phloem in the shoot downregulated the expression of both copper and iron
785 deficiency markers in roots of the *opt3* mutant (**Figure 9D**). Likewise, iron feeding *via* the
786 phloem in the shoot downregulated the expression of *FIT* and *IRT1* as well as *CITF1* and *COPT2*
787 in roots of the *opt3* mutant (**Figure 9B**). We note that the *opt3* mutant has a lower concentration
788 of both copper and iron in the phloem and thus, provides a sensitized genetic background for the
789 phloem feeding experiments with copper or iron. Therefore, we used wild type plants, subjected
790 them to copper and iron deficiency individually or simultaneously, and fed with either copper or
791 iron *via* the phloem in the shoot. We found that either copper or iron phloem feeding

792 downregulated the expression of both copper and iron-deficiency-responsive genes (**Figure 10B**
793 **and C**). These findings raised an intriguing possibility that mobile iron and copper in the phloem
794 can, in part, substitute each other's signaling function in regulating the expression of copper and
795 iron uptake genes in the root (**Figure 12**).
796
797 **AtOPT3-facilitated Copper and Iron Transport to the Phloem Companion Cells Mediates**
798 **Iron-Copper Crosstalk in Shoot-to-Root Signaling and Iron and Copper Homeostasis.**
799
800 As a corollary to finding that AtOPT3 loads copper to the phloem companion cells in the shoot
801 was the discovery that this function is important not only for feeding the developing sinks with
802 copper but also for conveying copper status of the shoot to the root; in addition, both copper and
803 iron can substitute each other signaling function in the phloem of the *opt3* mutant for fine-tuning
804 the expression of copper/iron uptake systems in the root (**Figures 9** and **12A**). Our finding that
805 iron deficiency significantly increases the expression of already highly expressed iron uptake
806 system in roots of the *opt3* mutant (**Figure 5D**), is especially relevant for the understanding of
807 the OPT3-mediated copper-iron crosstalk in long distance signaling as discussed below.
808 We propose that in *A. thaliana* wild type grown under copper and iron sufficiency,
809 copper and iron ions, absorbed by the root and delivered to the shoot, loaded to the phloem
810 companion cells in leaves by AtOPT3 to convey copper/iron sufficiency (**Figure 12A**). *Under*
811 *iron deficiency,* AtOPT3 loads mainly copper into the phloem companion cells since iron is
812 limited, while copper absorption by roots and accumulation in leaves increases under iron
813 deficiency (**Figure 12B**) and (Waters et al., 2012; Waters and Armbrust, 2013; Waters et al.,
814 2014). While the expression of iron uptake genes in roots of iron-deficient wild type increases, it
815 is significantly lower than in the *opt3* mutant under iron deficiency (**Figures 5D**).
816 Similarly, *under copper deficiency*, AtOPT3 loads mainly iron into the phloem
817 companion cells since copper is limited (**Figure 12C**). This AtOPT3 function fine-tunes the
818 expression of iron and copper transport systems to ensure adequate iron/copper uptake while
819 preventing toxicity. It is noteworthy that unlike copper or iron feeding *via* the vasculature in the
820 shoot, the function of AtOPT3 in the wild type does not entirely suppress copper or iron uptake
821 systems in the root under reciprocal deficiency since copper or iron uptake systems are still
822 upregulated (**Figure 12B, C**). It is possible that the concentration of iron or copper in the phloem

823 in *A. thaliana* grown under copper or iron may not be sufficient to fully repress the expression of
824 copper or iron uptake genes in the root. It is also possible that the sink strength and competition
825 (roots *vs.* shoot apices and developing leaves) are also important contributing factors that
826 determine the amount of copper and iron (as well as other components of the phloem sap)
827 recirculated to roots *via* the phloem to repress iron or copper uptake under the reciprocal
828 deficiency.

829 *Concerning the opt3 mutant*, we propose that the constitutive expression of copper and
830 iron uptake systems in its roots originates from the constitutive copper and iron deficiency in the
831 leaf phloem, most likely the phloem companion cells (**Figure 12D, E**). Copper and iron
832 deficiencies, co-occurring in the phloem of the *opt3* mutant, act autonomously in regulating
833 copper and iron deficiency genes in the roots. This suggestion is based on our finding that the
834 expression of *CITF1* and copper *miRNAs*, normally downregulated by iron deficiency while
835 upregulated by copper deficiency when applied independently, was upregulated under
836 simultaneous application of both deficiencies (**Figure 10A** and **12D**). Likewise, although *FIT* is
837 upregulated by iron deficiency and does not respond transcriptionally to copper deficiency, it
838 was upregulated by the simultaneous application of copper and iron deficiency (**Figure 10A**).

839 The question remains about how copper and iron act in systemic signaling. It is possible
840 that copper/iron availability in the phloem may be communicated *via* a common transduction
841 pathway and/or metal-binding ligand. In this regard, iron sensors, HRZs/BTS and IDEF1 in *A.*
842 *thaliana* and *O. sativa* bind not only ionic Fe^{2+} but also other transition metals and act in the root
843 to regulate the iron uptake system (Selote et al., 2014; Kobayashi, 2019). Phloem sap contains
844 potential iron and copper binding ligands such as NA and glutathione (GSH) (reviewed in
845 (Gayomba et al., 2015)). It is noteworthy that the *nas4x* mutant of *A. thaliana*, lacking functional
846 NA synthase genes, overaccumulates iron in the vasculature, similar to the *opt3* mutant (Nguyen
847 et al., 2022). Unlike the *opt3* mutant, copper accumulation in the vasculature of the *nas4x* mutant
848 was not observed, suggesting that in *A. thaliana* NA contributes mainly to iron homeostasis
849 (Klatte et al., 2009; Nguyen et al., 2022). While roots of the *nas4x* mutant exhibit somewhat
850 elevated levels of *FIT*, *IRT1* and *FRO2* expression compared to wild type both grown under
851 control conditions, unlike the *opt3* mutant (**Figure 5D**), the expression of iron uptake genes in
852 roots of *nas4x* does not increase further under iron deficiency (Klatte et al., 2009). It is tempting
853 to speculate that copper loaded by OPT3 to the phloem of the *nas4x* mutant is involved in

854 controlling the expression of iron uptake genes in its roots. The *nas4x* mutant will provide an
855 excellent complementary system for the study of crosstalk between copper and iron in systemic
856 signaling. A new family of phloem mobile peptides, IMA/FEP, has been proposed to coordinate
857 systemic iron deficiency signaling. Their contribution to the crosstalk between iron and copper
858 systemic signaling is unknown (Grillet et al., 2018; Hirayama et al., 2018).

859 While our data are consistent with the repressive role of the phloem-associated iron and
860 copper in systemic signaling and the expression of iron and copper uptake systems in the root, a
861 promotive mechanism of systemic signaling has been put forward as well (Grusak and Pezeshgi,
862 1996; Vert et al., 2003; Kumar et al., 2017). In this mechanism, iron-sufficient status in the shoot
863 would prevent a release of the promotive systemic signal, and iron deficiency-responsive genes
864 will not be expressed in the root. Considering this scenario, it is possible that iron and/or copper
865 abundance in the phloem companion cells would sequester or inhibit synthesis of the promotive
866 signal(s) preventing the upregulation of genes encoding the root iron and/or copper uptake
867 systems (**Figure 12**). We note that both repressive and promotive mechanisms rely on the
868 availability of iron and copper in the phloem, most likely the phloem companion cells.

869 To conclude, our studies have assigned new functions to AtOPT3 in loading copper into
870 the phloem, subsequent distribution to sink tissues and systemic signaling of copper deficiency.
871 We have also discovered that copper can, in part, substitute for iron in long-distance signaling.
872 We have also shown the important role for OPT3 in copper-iron crosstalk in normal homeostasis
873 of both elements. Understanding the basic mechanisms plants use to coordinate iron and copper
874 demands with their uptake, transport and utilization will provide promising avenues for targeted
875 biofortification strategies directed at increasing iron density in the edible portions of crops and
876 improving agricultural productivity on iron and copper-deficient soils.

877

878 ## Materials and Methods

879

880 ### Plant Material and Growth Conditions

881 *Arabidopsis thaliana* (*cv*. Col-0) and a previously described *opt3-3* T-DNA insertion mutant (cv.
882 Col-0; SALK_058794C; (Zhai et al., 2014) were obtained from ABRC. Soil-grown plants were
883 directly sown onto Lambert 111 irrigated with regular fertilizer. For copper deficiency treatments,
884 plants were either grown on half-strength Murashige and Skoog (MS) medium (Sigma-Aldrich,

885 M5519) with 1% sucrose and 0.7% agar or hydroponically in a medium containing 1.25 mM
886 KNO_3, 0.625 mM KH2PO_4, 0.5 mM $MgSO_4$, 0.5 mM $Ca(NO_3)$, 10 µM Fe(III)HBED and the
887 following micronutrients: 17.5 µM H_3BO_3, 3.5 µM $MnCl_2$, 0.25 µM $ZnSO_4$, 0.05 µM $NaMoO_4$,
888 2.5 µM NaCl and 0.0025 µM $CoCl_2$ (Arteca and Arteca 2000), and the indicated concentrations
889 of copper with 125 nM copper considered as control (Yan et al., 2017). For growing plants
890 hydroponically, seeds were surface sterilized before sowing onto 0.7% (w/v) agar aliquoted in 10
891 µL pipette tips. Pipette tips were cut before placing them into floats made of foam boards. The
892 roots of seedlings were immersed into the hydroponic solution after 7-8 days of growth. To
893 ensure that both wild type and the *opt3-3* mutant were treated at the same growth stage, all plants
894 were transferred when the rosette reached to 50% of final size (principal growth stage 3.5 as
895 documented in (Boyes et al., 2001)). In this case, wild type and the *opt3-3* plants were
896 transferred 3 and 4 weeks after sowing seeds, respectively. The solution was replaced on a
897 weekly basis and was replaced for one more time 24 hours before collecting samples All plants
898 were grown in a growth chamber at 22°C, 14 h light/10 h dark photoperiod at a photon flux
899 density of 110 µmol m^{-2} s^{-1}.
900

901 **High-Throughput Sequencing of mRNA, Sequence Mapping and Differential Gene**
902 **Expression Analysis**

903 *A. thaliana* wild type and *opt3-3* plants were grown hydroponically with 0.125 µM $CuSO_4$ for
904 four weeks. The total RNA was isolated from roots, mature and young leaves using the TRIzol
905 reagent (Invitrogen). To achieve iron deficiency, a subset of plants grown as described above
906 were transferred to a medium without iron for four days before roots were collected. Tissues
907 were pooled from four plants grown in the same container and three containers were used per
908 each genotype. The strand-specific RNA-Seq libraries were constructed using 3 µg of total RNA
909 according to procedures described previously (Zhong et al., 2011). RNA-Seq libraries were
910 sequenced on the Illumina HiSeq 2500 system using the single-end mode. Three replicates were
911 used for RNA-seq. Each replicate consisted of tissues (roots, young and mature leaves) pooled
912 from four plants per genotype grown in the same container. Trimmomatic (Bolger et al. 2014)
913 was employed to remove adaptor and low-quality sequences in the Illumina raw reads. Reads
914 shorter than 40 bp were discarded. The resulting reads were aligned to the ribosomal RNA
915 database using Bowtie with 3 mismatches allowed (Langmead et al., 2009; Quast et al., 2013),

916 and those aligned were discarded. The final clean reads were aligned to the Arabidopsis genome
917 sequence (TAIR 10) using TopHat with 1 mismatch allowed (Trapnell et al., 2009). Finally, the
918 counts of mapped reads for each gene model from each sample were derived and normalized to
919 RPKM (reads per kilobase of exon model per million mapped reads). DESeq2 was used to
920 identify differentially expressed genes (DEGs) with the raw count data (Love et al., 2014). Raw
921 *p* values were corrected for multiple testing using the false discovery rate (FDR; (Benjamini and
922 Hochberg, 1995). Genes with an FDR less than 0.05 and fold-changes greater than or equal to
923 1.5 were regarded as DEGs. GO term enrichment and gene functional classification analyses
924 were performed using Plant MetGenMap (Joung et al., 2009).
925
926 **ICP-MS Analysis of Copper Concentration in Plant Tissues**
927 Root and shoot tissues were collected from five-week-old plants grown hydroponically as
928 described above. The seeds and siliques were collected from 11–12-week-old plants grown in
929 soil as described above. Iron and other elements were desorbed from root cell walls by washing
930 roots in 10 mM EDTA for five minutes and a solution with 0.3 mM bathophenanthroline
931 disulphonate (BPS) and 5.7 mM sodium dithionite for ten minutes followed by three consecutive
932 washes in deionized water. The fully expanded mature leaves (three leaves/plant) and two-to-
933 three upmost leaves less than five millimeters long (young leaves) were rinsed with deionized
934 water three times and then pooled separately as mature leaves and young leaves. The dry seeds
935 and valves were collected from plants grown in soil, and the seeds were separated from the
936 valves with 500 μm mesh. Four to eight plants were pooled for one measurement in each
937 experiment. Three measurements and three independent experiments were conducted. All the
938 samples were dried in an 80°C oven before measuring the weight. Elemental analysis was
939 performed using ICP-MS.
940
941 **RT-qPCR Analysis**
942 Roots and leaves were collected from plants at Zeitgeber time 7 (Zeitgeber time is defined as the
943 hours after lights-on) and flash-frozen in liquid nitrogen before the homogenization. Total RNA
944 was isolated using TRIzol reagent (Invitrogen) according to the manufacturer's instructions.
945 cDNA templates used for qPCR analysis were synthesized by using AffinityScript QPCR cDNA
946 synthesis kit. One μg of total RNA was treated with DNase I (New England Biolabs) prior to the

947 first-strand cDNA synthesis to eliminate genomic DNA contamination. Real-time PCR analysis
948 was performed in a total volume of 15 mL containing 1x iQSYBR GreenSupermix (Bio-Rad),
949 500 nM concentration of each PCR primer and 2 µL of 15x diluted cDNA templates using
950 CFX96 real-time PCR system (Bio-Rad) as described (Gayomba et al., 2013). Data were
951 normalized to the expression of *ACTIN2* (AT3G18780), whose expression was stable under
952 investigated conditions and in studied genotypes (Supplemental Dataset 5 online). The fold
953 difference (2^{-DDCt}) and the statistical parameters were calculated using the CFX Manager
954 Software, version 3.1 (Bio-Rad).
955

956 **Grafting Experiments**

957 The grafting method was described previously with slight modification (Marsch-Martínez et al.
958 2013). All of the procedures were performed under Leica S6E microscope. Briefly, wild type and
959 *opt3-3* seeds were germinated and grown vertically on half-strength MS medium with 0.5%
960 sucrose for 6-7 days. Cotyledons were removed by using sterile scalpels with No.11 blades right
961 before grafting. The scions and rootstocks were then separated and moved to half-strength MS
962 plates with 0.5% sucrose and 0.7% agar for alignment. After grafting, the plants were grown
963 vertically on the plates for another 10 days. Successfully grafted plants without adventitious
964 roots above the graft junction were then transferred to the hydroponic system with 0.25 µM
965 $CuSO_4$ for 24 days before qPCR analysis.
966

967 **Synchrotron X-Ray Fluorescence Imaging**

968 Fresh samples were detached immediately before the analysis and were placed in a wet chamber
969 made between two layers of metal-free Kaptonfilm and mounted onto 35-mm slide frames. The
970 spatial distribution of Cu and Fe was imaged via SXRF microscopy at the F3 station at the
971 Cornell High Energy Synchrotron Source (CHESS). The 2D Cu and Fe raster maps were
972 acquired at the 25-µm resolution, 0.2 s/pixel dwell time using a focused, monochromatic incident
973 x-ray beam at 12.8 keV and photon flux of ~10^{10}photons/s. The monochromatic beam was
974 generated with 0.6% energy bandwidth multilayers. Focusing was achieved using a single-
975 bounce moncapillary (named PEB605) fabricated at CHESS. These settings did not cause
976 detectable damage to plant tissues within the 6- to 9-h scans required for analysis of the full set
977 of samples. Element-specific x-ray fluorescence was detected using a Vortex ME-4 silicon drift

978 detector. Quantifications were done by calibrating using a thin copper foil film standard (15.9 µg
979 copper/cm^2, the metal was deposited on 6.3 µm thick Mylar) during each experiment and
980 concentrations were expressed as µg cm^{-2}. Data was processed with the software Praxes, which
981 was developed at CHESS and employs PyMCA libraries in batch mode (Solé et al., 2007).
982

983 **Synchrotron-based Confocal XRF Microscopy**

984 Confocal XRF experiments were obtained at beamline 5-ID (SRX). The beamline
985 monochromator and focusing optics were employed to deliver 3x10^{11} photons/second in a 1x1
986 µm^2 beam, with incident beam energy of 10.0 keV and bandwidth of approximately 1 eV. The
987 confocal geometry was achieved by placing a collimating channel array (CCA) (Agyeman-Budu
988 et al., 2016) onto a single-element Vortex SDD detector perpendicular to the beam. The sample
989 stage was oriented such that the horizontal translation axis of the stage is 35 degrees from that of
990 the incident beam, and 55 degrees from the detector axis. The particular CCA employed for these
991 measurements has a series of 175, 2-µm channels etched into a 1-mm thick Germanium substrate,
992 etched to an approximate depth of 300 µm. The working distance between the sample and optic
993 is 1.5 mm. Due to the finite width of the optic at its front tip, the maximum probe depth of the
994 system in this configuration is 0.8 mm. Quantitative calibration of the confocal XRF system was
995 achieved by methods described in (Malzer and Kanngießer, 2005; Mantouvalou et al., 2012).
996

997 **Synchrotron-based X-ray Fluorescence Computed Microtomography (F-CMT)**

998 Internal distributions of copper, iron and other micronutrient elements in wild type and the *opt3-*
999 *3* mutant seeds were measured *in vivo* by synchrotron-based X-ray Fluorescence Computed
1000 Microtomography (F-CMT) at the X-ray Fluorescence Microprobe (XFM) beamline at the
1001 National Synchrotron Light Source II (NSLS-II) in Upton, NY. XFM (4-BM) beamline is
1002 designed for monochromatic operation in the 2.3 to 23 keV range and optimized for high-quality,
1003 spatially-resolved X-ray absorption spectroscopy (Sulfur to Technetium K-edges) in conjunction
1004 with element-specific imaging and microdiffraction. XFM beamline can also be operated in a
1005 pink beam "imaging" mode that delivers a 1-micron spot with up to 1000X more flux than the
1006 XFM monochromatic beam. XFM filtered pink beam (12 – 20 keV broadband) was focused by
1007 Kirkpatrick-Baez (KB) mirrors to a 1-micron spot for F-CMT measurements of seeds. Seeds
1008 were mounted to a quartz post that interfaces with a Huber goniometer head on a rotation stage

attached to a fast-scanning translation stage. F-CMT images were acquired at the seed center by rotating and translating the specimen in the microbeam while recording the fluorescence intensities with a Hitachi 4-element Vortex SDD coupled to Quantum Detectors Xspress3 electronics. F-CMT data were collected using 0.75 – 3.0^{-} degree angular steps, 2 – 8 µm translation steps and 50 ms dwell time. Tomographic image reconstructions using a conventional filtered back projection algorithm were processed using tomo-Py plugin to GSE Mapviewer in the LARCH package (Newville, 2013). Thin-film standard reference materials (SRM 1832 & 1833) were measured as part of the data set to establish elemental sensitivities (counts per second per mg cm^{-2}). The intensity of elements between wild type and the *opt3* mutant was set to the same scale.

Copper Uptake in *Xenopus laevis* Oocytes

Oocyte harvesting, cRNA synthesis, microinjections, and OPT3 expression in *Xenopus* oocytes was performed as described previously (Zhai et al., 2014). All animal procedures were performed in accordance with Cornell University IACUC Protocol number 2017-0139. *X. laevis* oocytes were injected with 50 nL of water (control) or 50 nL of water containing 50 ng of OPT3 cRNA and incubated in ND96 solution at 18°C for 4 d prior to the uptake measurements. The basal uptake solution consisted of a modified ND96 solution containing 96 mM NaCl, 1 mM KCl, 0.9 mM $CaCl_2$, buffered with 5 mM 2-(N-morpholino) ethanesulfonic acid/NaOH to pH 6.0, as previous studies determined these conditions were suitable to minimize endogenous transport in oocytes (Zhai et al., 2014; Sheng et al., 2021). The uptake solution was supplemented with 25 µM Cu-NA or 100 µM CuSO4 [the final free Cu^{2+} activity in the uptake solution being estimated to be 35 µM as determined by GEOCHEM-EZ (Shaff et al., 2010). Each sample contained 8 – 10 oocytes, with 5 replicates per data point. At a given time point, the uptake was terminated by washing oocytes six consecutive times with an ice-cold basal uptake solution. Oocytes were collected and samples were digested in 100 µL of 70% HClO4, re-suspended in 5 ml of 0.1 M nitric acid, and analyzed using inductively coupled plasma mass spectrometry (Sciex ICP-MS). Resting membrane potentials were measured as described previously(Zhai et al., 2014).

Functional Complementation Assays in *Saccharomyces cerevisiae*

1039 *S. cerevisiae* SEY6210 (*MATa ura3-52 leu2-3,-112 his3Δ200 trp1Δ901 lys2-801 suc2Δ9*) wild
1040 type and the *ctr1Δctr2Δctr3Δ* triple mutant (*MATa ura3-52 his3Δ200 trp1-901 ctr1*::*ura3*::*Knr*
1041 *ctr2*::*HIS3 ctr3*::*TRP1*) were used for functional complementation assays. *YES3-Gate-OPT3*
1042 construct or *YES3-Gate* lacking the cDNA insert were transformed into appropriate yeast line
1043 using the Frozen-EZ Yeast Transformation II kit (Zymo Research). Transformants were selected
1044 for uracil prototrophy on YNB medium containing 6.7% (w/v) yeast nitrogen base without amino
1045 acids (Difco), 0.77% (w/v) CSM-URA, 0.5% (w/v) NaCl, 2% glucose, 2% (w/v) agar.
1046 Functional complementation assays included analyses of the respiration competence and
1047 copper accumulation in yeast cells as described (Jung et al., 2012). Specifically, the respiration
1048 competence of different cell lines was tested by the ability of cells to grow on non-fermentable
1049 carbon sources (Dancis et al., 1994). To do so, different cell lines transformed with *YES3-Gate*
1050 with or without *OPT3* cDNA insert were grown in liquid YNB-URA to an $OD_{600\ nm}$ = 1.0,
1051 serially 10-fold diluted, and spotted onto YPEG medium containing 1% (w/v) yeast extract, 2%
1052 (w/v) bacto-peptone, 3% (v/v) glycerol, 2% (v/v) ethanol, and 2% (w/v) agar and the indicated
1053 concentrations of $CuSO_4$. Plates were incubated for 3 days at 30°C.
1054 Different yeast lines were grown to exponential log phase in liquid YNB media described
1055 above to analyze copper accumulation. An aliquot (150 µl) of the overnight grown culture was
1056 inoculated into 20 ml of the fresh YNB media with 20 µM $CuSO_4$ and cells were grown at 30°C.
1057 After 24 h, cells were collected by centrifugation, washed with deionized water before copper
1058 was desorbed from yeast cell wall by washings in desorbing buffer containing 1mM EDTA and
1059 100 µM of a copper chelator, bathocuproine disulfonate BCS, pH8.0. Cells were then washed
1060 two more times in de-ionized water and collected by centrifugation. The cell pellet was dried,
1061 digested by heating with a combination of purified concentrated nitric and perchloric acids, and
1062 finally dissolved in 10 ml of 5% nitric acid. The concentration of copper in processed yeast cells
1063 was analyzed by inductively coupled plasma mass spectroscopy (ICP-MS; Agilent 7500).
1064

1065 **Collection of the Phloem Sap**

1066 Phloem sap was collected from wild type and *opt3-3* mutant plants grown hydroponically at the
1067 late vegetative stage as described (Zhai et al., 2014). Briefly, leaves # 9 and 10 collected from
1068 one plant were pooled together, and the xylem sap was flashed by placing the petioles in a tube
1069 filled with 300 µL of deionized water and incubated in an illuminated growth chamber for 15

1070 min followed by further incubation in darkness for 1 h. To collect phloem sap, the petioles were
1071 then recut in 5 mM Na_2-EDTA (pH 7.5) under low light before placing the petioles in pre-
1072 weighed Eppendorf tubes containing 250 µL of 5 mM Na_2-EDTA (pH 7.5). Leaves were then
1073 incubated in darkness for 1 h in a high-humidity chamber lined with wet paper towels and sealed
1074 with Vaseline. Samples with the collected phloem sap were weighed again to determine the
1075 volume of phloem sap obtained per sample to calculate concentrations of copper or potassium
1076 (abundant in the phloem) after ICP-MS.
1077
1078 **Copper and Iron Feeding to the Phloem**
1079 The phloem feeding procedure was performed as described by (Oparka et al., 1994; Oparka et al.,
1080 1995; Knox, 2019). The procedure is based on the abrasion of the source leaf vein that results in
1081 some phloem 'trapping' of the applied sample. To test the phloem loading effectiveness, we used
1082 a phloem tracer carboxyfluorescein diacetate succinimidyl ester (CFDA), that after diffusing into
1083 plant cells, is cleaved by cellular esterases into a membrane-impermeable form,
1084 carboxyfluorescein (CF) (Grignon et al., 1989). *A. thaliana* wild type was grown hydroponically
1085 in control conditions for 33 days. Ten microliters of 10 mM CFDA was applied to the leaf
1086 surface around the major vein of six to seven bottommost leaves before the leaf surface at the
1087 major vein was abrased with a carbon steel blade. CF-mediated fluorescence in roots was
1088 visualized after 6 hours using a FITC filter set of the Axio Imager M2 microscope equipped with
1089 the motorized Z-drive (Zeiss). Images were collected using the high-resolution 25 AxioCam MR
1090 Camera and processed using the Adobe Photoshop software package, version 12.0.
1091 For iron or copper phloem feeding, *A. thaliana* wild type was grown hydroponically with
1092 or without 125 nM $CuSO_4$ for 33 days. To impose iron deficiency, plants were grown
1093 hydroponically in a control solution for 31 days and then a subset was transferred to a fresh
1094 medium without iron and grown for two more days. The *opt3* mutant was grown hydroponically
1095 under control conditions for 33 days. Ten microliters of 5 mM $CuSO_4$ or 10 mM $FeCl_2$ dissolved
1096 in 10 mM citrate were applied to the major vein of 6 to 7 bottommost leaves before the leaf
1097 surface at the major vein was abrased with a carbon steel blade. For control, water (a mock
1098 treatment for $CuSO_4$) or 10 mM citrate (a mock treatment for Fe(II)-citrate) were fed to the
1099 phloem as described above. This procedure was performed on 8 fully developed leaves per each
1100 plant. In all experiments, roots were collected after 24 hours of phloem feeding and at Zeitgeber

1101 time 4-5. Roots were pooled from four plants per experiment and all experiments were repeated
1102 at least three times.
1103
1104 **Statistical analysis**
1105 Statistical analyses of experimental data were performed using the ANOVA single-factor
1106 analysis and Tukey HSD using JMP® Pro 14 (SAS Institute Inc., Cary, NC, 1989-2007).
1107
1108 **Accession numbers**
1109 Sequence data of the genes from this article can be found in the Arabidopsis Genome Initiative
1110 or GenBank/EMBL databases under the following accession numbers: *OPT3* (AT4G16370),
1111 *CITF1* (AT1G71200), *FRO4* (AT5G23980), FRO5 (AT5G23990), *COPT1* (AT5G59030),
1112 *COPT2* (AT3G46900), *YSL1* (AT4G24120), *YSL2* (AT5G24380), *YSL3* (AT5G53550), *CSD1*
1113 (AT1G08830), *CSD2* (AT2G28190), *IRT1* (AT4G19690), *FRO2* (AT1G01580), *FRO6*
1114 (AT5G49730), *FRO7* (AT5G49740), *FSD1* (AT4G25100), *ARPN* (AT2G02850), *BCB*
1115 (AT5G20230), *CCS1* (AT1G12520), *UCC2* (AT2G44790), *FER1* (AT5G01600), *FER3*
1116 (AT3G65090), *FER4* (AT2G40300), *ZIP2* (AT5G59520), *bHLH23* (AT4G28790), TCH4
1117 (AT5G57560), *BTSL1* (AT1G74770), *ZAT12* (AT5G59820), *FEP2/IMA2* (AT1G47395),
1118 *FEP1/IMA3* (AT2G30766), *IREG2/FPN2* (AT5G03570), *VTL1* (AT1G21140), *VTL2*
1119 (AT1G76800), *VTL5* (AT3G25190), *NAS3* (AT1G09240), *PETE2* (AT1G20340), *MT1B*
1120 (AT5G56795), *NRT2.7* (AT5G14570), *MT1B* (AT5G56795), *MT1A* (AT1G07600), *MT2A*
1121 (AT3G09390), *AT2G47010, AT4G10500, At1G31710, At1G32350, At5G02670,* and *At5g05250*.
1122

1123 ## Author Contributions and Acknowledgements:

1124 J-C. C. and O. K. V. designed experiments; all authors contributed to different experiments
1125 presented in this manuscript. J.C. and O. K. V. wrote the manuscript with contributions from all
1126 authors. We thank Mary Lou Guerinot (Dartmouth, USA) for providing the seed of the *fit-2*
1127 mutant and for constructive comments on the manuscript. We thank David Mendoza-Cózatl
1128 (University of Missouri) for providing seeds of the *opt3-2* mutant. We thank a former member of
1129 the Vatamaniuk lab, Nanditha Vimalakumari for her contribution to Figure 3 and all current lab
1130 members for constructive comments on the manuscript. We thank Prof. Margaret Frank and her
1131 Ph.D. student, Hannah Thomas (Cornell University) for assisting with the phloem feeding

experiments. We thank Dr. John Grazul at the Cornell Center for Materials Research (CCMR) for assisting in the preparation samples for 2D-CXRF. The CCMR facility is supported by the National Science Foundation under Award Number DMR-1719875. Parts of this research used the XFM and SRX Beamlines of the National Synchrotron Light Source II, a U.S. Department of Energy (DOE) Office of Science User Facility operated for the DOE Office of Science by Brookhaven National Laboratory under Contract No. DE-SC0012704. This work is based upon research conducted at the Cornell High Energy Synchrotron Source (CHESS), which during the period of research was supported by the National Science Foundation under award DMR-1332208; the Center for High Energy X-ray Sciences (CHEXS) is presently supported by the National Science Foundation under award DMR-1829070. This study was funded by NSF-IOS #1656321 to O. K. V. and NSF-IOS #1754966 to E. W., O. K. V. and M. P.

References

Agyeman-Budu DN, Choudhury S, Coulthard I, Gordon R, Hallin E, Woll AR (2016) Germanium Collimating micro-Channel Arrays For High Resolution, High Energy Confocal X-ray Fluorescence Microscopy. Icxom23: International Conference on X-Ray Optics and Microanalysis **1764**

Alexander SPH, Kelly E, Mathie A, Peters JA, Veale EL, Armstrong JF, Faccenda E, Harding SD, Pawson AJ, Sharman JL, et al. (2019) THE CONCISE GUIDE TO PHARMACOLOGY 2019/20: Transporters. British Journal of Pharmacology **176:** S397-S493

Araki R, Mermod M, Yamasaki H, Kamiya T, Fujiwara T, Shikanai T (2018) SPL7 locally regulates copper-homeostasis-related genes in Arabidopsis. J Plant Physiol **224-225:** 137-143

Bashir K, Ishimaru Y, Itai RN, Senoura T, Takahashi M, An G, Oikawa T, Ueda M, Sato A, Uozumi N, et al. (2015) Iron deficiency regulated OsOPT7 is essential for iron homeostasis in rice. Plant Molecular Biology **88:** 165-176

Baxter IR, Vitek O, Lahner B, Muthukumar B, Borghi M, Morrissey J, Guerinot ML, Salt DE (2008) The leaf ionome as a multivariable system to detect a plant's physiological status. Proceedings of the National Academy of Sciences **105:** 12081-12086

Benjamini Y, Hochberg Y (1995) Controlling the False Discovery Rate: A Practical and Powerful Approach to Multiple Testing. Journal of the Royal Statistical Society. Series B (Methodological) **57:** 289-300

Bernal M, Casero D, Singh V, Wilson GT, Grande A, Yang H, Dodani SC, Pellegrini M, Huijser P, Connolly EL, et al. (2012) Transcriptome Sequencing Identifies SPL7 - Regulated Copper Acquisition Genes FRO4 FRO5 and the Copper Dependence of Iron Homeostasis in Arabidopsis The Plant Cell **24:** 738-761

Bogs J, Bourbouloux A, Cagnac O, Wachter A, Rausch T, Delrot S (2003) Functional characterization and expression analysis of a glutathione transporter, BjGT1, from

1171 Brassica juncea: evidence for regulation by heavy metal exposure. Plant, Cell &
1172 Environment **26:** 1703-1711
1173 **Broadley M, Brown P, Cakmak I, Rengel Z, Zhao F** (2012) Chapter 7 - Function of Nutrients:
1174 Micronutrients A2 - Marschner, Petra. *In* Marschner's Mineral Nutrition of Higher Plants
1175 (Third Edition). Academic Press, San Diego, pp 191-248
1176 **Burkhead JL, Gogolin Reynolds KA, Abdel-Ghany SE, Cohu CM, Pilon M** (2009) Copper
1177 homeostasis. New Phytologist **182:** 799-816
1178 **Cagnac O, Bourbouloux A, Chakrabarty D, Zhang MY, Delrot S** (2004) AtOPT6 transports
1179 glutathione derivatives and is induced by primisulfuron. Plant Physiology **135:** 1378-
1180 1387
1181 **Chang CJ** (2015) Searching for harmony in transition-metal signaling. Nat Chem Biol **11:** 744-
1182 747
1183 **Chao Z-F, Wang Y-L, Chen Y-Y, Zhang C-Y, Wang P-Y, Song T, Liu C-B, Lv Q-Y, Han**
1184 **M-L, Wang S-S, et al.** (2021) NPF transporters in synaptic-like vesicles control delivery
1185 of iron and copper to seeds. Science advances **7:** eabh2450-eabh2450
1186 **Chen C, Galon Y, Rahmati Ishka M, Malihi S, Shimanovsky V, Twito S, Rath A,**
1187 **Vatamaniuk OK, Miller G** (2020) ASCORBATE PEROXIDASE6 delays the onset of
1188 age-dependent leaf senescence. Plant Physiology
1189 **Colangelo EP, Guerinot ML** (2004) The essential basic helix-loop-helix protein FIT1 is
1190 required for the iron deficiency response. Plant Cell **16:** 3400-3412
1191 **Cui Y, Chen CL, Cui M, Zhou WJ, Wu HL, Ling HQ** (2018) Four IVa bHLH Transcription
1192 Factors Are Novel Interactors of FIT and Mediate JA Inhibition of Iron Uptake in
1193 Arabidopsis. Mol Plant **11:** 1166-1183
1194 **Dancis A, Haile D, Yuan DS, Klausner RD** (1994) The Saccharomyces cerevisiae copper
1195 transport protein (Ctr1p). Biochemical characterization, regulation by copper, and
1196 physiologic role in copper uptake. J Biol Chem **269:** 25660-25667
1197 **Emmerstorfer A, Wriessnegger T, Hirz M, Pichler H** (2014) Overexpression of membrane
1198 proteins from higher eukaryotes in yeasts. Applied Microbiology and Biotechnology **98:**
1199 7671-7698
1200 **Epstein E, Bloom A** (2005) Mineral nutrition of plants: principles and perspectives, 2nd eds.
1201 Sunderland, Mass Sinaur**:** 292-305
1202 **Gao F, Robe K, Bettembourg M, Navarro N, Rofidal V, Santoni V, Gaymard F, Vignols F,**
1203 **Roschzttardtz H, Izquierdo E, et al.** (2020) The Transcription Factor bHLH121
1204 Interacts with bHLH105 (ILR3) and Its Closest Homologs to Regulate Iron Homeostasis
1205 in Arabidopsis. Plant Cell **32:** 508-524
1206 **Garcia MJ, Romera FJ, Stacey MG, Stacey G, Villar E, Alcantara E, Perez-Vicente R**
1207 (2013) Shoot to root communication is necessary to control the expression of iron-
1208 acquisition genes in Strategy I plants. Planta **237:** 65-75
1209 **Gayomba SR, Jung HI, Yan J, Danku J, Rutzke MA, Bernal M, Kramer U, Kochian LV,**
1210 **Salt DE, Vatamaniuk OK** (2013) The CTR/COPT-dependent copper uptake and SPL7-
1211 dependent copper deficiency responses are required for basal cadmium tolerance in A.
1212 thaliana. Metallomics **5:** 1262-1275
1213 **Gayomba SR, Zhai Z, Jung HI, Vatamaniuk OK** (2015) Local and systemic signaling of iron
1214 status and its interactions with homeostasis of other essential elements. Front Plant Sci **6:**
1215 716

1216 **Green LS, Rogers EE** (2004) FRD3 Controls Iron Localization in Arabidopsis. Plant
1217 Physiology **136:** 2523-2531
1218 **Grignon N, Touraine B, Durand M** (1989) 6(5)Carboxyfluorescein as a tracer of phloem sap
1219 translocation. American Journal of Botany **76:** 871-877
1220 **Grillet L, Lan P, Li W, Mokkapati G, Schmidt W** (2018) IRON MAN is a ubiquitous family
1221 of peptides that control iron transport in plants. Nat Plants **4:** 953-963
1222 **Grusak MA, Pezeshgi S** (1996) Shoot-to-Root Signal Transmission Regulates Root Fe(III)
1223 Reductase Activity in the dgl Mutant of Pea. Plant Physiology **110:** 329-334
1224 **Ha JH, Doguer C, Wang X, Flores SR, Collins JF** (2016) High-Iron Consumption Impairs
1225 Growth and Causes Copper-Deficiency Anemia in Weanling Sprague-Dawley Rats.
1226 PLoS One **11:** e0161033
1227 **Hirayama T, Lei GJ, Yamaji N, Nakagawa N, Ma JF** (2018) The Putative Peptide Gene FEP1
1228 Regulates Iron Deficiency Response in Arabidopsis. Plant Cell Physiol **59:** 1739-1752
1229 **Jain A, Wilson G, Connolly E** (2014) The diverse roles of FRO family metalloreductases in
1230 iron and copper homeostasis. Frontiers in Plant Science **5**
1231 **Jeong J, Merkovich A, Clyne M, Connolly EL** (2017) Directing iron transport in dicots:
1232 regulation of iron acquisition and translocation. Curr Opin Plant Biol **39:** 106-113
1233 **Jiang A, Guo Z, Pan J, Zhuang Y, Zuo D, Hao C, Gao Z, Xin P, Chu J, Zhong S, et al.**
1234 (2020) The *PIF1-MIR408-Plantacyanin* Repression Cascade Regulates Light Dependent
1235 Seed Germination. bioRxiv**:** 2020.2007.2020.212340
1236 **Joung J-G, Corbett AM, Fellman SM, Tieman DM, Klee HJ, Giovannoni JJ, Fei Z** (2009)
1237 Plant MetGenMAP: An Integrative Analysis System for Plant Systems Biology. Plant
1238 Physiology **151:** 1758-1768
1239 **Jung HI, Gayomba SR, Rutzke MA, Craft E, Kochian LV, Vatamaniuk OK** (2012) COPT6
1240 is a plasma membrane transporter that functions in copper homeostasis in *Arabidopsis*
1241 and is a novel target of SQUAMOSA promoter-binding protein-like 7. J Biol Chem **287:**
1242 33252-33267
1243 **Kastoori Ramamurthy R, Xiang Q, Hsieh EJ, Liu K, Zhang C, Waters BM** (2018) New
1244 aspects of iron-copper crosstalk uncovered by transcriptomic characterization of Col-0
1245 and the copper uptake mutant spl7 in Arabidopsis thaliana. Metallomics **10:** 1824-1840
1246 **Khan MA, Castro-Guerrero NA, McInturf SA, Nguyen NT, Dame AN, Wang J, Bindbeutel**
1247 **RK, Joshi T, Jurisson SS, Nusinow DA, et al.** (2018) Changes in iron availability in
1248 Arabidopsis are rapidly sensed in the leaf vasculature and impaired sensing leads to
1249 opposite transcriptional programs in leaves and roots. Plant Cell Environ **41:** 2263-2276
1250 **Kim SA, LaCroix IS, Gerber SA, Guerinot ML** (2019) The iron deficiency response in
1251 *Arabidopsis thaliana* requires the phosphorylated transcription factor URI. Proceedings
1252 of the National Academy of Sciences **116:** 24933-24942
1253 **Kim SA, Punshon T, Lanzirotti A, Li L, Alonso JM, Ecker JR, Kaplan J, Guerinot ML**
1254 (2006) Localization of Iron in *Arabidopsis* Seed Requires the Vacuolar Membrane
1255 Transporter VIT1. Science **314:** 1295-1298
1256 **Klatte M, Schuler M, Wirtz M, Fink-Straube C, Hell R, Bauer P** (2009) The analysis of
1257 Arabidopsis nicotianamine synthase mutants reveals functions for nicotianamine in seed
1258 iron loading and iron deficiency responses. Plant physiology **150:** 257-271
1259 **Klevay LM** (2001) Iron overload can induce mild copper deficiency. J Trace Elem Med Biol **14:**
1260 237-240

Knox K (2019) Measuring Phloem Transport Velocity in Arabidopsis Seedlings Using the Fluorescent Coumarin Glucoside, Esculin. *In* J Liesche, ed, Phloem: Methods and Protocols. Springer New York, New York, NY, pp 195-201

Kobayashi T (2019) Understanding the Complexity of Iron Sensing and Signaling Cascades in Plants. Plant Cell Physiol **60:** 1440-1446

Kumar RK, Chu H-H, Abundis C, Vasques K, Rodriguez DC, Chia J-C, Huang R, Vatamaniuk OK, Walker EL (2017) Iron-Nicotianamine Transporters Are Required for Proper Long Distance Iron Signaling Plant Physiology **175:** 1254-1268

Kurt F (2021) An Insight into Oligopeptide Transporter 3 (OPT3) Family Proteins. Protein and Peptide Letters **28:** 43-54

Langmead B, Trapnell C, Pop M, Salzberg SL (2009) Ultrafast and memory-efficient alignment of short DNA sequences to the human genome. Genome Biology **10:** R25

Li WF, Lan P (2017) The Understanding of the Plant Iron Deficiency Responses in Strategy I Plants and the Role of Ethylene in This Process by Omic Approaches. Frontiers in Plant Science **8**

Long TA, Tsukagoshi H, Busch W, Lahner B, Salt DE, Benfey PN (2010) The bHLH transcription factor POPEYE regulates response to iron deficiency in Arabidopsis roots. Plant Cell **22:** 2219-2236

Love MI, Huber W, Anders S (2014) Moderated estimation of fold change and dispersion for RNA-seq data with DESeq2. Genome Biology **15:** 550

Lubkowitz M (2011) The Oligopeptide Transporters: A Small Gene Family with a Diverse Group of Substrates and Functions? Mol Plant **4:** 407-415

Mai HJ, Lindermayr C, von Toerne C, Fink-Straube C, Durner J, Bauer P (2015) Iron and FER-LIKE IRON DEFICIENCY-INDUCED TRANSCRIPTION FACTOR-dependent regulation of proteins and genes in Arabidopsis thaliana roots. Proteomics **15:** 3030-3047

Malzer W, Kanngießer B (2005) A Model for the Confocal Volume of 3D Micro X-ray Fluorescence Spectrometer. Spectrochimica Acta Part B: Atomic Spectroscopy **60:** 1334-1341

Mantouvalou I, Malzer W, Kanngiesser B (2012) Quantification for 3D micro X-ray fluorescence. Spectrochimica Acta Part B-Atomic Spectroscopy **77:** 9-18

Mendoza-Cózatl DG, Xie Q, Akmakjian GZ, Jobe TO, Patel A, Stacey MG, Song L, Demoin DW, Jurisson SS, Stacey G, et al. (2014) OPT3 is a component of the iron-signaling network between leaves and roots and misregulation of OPT3 leads to an over-accumulation of cadmium in seeds. Mol Plant **7:** 1455-1469

Morrissey J, Baxter IR, Lee J, Li L, Lahner B, Grotz N, Kaplan J, Salt DE, Guerinot ML (2009) The Ferroportin Metal Efflux Proteins Function in Iron and Cobalt Homeostasis in Arabidopsis. The Plant Cell **21:** 3326-3338

Mukherjee I, Campbell NH, Ash JS, Connolly EL (2006) Expression profiling of the Arabidopsis ferric chelate reductase (FRO) gene family reveals differential regulation by iron and copper. Planta **223:** 1178-1190

Mustroph A, Zanetti ME, Jang CJH, Holtan HE, Repetti PP, Galbraith DW, Girke T, Bailey-Serres J (2009) Profiling translatomes of discrete cell populations resolves altered cellular priorities during hypoxia in Arabidopsis. Proceedings of the National Academy of Sciences **106:** 18843-18848

Newville M (2013) Larch: An Analysis Package for XAFS and Related Spectroscopies. J. Phys.: Conf. Ser. **430**

Nguyen NT, Khan MA, Castro-Guerrero NA, Chia J-C, Vatamaniuk OK, Mari S, Jurisson SS, Mendoza-Cozatl DG (2022) Iron Availability Within the Leaf Vasculature Determines the Magnitude of Iron Deficiency Responses in Source and Sink Tissues in Arabidopsis. Plant and Cell Physiology

Oparka KJ, Duckett CM, Prior DAM, Fisher DB (1994) Real-time imaging of phloem unloading in the root tip of Arabidopsis. The Plant Journal **6:** 759-766

Oparka KJ, Prior DAM, Wright KM (1995) Symplastic communication between primary and developing lateral roots of Arabidopsis thaliana. Journal of Experimental Botany **46:** 187-197

Osawa H, Stacey G, Gassmann W (2006) ScOPT1 and AtOPT4 function as proton-coupled oligopeptide transporters with broad but distinct substrate specificities. Biochemical Journal **393:** 267-275

Pilon M (2017) The copper microRNAs. New Phytologist **213:** 1030-1035

Pottier M, Dumont J, Masclaux-Daubresse C, Thomine S (2019) Autophagy is essential for optimal translocation of iron to seeds in Arabidopsis. Journal of experimental botany **70:** 859-869

Quast C, Pruesse E, Yilmaz P, Gerken J, Schweer T, Yarza P, Peplies J, Glöckner FO (2013) The SILVA ribosomal RNA gene database project: improved data processing and web-based tools. Nucleic Acids Research **41:** 7

Rahmati Ishka M, Chia J-C, Vatamaniuk OK (2022) Chapter 12 - Advances in understanding of copper function and transport in plants. *In* SK Upadhyay, ed, Cation Transporters in Plants. Academic Press, pp 205-226

Rahmati Ishka M, Vatamaniuk OK (2020) Copper deficiency alters shoot architecture and reduces fertility of both gynoecium and androecium in Arabidopsis thaliana. Plant Direct **4:** e00288

Rai S, Singh PK, Mankotia S, Swain J, Satbhai SB (2021) Iron homeostasis in plants and its crosstalk with copper, zinc, and manganese. Plant Stress **1:** 100008

Ravet K, Pilon M (2013) Copper and Iron Homeostasis in Plants: The Challenges of Oxidative Stress. Antioxidants & Redox Signaling **19:** 23

Rees EM, Lee J, Thiele DJ (2004) Mobilization of Intracellular Copper Stores by the Ctr2 Vacuolar Copper Transporter. Journal of Biological Chemistry **279:** 54221-54229

Rellán-Álvarez R, Giner-Martínez-Sierra J, Orduna J, Orera I, Rodríguez-Castrillón JÁ, García-Alonso JI, Abadía J, Álvarez-Fernández A (2009) Identification of a Tri-Iron(III), Tri-Citrate Complex in the Xylem Sap of Iron-Deficient Tomato Resupplied with Iron: New Insights into Plant Iron Long-Distance Transport. Plant and Cell Physiology **51:** 91-102

Rodríguez FI, Esch JJ, Hall AE, Binder BM, Schaller GE, Bleecker AB (1999) A Copper Cofactor for the Ethylene Receptor ETR1 from *Arabidopsis*. Science **283:** 996-998

Rogers EE, Guerinot ML (2002) FRD3, a Member of the Multidrug and Toxin Efflux Family, Controls Iron Deficiency Responses in Arabidopsis. The Plant Cell **14:** 1787-1799

Ross-Elliott TJ, Jensen KH, Haaning KS, Wager BM, Knoblauch J, Howell AH, Mullendore DL, Monteith AG, Paultre D, Yan D, et al. (2017) Phloem unloading in Arabidopsis roots is convective and regulated by the phloem-pole pericycle. eLife **6:** e24125

Schott-Verdugo S, Müller L, Classen E, Gohlke H, Groth G (2019) Structural Model of the ETR1 Ethylene Receptor Transmembrane Sensor Domain. Scientific Reports **9:** 8869

Schwarz B, Bauer P (2020) FIT, a regulatory hub for iron deficiency and stress signaling in roots, and FIT-dependent and -independent gene signatures. J Exp Bot **71:** 1694-1705

Selote D, Samira R, Matthiadis A, Gillikin JW, Long TA (2014) Iron-Binding E3 Ligase Mediates Iron Response in Plants by Targeting Basic Helix-Loop-Helix Transcription Factors Plant Physiology **167:** 273-286

Shaff JE, Schultz BA, Craft EJ, Clark RT, Kochian LV (2010) GEOCHEM-EZ: a chemical speciation program with greater power and flexibility. Plant and Soil **330:** 207-214

Sheng H, Jiang Y, Ishka MR, Chia JC, Dokuchayeva T, Kavulych Y, Zavodna TO, Mendoza PN, Huang R, Smieshka LM, et al. (2021) YSL3-mediated copper distribution is required for fertility, seed size and protein accumulation in Brachypodium. Plant Physiol **186:** 655-676

Solé VA, Papillon E, Cotte M, Walter P, Susini J (2007) A multiplatform code for the analysis of energy-dispersive X-ray fluorescence spectra. Spectrochimica Acta Part B: Atomic Spectroscopy **62:** 63-68

Spielmann J, Vert G (2020) The many facets of protein ubiquitination and degradation in plant root iron-deficiency responses. Journal of Experimental Botany **72:** 2071-2082

Stacey MG, Koh S, Becker J, Stacey G (2002) AtOPT3, a Member of the Oligopeptide Transporter Family, Is Essential for Embryo Development in Arabidopsis. The Plant Cell **14:** 2799-2811

Stacey MG, Patel A, McClain WE, Mathieu M, Remley M, Rogers EE, Gassmann W, Blevins DG, Stacey G (2008) The Arabidopsis AtOPT3 Protein Functions in Metal Homeostasis and Movement of Iron to Developing Seeds. Plant Physiology **146:** 589-601

Trapnell C, Pachter L, Salzberg SL (2009) TopHat: discovering splice junctions with RNA-Seq. Bioinformatics **25:** 7

Tsang T, Posimo JM, Gudiel AA, Cicchini M, Feldser DM, Brady DC (2020) Copper is an essential regulator of the autophagic kinases ULK1/2 to drive lung adenocarcinoma. Nature cell biology **22:** 412-424

Turski ML, Brady DC, Kim HJ, Kim BE, Nose Y, Counter CM, Winge DR, Thiele DJ (2012) A novel role for copper in Ras/mitogen-activated protein kinase signaling. Mol Cell Biol **32:** 1284-1295

Turski ML, Thiele DJ (2009) New roles for copper metabolism in cell proliferation, signaling, and disease. J Biol Chem **284:** 717-721

Vert GA, Briat J-F, Curie C (2003) Dual regulation of the Arabidopsis high-affinity root iron uptake system by local and long-distance signals. Plant physiology **132:** 796-804

Waters BM, Armbrust LC (2013) Optimal copper supply is required for normal plant iron deficiency responses. Plant Signal Behav **8:** e26611

Waters BM, McInturf SA, Amundsen K (2014) Transcriptomic and physiological characterization of the fefe mutant of melon (Cucumis melo) reveals new aspects of iron-copper crosstalk. New Phytol **203:** 1128-1145

Waters BM, McInturf SA, Stein RJ (2012) Rosette iron deficiency transcript and microRNA profiling reveals links between copper and iron homeostasis in Arabidopsis thaliana. J Exp Bot **63:** 5903-5918

Wongkaew A, Asayama K, Kitaiwa T, Nakamura SI, Kojima K, Stacey G, Sekimoto H, Yokoyama T, Ohkama-Ohtsu N (2018) AtOPT6 Protein Functions in Long-Distance Transport of Glutathione in Arabidopsis thaliana. Plant and Cell Physiology **59:** 1443-1451

Wu Y, Zhang D, Chu Jee Y, Boyle P, Wang Y, Brindle Ian D, De Luca V, Després C (2012) The Arabidopsis NPR1 Protein Is a Receptor for the Plant Defense Hormone Salicylic Acid. Cell Reports **1:** 639-647

Yamasaki H, Hayashi M, Fukazawa M, Kobayashi Y, Shikanai T (2009) SQUAMOSA Promoter Binding Protein-Like7 Is a Central Regulator for Copper Homeostasis in *Arabidopsis*. Plant Cell **21:** 347-361

Yan J, Chia J-C, Sheng H, Jung H-i, Zavodna T-O, Zhang L, Huang R, Jiao C, Craft EJ, Fei Z, et al. (2017) Arabidopsis Pollen Fertility Requires the Transcription Factors CITF1 and SPL7 That Regulate Copper Delivery to Anthers and Jasmonic Acid Synthesis. The Plant Cell **29:** 3012-3029

Zhai Z, Gayomba SR, Jung H-I, Vimalakumari NK, Piñeros M, Craft E, Rutzke MA, Danku J, Lahner B, Punshon T, et al. (2014) OPT3 Is a Phloem-Specific Iron Transporter That Is Essential for Systemic Iron Signaling and Redistribution of Iron and Cadmium in Arabidopsis. The Plant cell **26:** 2249-2264

Zhang Z, Xie Q, Jobe TO, Kau AR, Wang C, Li Y, Qiu B, Wang Q, Mendoza-Cózatl DG, Schroeder JI (2016) Identification of AtOPT4 as a Plant Glutathione Transporter. Mol Plant **9:** 481-484

Zhong S, Joung J-G, Zheng Y, Chen Y-r, Liu B, Shao Y, Xiang JZ, Fei Z, Giovannoni JJ (2011) High-Throughput Illumina Strand-Specific RNA Sequencing Library Preparation. Cold Spring Harbor Protocols **2011:** pdb.prot5652

1420 **Figure Legends**

1421

1422 **Figure 1. OPT3 mediates copper loading to the phloem.**

1423 (**A**) Hand-cut cross sections through the petiole of transgenic wild-type plants expressing the
1424 OPT3pro-GFP construct (Zhai et al. 2014). **B** to **E** show 2D XRF maps of the indicated minerals
1425 in mature leaves. **F** to **J** show 2D-CXRF maps of indicated elements in the vasculature of mature
1426 leaf petioles. (**K**) Merged images of calcium (Ca) and indicated elements. Calcium maps show
1427 the overall structures of the vascular tissues, and the majority of copper and iron in the *opt3*
1428 mutant is associated with the xylem and fascicular cambium (**FC**). Plants were grown
1429 hydroponically with 250 nM $CuSO_4$ for 26 days (in **B** to **E**) or five weeks (in **F** to **I**) before
1430 tissues were collected In **B** to **K** bar = 1 mm. Xy, FC and Ph indicate the location of the xylem,
1431 fascicular cambium and the phloem, respectively. **B** to **K** show representative images from three
1432 analyzed plants. Results from two other independent experiments are shown in **Supplemental**
1433 **Figure 1C, D online**).

1434

1435 **Figure 2. The *opt3* mutant accumulates less copper in the phloem sap, roots, young leaves**
1436 **and developing embryos.**

1437 (**A**) The concentration of copper in the phloem sap and the indicated plant tissues of wild type
1438 and the *opt3* mutant. Plants were grown hydroponically under iron and copper sufficient
1439 conditions. Shown values are arithmetic means ± S.E. Asterisks indicate statistically significant
1440 differences from wild type ($p < 0.05$, Student's *t* test, n = 4 independent phloem sap collections).
1441 An independent analysis of copper concentration in the phloem sap is shown in **Supplemental**
1442 **Figure 1E online**. (**B**) ICP-MS analysis of mineral accumulation in dry silique valves collected
1443 from soil-grown plants. Shown values are arithmetic means ± S.E. Asterisks indicate statistically
1444 significant differences from wild type ($p < 0.05$, Student's t test, n = 3 independent experimental
1445 set-ups. In each experimental set-up, tissues from four to five plants grown in the same container
1446 were pooled and represented an independent measurement. Data for the wild type *vs.* the *opt3-2*
1447 allele are shown in **Supplemental Figure 3 online**. (**C**) Fifteen-mm-long developing siliques
1448 were collected from soil-grown plants and subjected to 2D-SXRF analysis. White arrows point to
1449 embryos. A representative image from three independent experiments is shown; results from
1450 another independent experiment are shown in **Supplemental Figure 4A online**.

1451

1452 **Figure 3. OPT3 transports copper in *X. laevis* oocytes and *S. cerevisiae***

1453 (**A**) Copper uptake into X*enopus* oocytes injected with either *OPT3* cRNA (**OPT3**) or water
1454 (**Moc**k). Copper uptake was measured at 3 h. The uptake solution was supplemented with 25 µM
1455 Cu-NA (**Cu-NA**) or 100 µM $CuSO_4$ (**Cu^{2+}**, the final free Cu^{2+} activity in the uptake solution
1456 being estimated to be 35 µM as determined by GEOCHEM-EZ (Shaff et al., 2010)). Presented
1457 values are arithmetic means ± S.E. (n = 5 independent measurements). Asterisks indicate
1458 statistically significant differences (**, $p < 0.01$, using Student's *t*-test). **(B)** Copper
1459 concentration in *S. cerevisiae* wild-type, SEY6210 and its isogenic *ctr1*Δ*2*Δ*3*Δ mutant both
1460 expressing the empty *YES3-Gate* vector (***Wt*** and ***ctrΔ***, respectively) or the *ctr1*Δ*2*Δ*3*Δmutant
1461 expressing *YES3-Gate-OPT3* (***ctrΔ*–OPT3**) all grown with 20 µM $CuSO_4$. Levels not connected
1462 with the same letter are statistically different (n = 4 to 5 independent ICP-MS measurements
1463 [independently grown cells]), Tukey HSD test). (**C**) The wild type and the *ctr1*Δ*2*Δ*3*Δ *S.*
1464 *cerevisiae* mutant transformed with the empty YES3-Gate vector or the *ctr1*Δ*2*Δ*3*Δ transformed
1465 with the vector containing the *OPT3* cDNA or the *A. thaliana* copper transporter, *COPT2*, were
1466 serially 10-fold diluted and spotted onto solid YPEG medium supplemented with different
1467 concentrations of $CuSO_4$. Colonies were visualized after incubating plates for three days at 30°C.
1468 Dilution series are indicated on the right. *S. cerevisiae* lines were designated as in (**B**), except
1469 that ***OPT3-1*** and ***OPT3-2*** designate two distinct *OPT3* expressing clones selected and
1470 propagated after yeast transformation.

1471

1472 **Figure 4. The *opt3* mutant is sensitive to copper deficiency.**

1473 In (**A**) and (**B**), wild type and the *opt3* mutant were grown hydroponically with or without 125
1474 nM $CuSO_4$ (+ Cu or – Cu, respectively). Images were taken after four weeks (**A**) or nine weeks
1475 (**B**) from the seed sowing. (**C**), (**D**) and (**E**) show time to flowering, primary rosette leaf number
1476 and leaf length, respectively. Plants were germinated and grown hydroponically without or with
1477 copper (**0** or **125**, respectively and **white bars**). After four weeks of growth, a subset of plants
1478 grown with or without copper was transferred to 500 nM $CuSO_4$ (**500** and **grey bars**).
1479 Measurements were taken after one week of growth and when plants were eight-week-old. Data
1480 show mean values ± S.E. Levels not connected by the same letter are statistically different
1481 (Tukey HSD, JMP Pro 14 software package, n = 3 to 6 measurements (plants) showing a

1482 representative outcome of at least three independent experiments). Data for the *opt3-2* allele *vs.*
1483 wild type are shown in **Supplemental Figure 6A.** (**F**) shows a representative image of leaves
1484 (from young to old in the direction from left to right) of wild type and the *opt3* mutant, both
1485 grown hydroponically for four weeks with or without copper (**125 nM Cu** or **0 nM Cu**,
1486 respectively). **A**, **B** and **F** show a representative image of plants from three independent
1487 experimental set-ups.
1488

1489 **Figure 5. The *opt3* mutant mounts copper deficiency response in roots and young leaves.**
1490 **(A**) Total number of differentially expressed genes in roots, mature leaves and young leaves of
1491 the *opt3* mutant *vs.* wild type, according to RNA-seq data (ratio >= 1.5 or <=0.67, false-
1492 discovery rate [FDR] < 0.05). Venn diagrams show the number of upregulated (**B**) or
1493 downregulated (**C**) genes in roots, mature and young leaves. Overlaps indicate the number of
1494 genes co-regulated in indicated tissues. Genes associated with iron and copper homeostasis are
1495 shown in (**B**) and (**C**). Genes involved in copper homeostasis are marked in bold; genes
1496 associated with iron and copper deficiency responses are marked in bold and underlined. (**D**) The
1497 expression of the iron transport system is upregulated in the roots of the *opt3* mutant under iron
1498 deficiency. Plants were grown hydroponically for 31 days. A subset of plants was transferred to a
1499 fresh medium without iron. Roots were collected after four days of additional growth with or
1500 without iron. Shown are mean values ± S.E. (n = 3 independent RT-qPCR experiments per
1501 genotype. In each experiment, roots were pooled from four plants grown in one container for
1502 RNA extraction). Asterisks indicate statistically significant differences in gene expression in
1503 wild type grown with or without iron ($p < 0.05$, Student-*t* test). Levels not connected by the same
1504 letter are statistically different ($p < 0.05$; Tukey HSD, JMP Pro 14 software package.
1505

1506 **Figure 6. The expression of copper micro-RNA genes is upregulated in the *opt3* mutant.**
1507 **(A)** shows the transcript abundance of *miRNA397a/b*, *miR857a*, *miR39b/c*, and *miR408* in roots
1508 of 5-week-old wild type (open bars) or the *opt3* mutant (black bars) grown hydroponically with
1509 125 nM $CuSO_4$. Shown are mean values ± S.E. Asterisks indicate statistically significant
1510 differences from the expression of genes in wild type, set to one ($p < 0.05$, Student-*t* test, n = 4
1511 independent RT-qPCR experiments per genotype. In each experiment, roots were pooled from
1512 four plants grown in one container for RNA extraction). (**B**) Expression of *OPT3*, *IRT1* and

1513 *CITF1* in roots of wild type subjected to one or four days under copper deficiency. *CITF1* was
1514 used as a marker of copper deficiency to validate treatment efficiency. Shown are mean values ±
1515 S.E. Levels not connected by the same letter are statistically different ($p < 0.05$; Tukey HSD,
1516 JMP Pro 14 software package, n = 4 independent RT-qPCR experiments per condition. In each
1517 experiment, roots were pooled from four plants grown in one container for RNA extraction.
1518

1519 **Figure 7. Copper supplementation partially rescues the molecular symptoms of copper**
1520 **deficiency in roots of the *opt3* mutant.**

1521 Plants were grown hydroponically under control conditions (**white bars**) until the late-vegetative
1522 stage before a subset of plants was transferred to a fresh medium with higher copper
1523 concentrations (250 nM $CuSO_4$, **light grey bars** in **A, B, E, F, J, K** or 500 nM $CuSO_4$, **dark**
1524 **grey bars** in **C, D, G, H, L, M**). Plants were grown for another week before tissue collection and
1525 RT-qPCR analysis. The transcript abundance of indicated genes was normalized to the wild type
1526 grown under control conditions. Data show mean values ± S.E. Levels not connected by the
1527 same letter are statistically different (Tukey HSD, JMP Pro 14 software package, n= 3 RT-qPCR
1528 experiments per genotype. In each experiment, roots were pooled from three plants grown in one
1529 container for RNA extraction. Data are normalized to the expression of *Actin2*; the expression of
1530 genes in wild type grown under 125 nM $CuSO_4$ (control conditions) was set to one.
1531

1532 **Figure 8. The OPT3 function in the shoot controls the expression of copper deficiency**
1533 **markers.**

1534 The transcript abundance of copper- (**A**) and iron-deficiency (**B**) markers in roots of grafted
1535 plants. Wild type and the *opt3* mutant were used for reciprocal grafting. **Wt*S*/Wt*R*,** wild type
1536 scion grafted to wild type rootstock (control); ***opt3S/opt3R***, *opt3* scion grafted to *opt3* rootstock;
1537 **Wt*S*/opt3*R***, wild type scion grafted to *opt3* rootstock; ***opt3S/WtR***, *opt3* scion grafted to wild
1538 type rootstock. Shown values represent means ± S.E. (n = 4 independent experiments [PCR runs,
1539 each representing an independent experimental setup]; roots were pooled from four plants per
1540 experimental set-up). Levels not connected by the same letter are statistically different ($p < 0.05$;
1541 Tukey HSD, JMP Pro 14 software package). Data are normalized to the expression of *Actin2*; the
1542 expression of genes in wild type was set to one.
1543

1544 **Figure 9. Copper or iron feeding *via* the phloem in the shoot represses the molecular**
1545 **symptoms of copper and iron deficiency in the root of the wild type and the *opt3* mutant.**
1546 RT-qPCR analysis of copper and iron deficiency molecular markers in roots of the 33-day-old
1547 wild type (**A, B**) or the *opt3* mutant (**C, D**). Wild type plants were grown hydroponically and
1548 subjected to either iron or copper deficiency (**A** and **B**, respectively). The *opt3* mutant was grown
1549 hydroponically in copper and iron sufficient conditions (**C**, **D**). Roots were collected after 24h of
1550 phloem feeding with iron (**Fe**, black bars) or copper (**Cu**, grey bars) or control feeding (**mock**,
1551 open bars). Mock treatment for copper feeding was MiliQ water, and mock treatment for iron
1552 feeding was citrate. Asterisks indicate statistically significant differences from the expression of
1553 genes in mock-fed plants, set to one ($p < 0.05$, Student-*t* test, n = 4 [PCR runs, each representing
1554 an independent experimental set up]; roots were pooled from four plants per each experimental
1555 set-up). Data are normalized to the expression of *Actin2*; the expression of genes in a mock-
1556 treated wild type (**A**, **B**) or a mock-treated *opt3* mutant (**C**, **D**) was set to one.
1557

1558 **Figure 10. Copper and iron deficiency applied simultaneously increases the expression of**
1559 ***CITF1*, *copper miRNAs* and *FIT*.**
1560 (**A**) Transcript abundance of *CITF1* and indicated *copper miRNAs* and the *FIT* was analyzed in
1561 roots of plants grown under control conditions (**Ctr**) or without cooper but with iron (**–Cu**) for
1562 four weeks before tissue collection. To achieve iron deficiency, plants were grown under control
1563 conditions for three weeks, transferred to a solution without iron and grown for one additional
1564 week (**–Fe**). For the simultaneous iron and copper deficiency treatment, plants were grown
1565 without copper but with iron for three weeks and then transferred to a fresh hydroponic medium
1566 lacking both copper and iron. Tissues were collected and analyzed after an additional week of
1567 growth (**–Cu –Fe**). (**B**) Transcript abundance of indicated genes in roots of wild type grown
1568 under simultaneous copper and iron deficiency after phloem feeding with copper (**Cu**, grey bars)
1569 or control feeding (**mock**, open bars). (**C**) Transcript abundance of indicated genes in roots of
1570 wild type grown under simultaneous copper and iron deficiency after phloem feeding with iron
1571 (**Fe**, black bars or control feeding (**mock**, open bars). Mock treatment for copper feeding was
1572 MiliQ water, and mock treatment for iron feeding was citrate. In (**A**), (**B**) and (**C**), mean values ±
1573 S.E are shown. Levels not connected by the same letter are statistically different (Tukey HSD,
1574 JMP Pro 14 software package, n = 3 to 4 independent experiments (PCR runs, representing an

1575 independent experimental set-up where roots were pooled from three plants per experiment).
1576 Data are normalized to the expression of *Actin2*; the expression of genes in wild type grown
1577 under control conditions (**A**) or mock-treated wild type (**B, C**) was set to one.
1578
1579 **Figure 11. Copper and iron availability in the medium influence each other's uptake and**
1580 **accumulation in roots and shoot of *A. thaliana*.**
1581 (**A**) Iron concentration in roots and shoots of *A. thaliana* grown for five weeks in the control
1582 condition (**Ctr**), copper deficiency (**−Cu**), iron deficiency (**−Fe**), and simultaneous copper and
1583 iron deficiency (**−Cu −Fe**). Data are mean values ± S.E. Levels not connected by the same letter
1584 are statistically different (Tukey HSD, JMP Pro 14 software package, n = 3 to 5 independent
1585 ICP-MS measurements, each representing an independent experimental set-up; roots and shoots
1586 were pooled from four plants per each experimental set-up to obtain one measurement. (**B**)
1587 Copper concentration in roots and shoots of *A. thaliana,* grown for five weeks in the control
1588 condition (**10 µM Fe)** or with high iron (**50 µM Fe**). Mean values ± S.E is obtained with n = 5
1589 ICP-MS measurements from two batches of independently grown plants per condition. Tissues
1590 from four plants were pooled for each measurement. Asterisks indicate statistically significant
1591 differences ($p < 0.05$, Student-*t* test).
1592
1593 **Figure 12. AtOPT3-facilitated Copper and Iron Transport to the Phloem Companion Cells**
1594 **Mediates Iron-Copper Crosstalk in Shoot-to-Root Signaling.**
1595 (**A**) AtOPT3 mediates iron and copper loading to the phloem companion cells for the distribution
1596 to sink organs, including roots. Phloem-mobile iron and/or copper represses the expression of
1597 iron and copper uptake systems, either acting directly as a repressor or indirectly by sequestering
1598 or inhibiting the synthesis of a promotive signal. (**B**) Iron deficiency in the outside medium
1599 stimulates copper accumulation in roots and leaves (Waters et al., 2012; Waters and Armbrust,
1600 2013; Waters et al., 2014) and **Figure 11A**. Under these circumstances, AtOPT3 loads mainly
1601 copper to the phloem in the shoot. The concentration of iron in the phloem decreases, which
1602 causes the upregulation of the expression of the iron uptake system. Copper availability in the
1603 phloem, provided by the AtOPT3, fine tunes the expression of iron transport genes to avoid iron
1604 overload observed in the *opt3* mutant. The repressive role of copper on the expression of copper
1605 and iron uptake system can occur directly or indirectly *via* scavenging or inhibiting the

production of a promotive signal. A similar scenario occurs under copper deficiency, where OPT3 mainly loads iron to fine-tune the expression of copper uptake genes (**C**). Simultaneous iron and copper deficiencies in the outside medium autonomously upregulate the expression of both copper and iron uptake genes as both elements are less available in the phloem sap (**D**). The scenario is different in the *opt3* mutant (**E**): although both iron and copper are available in the outside medium, the *opt3* mutant experiences simultaneous iron and copper deficiency in the phloem. Low iron accumulation in the phloem stimulates transcriptional iron deficiency response, overriding local iron sufficiency response. Since iron is available in the outside medium, iron accumulates in the *opt3* mutant. Copper deficiency in the phloem, roots and leaves also leads to iron accumulation and transcriptional copper deficiency response. Increased iron accumulation from both pathways, in turn, decreases copper uptake, as shown in (**Figure 11B**) and documented in animal species (Klevay, 2001; Ha et al., 2016), further altering Fe-Cu crosstalk. Figure created in Biorender.com

Supplemental Figure S1 (Supports Figs. 1 and 2). Copper and iron maps and copper accumulation in the phloem exudates of wild type and the *opt3-3* mutant.

(**A**) and (**B**) show the representative leaves used for 2D-XRF analysis. Plants were grown hydroponically with 250 nM $CuSO_4$ for 22 days before 2D-XRF analysis. Numbers indicate the order of leaf from the oldest to the youngest. Red arrows indicate the fourth oldest true leaves that were analyzed in Figure 1. (**C**) and (**D**) show the 2D-XRF mapping of the 1st true leaf (**C**) and the 6th true leaf (**D**) of the wild type (***Wt***) and the *opt3* mutant (***opt3***) grown hydroponically with 250 nM Cu for 24-26 days. Bars = 1 mm. (**E**) ICP-MS analysis of the phloem sap collected from the wild-type and the *opt3* mutant. A minimum of ten individual phloem sap collections per genotype were performed. Plants were grown and phloem sap was collected as described in (Kumar et al., 2017).

Supplemental Figure S2 (Supports Fig. 2). The *opt3-3* mutant accumulates a high concentration of metals in vegetative tissues.

Plants were grown hydroponically with 125 nM (**A**) or 250 nM $CuSO_4$ (**B**) for 30 days before tissue collection for ICP-MS analysis. Shown values are arithmetic means ± S.E. Asterisks indicated statistically significant differences from wild type ($p < 0.05$, Student's t test, n = 3

independent experimental set-ups. In each experimental set-up, tissues from four to five plants grown in the same container were pooled and represented an independent measurement.

Supplemental Figure S3 (Supports Fig. 2). The *opt3-2* mutant accumulates less copper in roots and young leaves.

Plants were grown hydroponically with 125 nM $CuSO_4$ (**B**) for 30 days before tissue collection for ICP-MS analysis. Shown values are arithmetic means ± S.E. Asterisks indicated statistically significant differences from wild type ($p < 0.05$, Student's *t* test, n = 3 independent measurements. In each measurement, tissues were pooled from four to five plants grown in the same container).

Supplemental Figure S4 (Supports Fig. 2). OPT3 mediates copper and iron accumulation in developing embryos.

(A) Fifteen-mm-long developing siliques were collected from soil-grown plants and subjected to 2D-SXRF analysis. (**B**) Dry seeds collected from soil-grown wild-type and the *opt3-3* mutant were subjected to 2D CT-XRF. Blue arrows point to the vasculature, blue boxes to regions in the seed coat with contrasting copper accumulation. A representative image of at least three scanned specimens is shown. (**C**) ICP-MS analysis in seeds of wild type and the *opt3-3* mutant. Shown values are arithmetic means ± S.E. Asterisks indicate statistically significant differences from wild type ($p < 0.05$, Student's *t* test, n = 3 independent experimental set-ups. In each set-up, tissues were pooled from four to five plants to yield one ICP-MS measurement).

Supplemental Figure S5 (Supports Fig 3A). Cellular integrity of mock and OPT3-expressing oocytes in control or copper-containing solutions.

Cells were (**A**) exposed to a bath media containing 100 μM $CuSO_4$ for 3 hours and subsequently washed and allowed to recover in a bath media lacking copper for the remaining 21 hours, or (**B**) continuously exposed to a bath media containing 50 μM $CuSO_4$ during 24 hours. Cell integrity was monitored by measuring the cell's membrane potentials (bottom panel) and changes in morphological characteristics (top panel) over 24 hours at the end of the 3, 9, and 24 h time intervals denoted above each panel. Copper-induced cellular damage was visually evidenced by an early blotchiness of the dark pigment in the animal hemisphere and eventual complete

discoloration of the cell, predominantly in OPT3 expressing cells. Survival rates (middle row pane) were calculated as the % of damaged-looking cells at a given time point. Resting membrane potentials were measured in at least 4 different cells for each group at each given time point and were recorded as described previously (Zhai et al., 2014). Data for mock and OPT3-expressing cells exposed to copper treatment are color-coded blue and red, respectively. Mock and OPT3-expressing cells maintained in bath media lacking copper for the entire 24 hours of the experiment (labelled as non-treated) are color-coded black and grey, respectively.

Supplemental Figure S6 (Supports Fig. 4). Seedlings of the *opt3* mutant are sensitive to copper deficiency.

(**A**) A representative image of increased sensitivity of the *opt3-2* mutant allele to copper deficiency. Plants were grown hydroponically with or without copper supplements for 35 days. (**B**) to (**E**) The *opt3-3* mutant and wild type were grown on ½ MS solid medium with or without 250 µM or 500 µM of a copper chelator BCS. (**B**) shows a representative image of plants after ten days of growth, after which root length (**C**), fresh weight (**D**) and cupric reductase activity (**E**) were analyzed. In **C** to **E** data are means ± S.E. Levels not connected by the same letter are significantly different ($p < 0.05$, Tukey-Kramer HSD test). In **C**, three independent experiments were performed with 30 plants per genotype analyzed per experiment (n = 90); in **D,** n = 3 independent experiments with 30 to 40 seedlings pooled for analyses in each experiment; in **E**, n = 3 independent experiments with 20 seedlings analyzed in each experiment.

Supplemental Figure S7 (Supports Fig. 4). Transferring the *opt3-3* mutant to high copper rescues its growth.

(**A**) Wild type and the *opt3* mutant were germinated and grown hydroponically at 125 nM Cu for four weeks before transferring to a fresh hydroponic medium with 500 nM (**A**) or 250 nM (**B**) copper. Images were taken after one week of growth. A representative set-up/result from three independent experiments is shown.

Supplemental Figure S8 (Supports Fig. 5). The *opt3* mutant accumulates IRT1 protein in roots under Fe sufficient growth conditions.

1698 (**A**) Western blots analysis of IRT1 protein accumulation in roots of wild type and the *opt3-3*
1699 mutant. Plants were grown hydroponically with 125 nM $CuSO_4$ and 10 mM Fe-HBED for four
1700 weeks before tissue collection. (**B**) Western blots analysis of iron deficiency-induced IRT1
1701 accumulation in wild type roots. Plants were grown hydroponically with 125 nM $CuSO_4$ and 10
1702 µM Fe-HBED for three weeks and then transferred to a fresh medium without iron. Roots were
1703 collected after one week of growth under iron deficiency. The *fit-2* mutant was incorporated as a
1704 negative control for the IRT1 protein accumulation. In (**A**) and (**B**), the IRT1 signals are
1705 recognized by the antibody at 35 kD while actin (protein loading control) at 45 kD. For the
1706 immunodetection of actin epitope, the nitrocellulose blots were probed with the primary mouse-
1707 monoclonal anti-actin antibody (1:5,000 dilution, Sigma-Aldrich) and secondary, an HRP-
1708 conjugated goat-antimouse IgG antibody (1:10,000 Rockland Immunochemicals). In both cases,
1709 immunoreactive bands were visualized with Clarity Max ECL blotting substrates (BIORAD).
1710

1711 **Supplemental Figure 9 (Supports Fig. 9). Phloem feeding with carboxyfluorescein diacetate**
1712 **succinimidyl ester (CFDA) in leaves of wild type *Arabidopsis thaliana.***
1713 (**A**) The illustration of phloem feeding procedures as described in Materials and Methods. (**B)**
1714 Shows a representative image of carboxyfluorescein (**CF**)-mediated fluorescence and brightfield
1715 images of the root after feeding 10 mM CFDA *via* the phloem in the shoot. (**C**) Shows
1716 autofluorescence of mock-fed plants (**Buffer**). (**D**) shows that iron but not mock feeding via the
1717 phloem in the shoot of iron-deficient wild type eliminates degreening of young leaves (indicated
1718 by white arrows). In all cases, experiments were repeated at least three times with at least three
1719 planst analyzed per each experiment.
1720

1721 **Supplemental Figure 10 (Supports Fig. 11). Iron availability in the medium influence the**
1722 **expression of copper deficiency responsive genes in the roots of *A. thaliana.***
1723 (**A**) Shows a representative phenotype of *A. thaliana* grown hydroponically with 10 µM or 50
1724 µM FeHBED for five weeks. Twelve plants per condition were analysed in total in three
1725 independent experiments. (**B**) The accumulation of iron in roots and shoots of plants grown as in
1726 (**A**). Mean values ± S.E (n = 5 ICP-MS measurements obtained from two batches of
1727 independently grown plants per condition. Tissues from four plants were pooled for each
1728 measurement). Asterisks indicate statistically significant differences ($p < 0.05$, Student-*t* test).

1729 **Table 1.** Average day from the date of sawing to flowering in wild type and the *opt3-3* mutant grown
1730 hydroponically with 0 or 125 nM $CuSO_4$. A subset of plants was shifted to 500 nM copper[1].

	Cu concentrations, nM			
Genotype	**0**	**0 to 500**	**125**	**125 to 500**
Wild type (Col-0)	46.83 ± 2.86	40.17 ± 0.79	42.33 ± 0.76	41.80 ± 1.24
opt3-3 (Col-0)	N.A.[2]	48 ± 1.78	N.A.[2]	48.4 ± 1.80

1731 [1] data showing average ± standard errors (n = 3 to 6)
1732 [2] NA; not applicable. The mutant did not flower during the course of measurements which ranged from
1733 week 5 to week 8.
1734

1735 **Table 2. Expression of copper deficiency-responsive genes in roots, mature leaves and young leaves**
1736 **of the *opt3-3* mutant.** Upregulated or downregulated genes are shown in red or blue bold font,
1737 respectively, and marked with asterisks (ratio >= 1.5 or <=0.67, [FDR] < 0.05).
1738

AGI ID	Gene	Short description	RPKM*						Ratio (*opt3-3*/wt)			Ratio (*YL vs ML*†)	
			*opt3*_R†	wt_R†	*opt3*_ML†	wt_ML†	*opt3*_YL†	wt_YL†	R†	ML†	YL†	Wt	opt3
AT5G59030	*COPT1*	Cu transporter 1	7.28	3.46	164.42	98.92	68.26	60.38	2.1	**1.7***	1.1	**0.6***	**0.4***
AT3G46900	*COPT2*	Cu transporter 2	183.29	46.13	1.57	1.96	0.36	0.11	**4.0***	0.8	3.3	**0.1***	**0.2***
AT2G26975	*COPT6*	Cu transporter 6	0.3	0.28	38.02	26.09	16.48	17.73	1.1	1.5	0.9	0.7*	**0.4***
AT4G24120	*YSL1*	YELLOW STRIPE like 1	0.15	0.35	10.39	3.32	4.33	2.54	0.4	**3.1***	**1.7***	0.8	**0.4***
AT5G24380	*YSL2*	YELLOW STRIPE like 2	19.19	10.3	1.47	0.97	1.31	0.47	**1.9***	0.7	**2.8***	**0.5***	0.9
AT5G53550	*YSL3*	YELLOW STRIPE like 3	19.26	20.51	20.96	11.63	8.17	8.56	0.9	**1.8***	1.0	0.7*	**0.4***
AT5G23980	*FRO4*	Ferric reduction oxidase 4	221.4	103.4	5.6	8.7	0.6	0.8	**2.1***	0.7	0.7	**0.1***	**0.1***
AT5G23990	*FRO5*	Ferric reduction oxidase 5	326.7	39.5	0.5	0.7	0.1	0.0	**8.3***	0.8	NA	**0.2***	**0.1***
AT1G71200	*CITF1*	Cu-inducible transcription factor 1	9.6	1.5	0.0	0.0	0.0	0.0	**6.6***	NA	NA	1.0	0.3
AT1G08830	*CSD1*	Cu/Zn superoxide dismutase 1	100.0	243.4	69.3	102.0	28.2	181.1	**0.4***	0.7	**0.2***	1.8	**0.4***
AT2G28190	*CSD2*	Cu/Zn superoxide dismutase 2	72.7	123.3	68.8	151.0	138.6	452.8	**0.6***	0.5	**0.3***	**3.0***	2.0
AT2G02850	*ARPN*	Plantacyanin; copper ion binding protein	17.9	19.6	0.7	0.7	2.2	6.5	0.9	1.0	**0.3***	**9.8***	**3.3***
AT5G20230	*BCB*	Blue copper binding protein	1.4	3.6	258.6	325.8	41.3	110.8	**0.4***	0.8	0.4	**0.3***	**0.2***
AT1G12520	*CCS1*	Cu chaperone for superoxide dismutase 1	32.7	55.8	18.6	20.9	12.5	39.4	**0.6***	0.9	**0.3***	1.9	**0.7***
AT2G44790	*UCC2*	UCLACYANIN 2; Cu ion binding protein	1068.8	1418.9	4.5	1.9	1.3	4.4	0.8*	**2.4***	**0.3***	2.3	**0.3***
AT4G25100	*FSD1*	Fe superoxide dismutase 1	331.9	120.9	807.2	584.7	681.3	264.0	**2.7***	1.4	**2.6***	**0.5***	0.8*
AT3G56240	*CCH*	CCH (Cu chaperone)	242.96	171.84	103.78	96.9	42.55	39.82	1.4*	1.1	1.1	**0.4***	**0.4***
AT1G71040	*LPR2*	LPR2 (Low Phosphate Root2); Cu ion binding	30.11	30.98	102.9	83.53	35.62	43.25	1.0	1.2	0.8	**0.5***	**0.4***
AT2G07687		Cytochrome *c* oxidase subunit 3	1.14	2.26	1.03	1.29	0.26	0.7	0.5	0.8	0.4	0.5	**0.3***
AT1G18140	*LAC1*	LAC1 (Laccase 1); copper ion binding /oxidoreductase	2.44	2.92	0.03	0.01	0.39	0.98	0.8	NA	0.4	**98***	**14.6***
AT2G29130	*LAC2*	LAC2 (Laccase 2); Cu ion binding /oxidoreductase	22.42	28.28	0.06	0.3	0.44	0.95	0.8	0.2	0.5	3.2	**7.4***
AT2G46570	*LAC6*	LAC6 (Laccase 6); Cu ion binding /oxidoreductase	2.57	2.55	0.7	0.38	3.23	3.15	1.0	1.8	1.0	**8.2***	**4.6***

1739 *RPKM stands for Reads Per Kilobase of transcript per Million mapped reads. Asterisks (*, $P < 0.05$)
1740 indicate transcript levels that are significantly different between wild type and *opt3-3* mutant.
1741 †R, roots; ML, mature leaves, YL, young leaves.

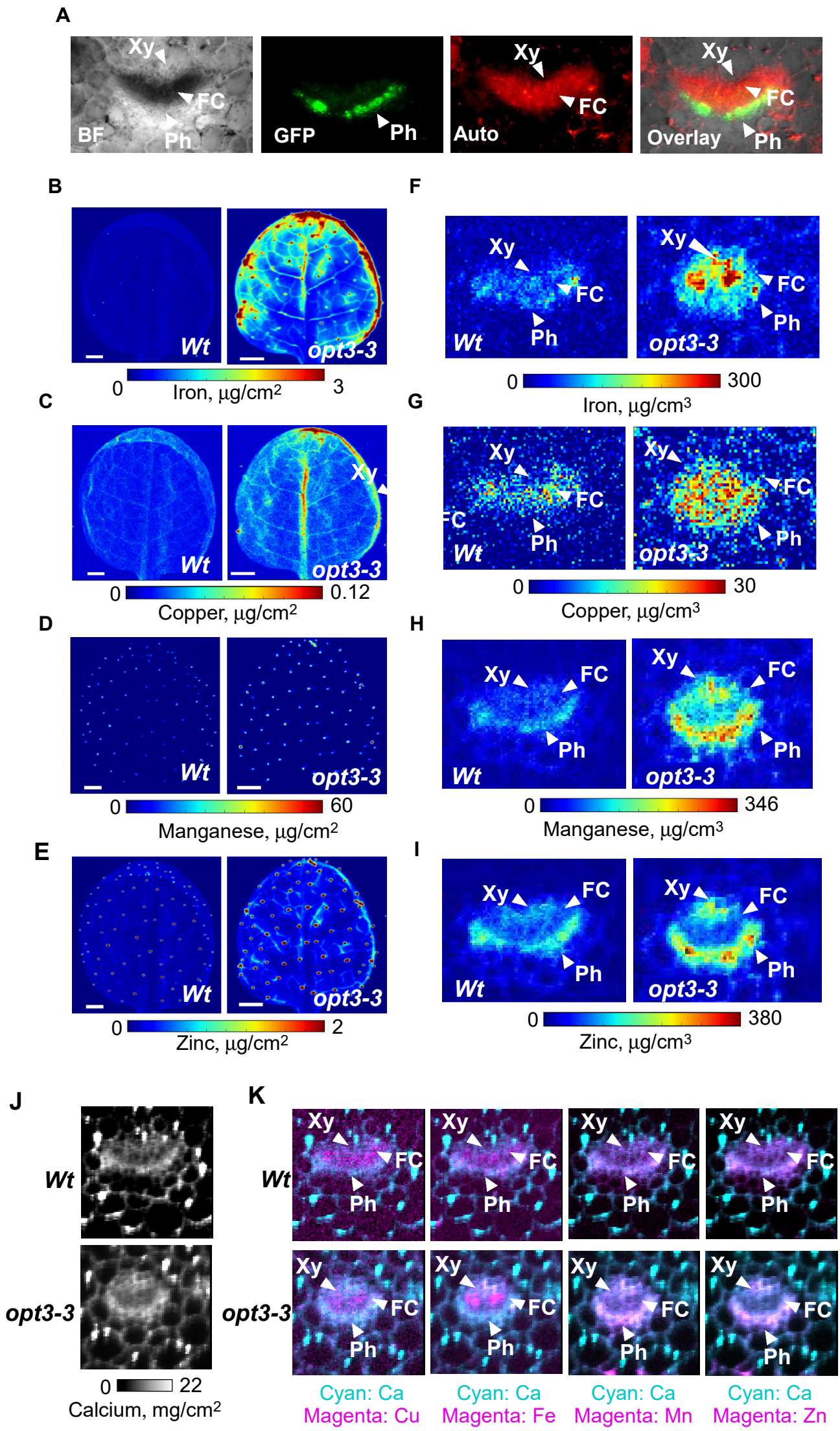

Figure 1. OPT3 mediates copper loading to the phloem.

(**A**) Hand-cut cross sections through the petiole of transgenic wild-type plants expressing the OPT3pro-GFP construct (Zhai et al. 2014). **B** to **E** show 2D XRF maps of the indicated minerals in mature leaves. **F** to **J** show 2D-CXRF maps of indicated elements in the vasculature of mature leaf petioles. (**K**) Merged images of calcium (Ca) and indicated elements. Calcium maps show the overall structures of the vascular tissues, and the majority of copper and iron in the *opt3* mutant is associated with the xylem and fascicular cambium (**FC**). Plants were grown hydroponically with 250 nM $CuSO_4$ for 26 days (in **B** to **E**) or five weeks (in **F** to **I**) before tissues were collected In **B** to **K** bar = 1 mm. Xy, FC and Ph indicate the location of the xylem, fascicular cambium and the phloem, respectively. **B** to **K** show representative images from three analyzed plants. Results from two other independent experiments are shown in **Supplemental Figure 1C, D online**).

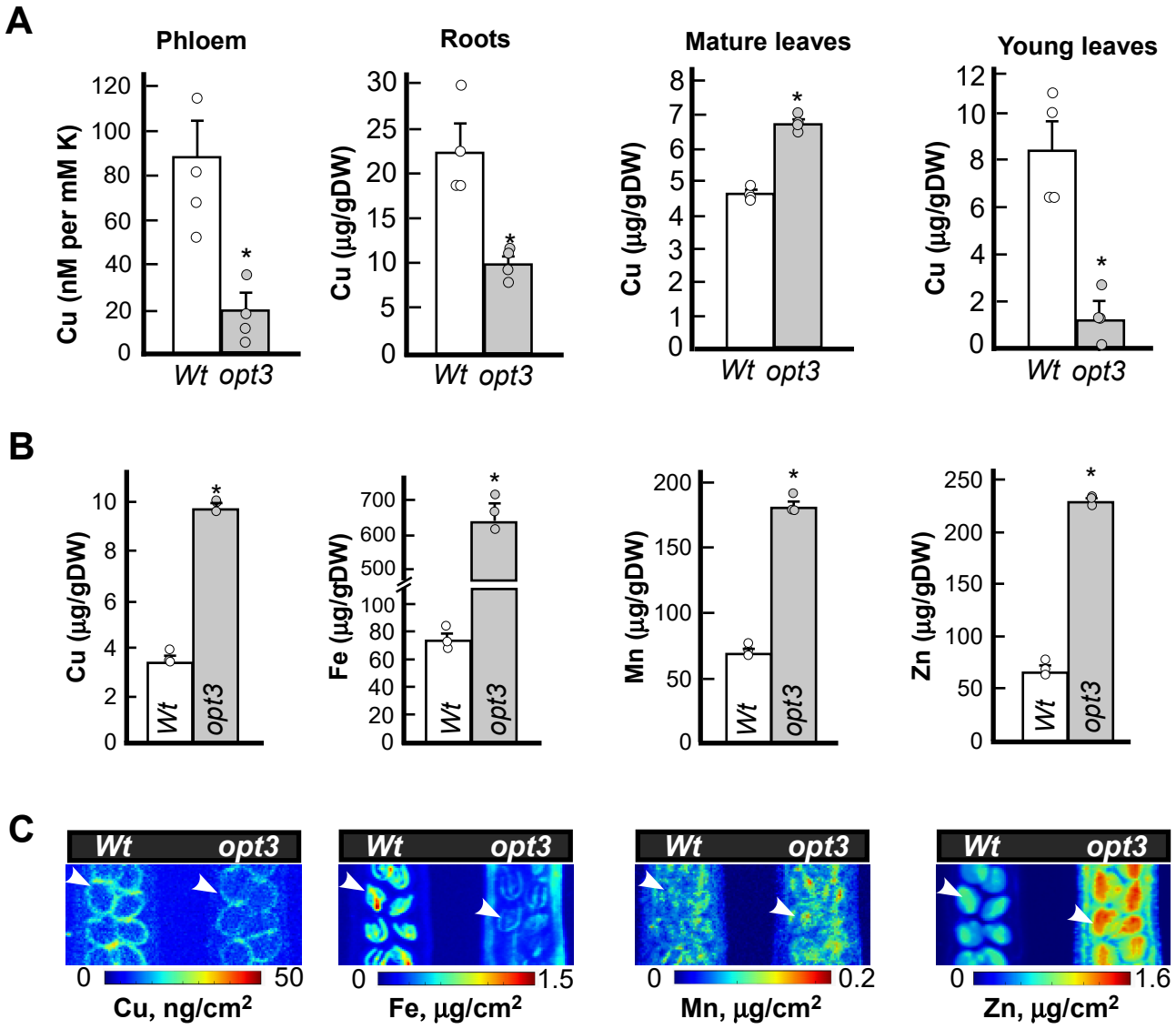

Figure 2. The *opt3* mutant accumulates less copper in the phloem sap, roots, young leaves and developing embryos. (**A**) The concentration of copper in the phloem sap and the indicated plant tissues of wild type and the *opt3* mutant. Plants were grown hydroponically under iron and copper sufficient conditions. Shown values are arithmetic means ± S.E. Asterisks indicate statistically significant differences from wild type ($p < 0.05$, Student's *t* test, n = 4 independent phloem sap collections). An independent analysis of copper concentration in the phloem sap is shown in **Supplemental Figure 1E online**. (**B**) ICP-MS analysis of mineral accumulation in dry silique valves collected from soil-grown plants. Shown values are arithmetic means ± S.E. Asterisks indicate statistically significant differences from wild type ($p < 0.05$, Student's t test, n = 3 independent experimental set-ups. In each experimental set-up, tissues from four to five plants grown in the same container were pooled and represented an independent measurement. Data for the wild type *vs.* the *opt3-2* allele are shown in **Supplemental Figure 3 online**. (**C**) Fifteen-mm-long developing siliques were collected from soil-grown plants and subjected to 2D-SXRF analysis. White arrows point to embryos. A representative image from three independent experiments is shown; results from another independent experiment are shown in **Supplemental Figure 4A online**.

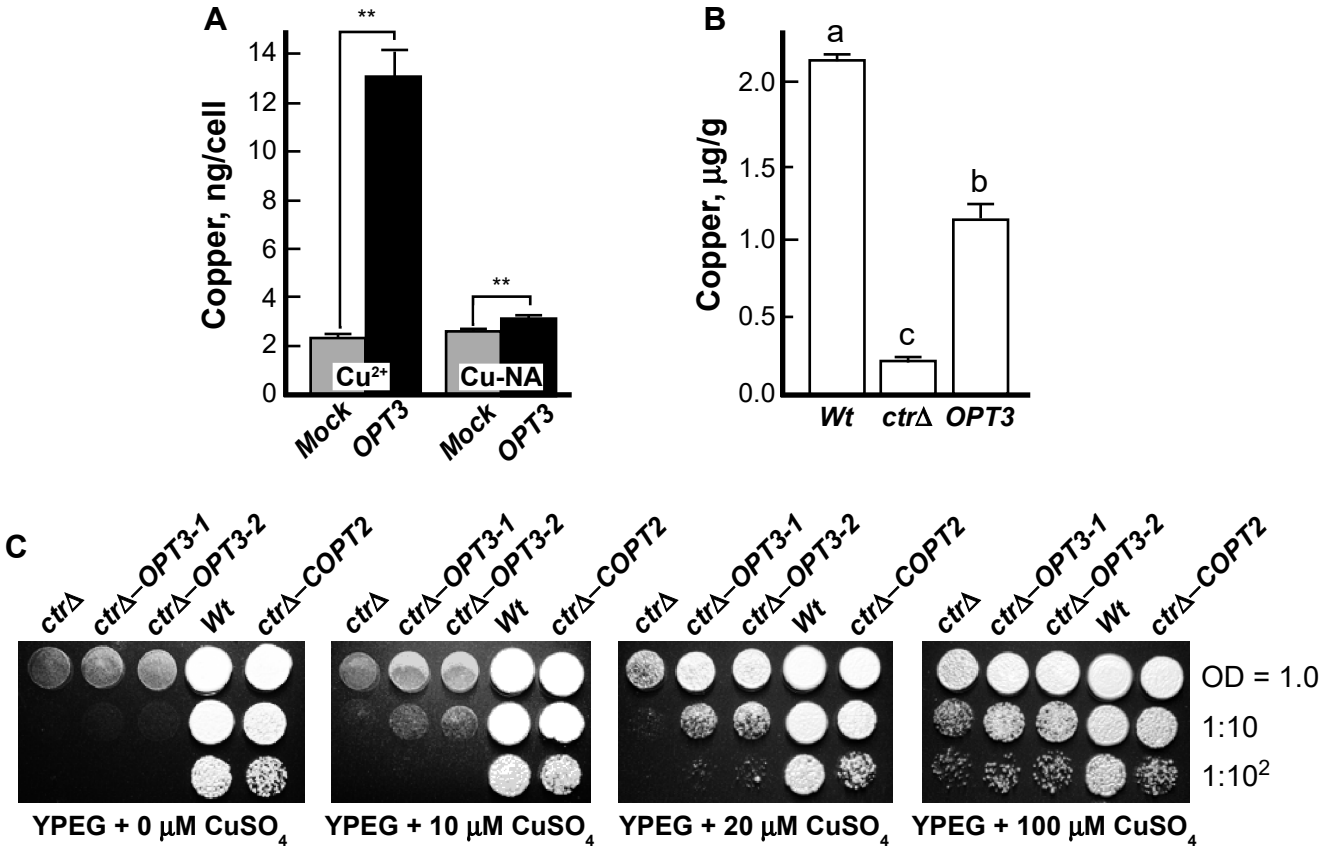

Figure 3. OPT3 transports copper in *X. laevis* oocytes and *S. cerevisiae*

(**A**) Copper uptake into X*enopus* oocytes injected with either *OPT3* cRNA (**OPT3**) or water (**Moc**k). Copper uptake was measured at 3 h. The uptake solution was supplemented with 25 µM Cu-NA (**Cu-NA**) or 100 µM $CuSO_4$ (**Cu^{2+}**, the final free Cu^{2+} activity in the uptake solution being estimated to be 35 µM as determined by GEOCHEM-EZ (Shaff et al., 2010)). Presented values are arithmetic means ± S.E. (n = 5 independent measurements). Asterisks indicate statistically significant differences (**, $p < 0.01$, using Student's *t*-test). **(B)** Copper concentration in *S. cerevisiae* wild-type, SEY6210 and its isogenic *ctr1*Δ*2*Δ*3*Δ mutant both expressing the empty *YES3-Gate* vector (***Wt*** and ***ctr*Δ**, respectively) or the *ctr1*Δ*2*Δ*3*Δ mutant expressing *YES3-Gate-OPT3* (***ctr*Δ–OPT3**) all grown with 20 µM $CuSO_4$. Levels not connected with the same letter are statistically different (n = 4 to 5 independent ICP-MS measurements [independently grown cells]), $p < 0.05$, Tukey HSD test). (**C**) The wild type and the *ctr1*Δ*2*Δ*3*Δ *S. cerevisiae* mutant transformed with the empty YES3-Gate vector or the *ctr1*Δ*2*Δ*3*Δ transformed with the vector containing the *OPT3* cDNA or the *A. thaliana* copper transporter, *COPT2*, were serially 10-fold diluted and spotted onto solid YPEG medium supplemented with different concentrations of $CuSO_4$. Colonies were visualized after incubating plates for three days at 30°C. Dilution series are indicated on the right. *S. cerevisiae* lines were designated as in (**B**), except that ***OPT3-1*** and ***OPT3-2*** designate two distinct *OPT3* expressing clones selected and propagated after yeast transformation.

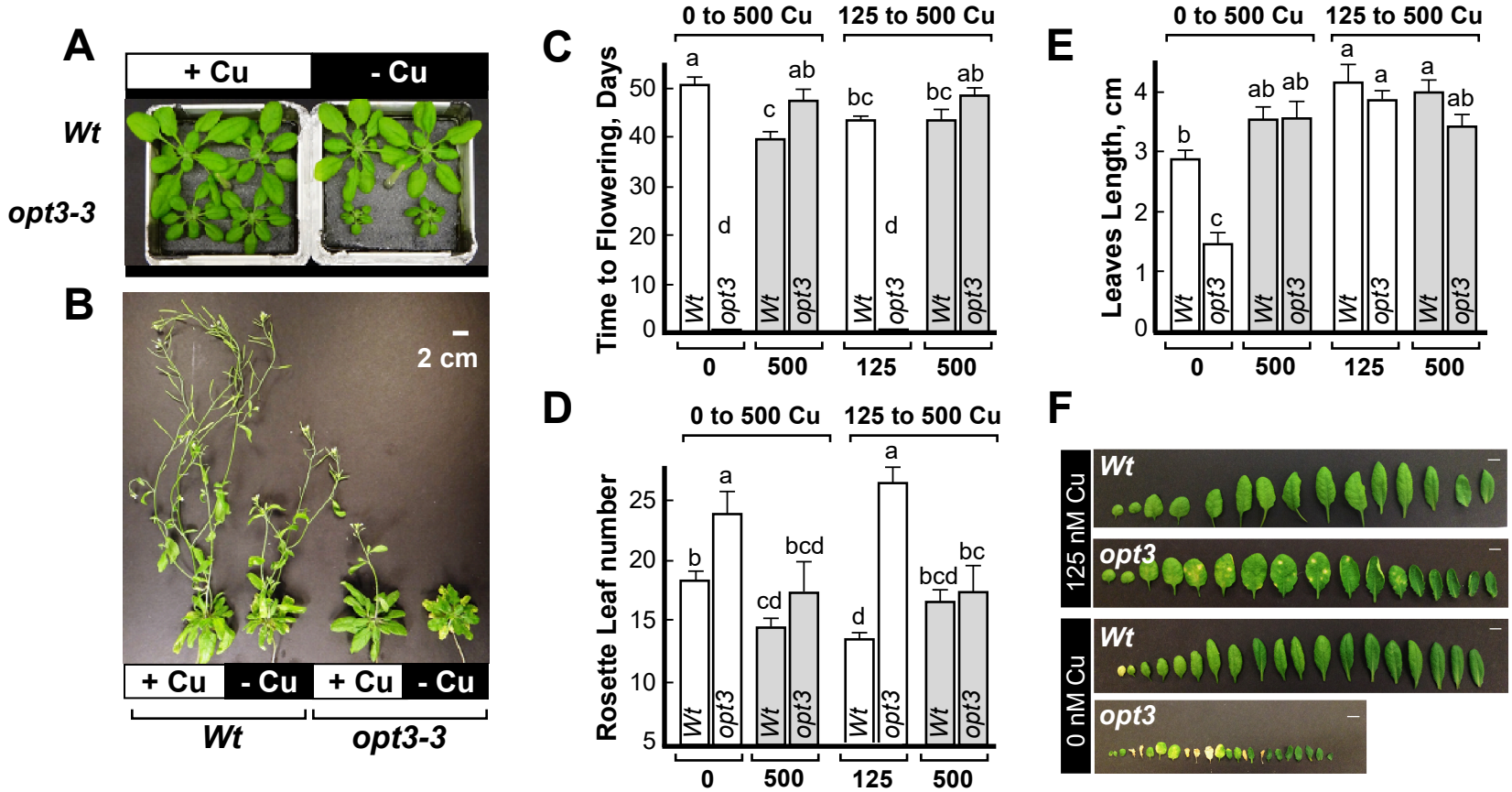

Figure 4. The *opt3* mutant is sensitive to copper deficiency.

In (**A**) and (**B**), wild type and the *opt3* mutant were grown hydroponically with or without 125 nM $CuSO_4$ (+ Cu or – Cu, respectively). Images were taken after four weeks (**A**) or nine weeks (**B**) from the seed sowing. (**C**), (**D**) and (**E**) show time to flowering, primary rosette leaf number and leaf length, respectively. Plants were germinated and grown hydroponically without or with copper (**0** or **125**, respectively and **white bars**). After four weeks of growth, a subset of plants grown with or without copper was transferred to 500 nM $CuSO_4$ (**500** and **grey bars**). Measurements were taken after one week of growth and when plants were eight-week-old. Data show mean values ± S.E. Levels not connected by the same letter are statistically different (Tukey HSD, JMP Pro 14 software package, n = 3 to 6 measurements (plants) showing a representative outcome of at least three independent experiments). Data for the *opt3-2* allele *vs.* wild type are shown in **Supplemental Figure 6A.** (**F**) shows a representative image of leaves (from young to old in the direction from left to right) of wild type and the *opt3* mutant, both grown hydroponically for four weeks with or without copper (**125 nM Cu** or **0 nM Cu**, respectively). **A**, **B** and **F** show a representative image of plants from three independent experimental set-ups.

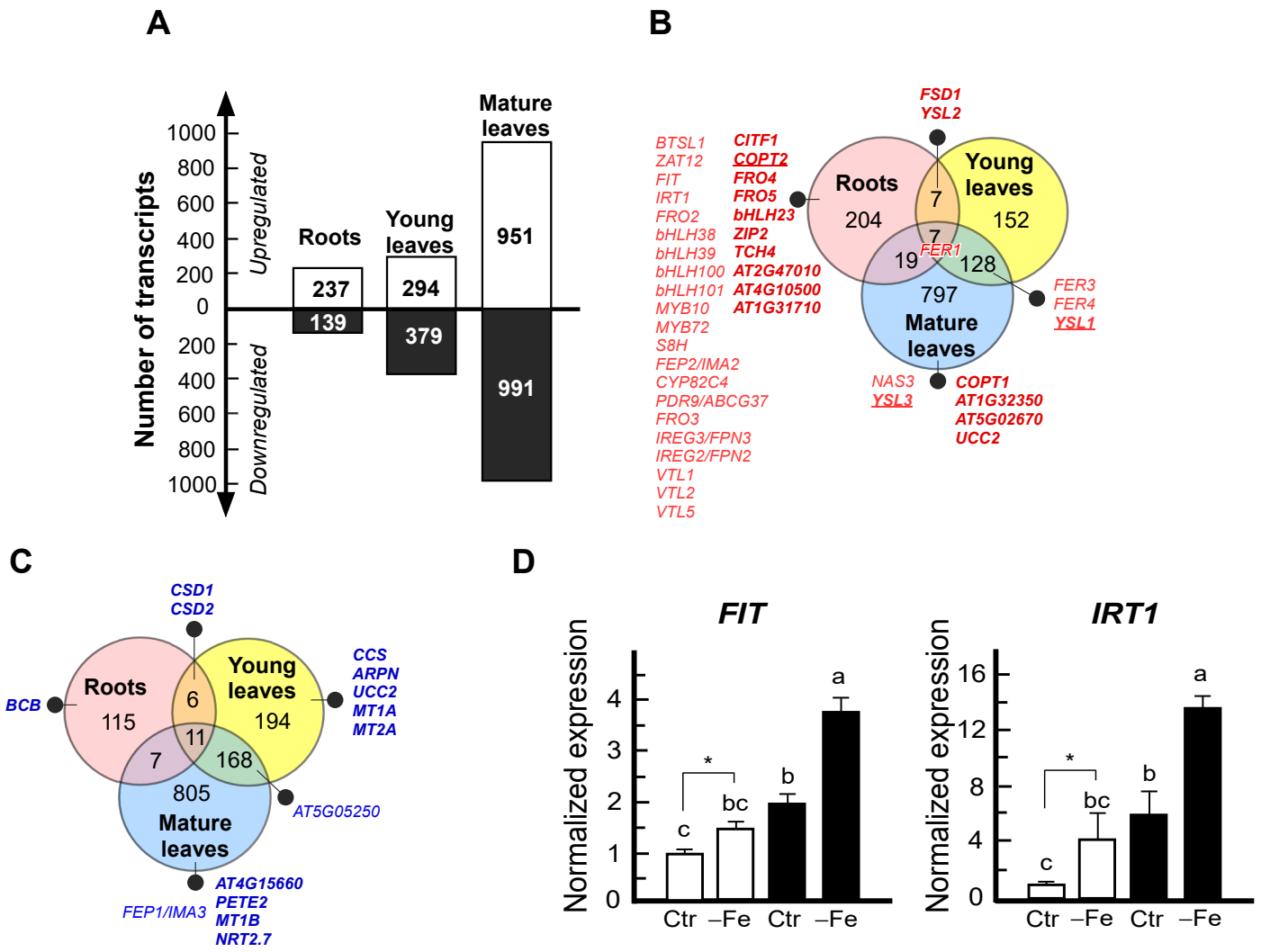

Figure 5. The *opt3* mutant mounts copper deficiency response in roots and young leaves.

(**A**) Total number of differentially expressed genes in roots, mature leaves and young leaves of the *opt3* mutant *vs.* wild type, according to RNA-seq data (ratio >= 1.5 or <=0.67, false-discovery rate [FDR] < 0.05). Venn diagrams show the number of upregulated (**B**) or downregulated (**C**) genes in roots, mature and young leaves. Overlaps indicate the number of genes co-regulated in indicated tissues. Genes associated with iron and copper homeostasis are shown in (**B**) and (**C**). Genes involved in copper homeostasis are marked in bold; genes associated with iron and copper deficiency responses are marked in bold and underlined. (**D**) The expression of the iron transport system is upregulated in the roots of the *opt3* mutant under iron deficiency. Plants were grown hydroponically for 31 days. A subset of plants was transferred to a fresh medium without iron. Roots were collected after four days of additional growth with or without iron. Shown are mean values ± S.E. (n = 3 independent RT-qPCR experiments per genotype. In each experiment, roots were pooled from four plants grown in one container for RNA extraction). Asterisks indicate statistically significant differences in gene expression in wild type grown with or without iron ($p < 0.05$, Student-*t* test). Levels not connected by the same letter are statistically different ($p < 0.05$; Tukey HSD, JMP Pro 14 software package.

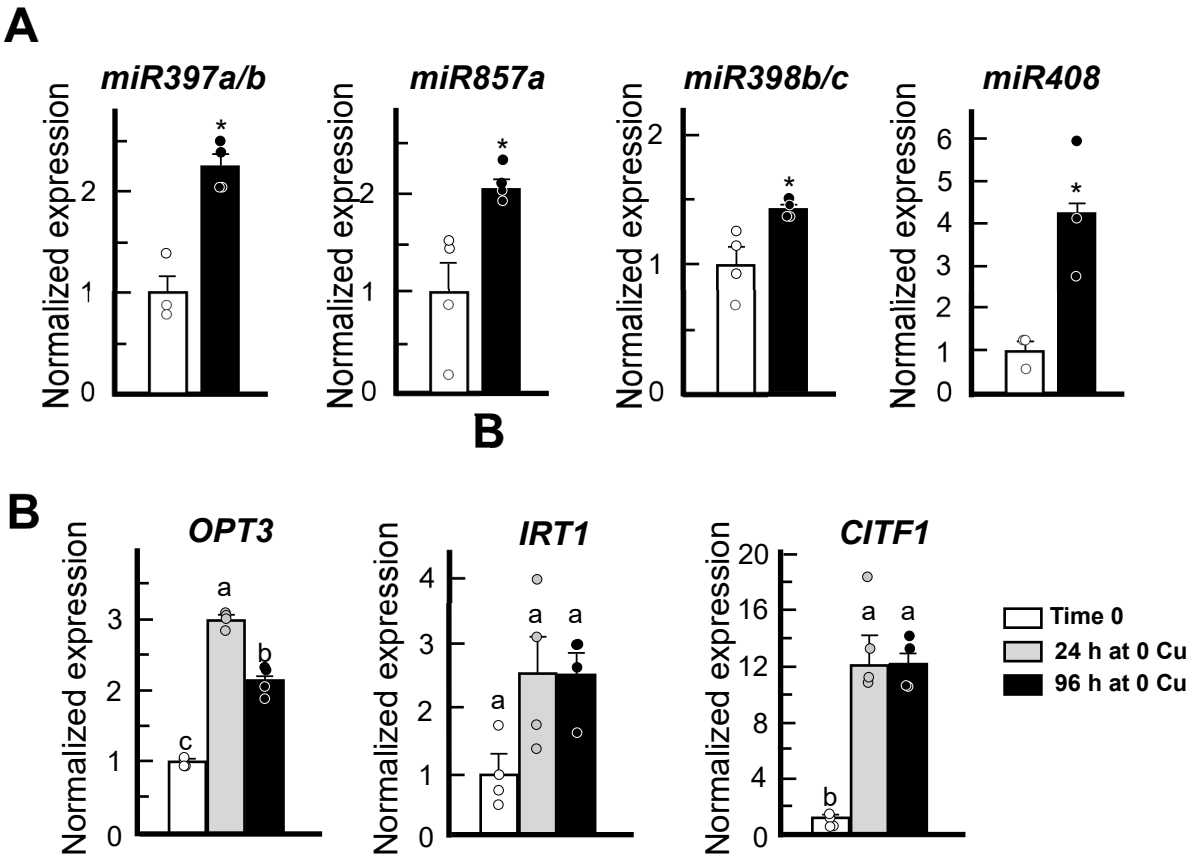

Figure 6. The expression of copper micro-RNA genes is upregulated in the *opt3* mutant.

(A) shows the transcript abundance of *miRNA397a/b*, *miR857a*, *miR39b/c*, and *miR408* in roots of 5-week-old wild type (open bars) or the *opt3* mutant (black bars) grown hydroponically with 125 nM $CuSO_4$. Shown are mean values ± S.E. Asterisks indicate statistically significant differences from the expression of genes in wild type, set to one ($p < 0.05$, Student-*t* test, n = 4 independent RT-qPCR experiments per genotype. In each experiment, roots were pooled from four plants grown in one container for RNA extraction). (**B**) Expression of *OPT3*, *IRT1* and *CITF1* in roots of wild type subjected to one or four days under copper deficiency. *CITF1* was used as a marker of copper deficiency to validate treatment efficiency. Shown are mean values ± S.E. Levels not connected by the same letter are statistically different ($p < 0.05$; Tukey HSD, JMP Pro 14 software package, n = 4 independent RT-qPCR experiments per condition. In each experiment, roots were pooled from four plants grown in one container for RNA extraction.

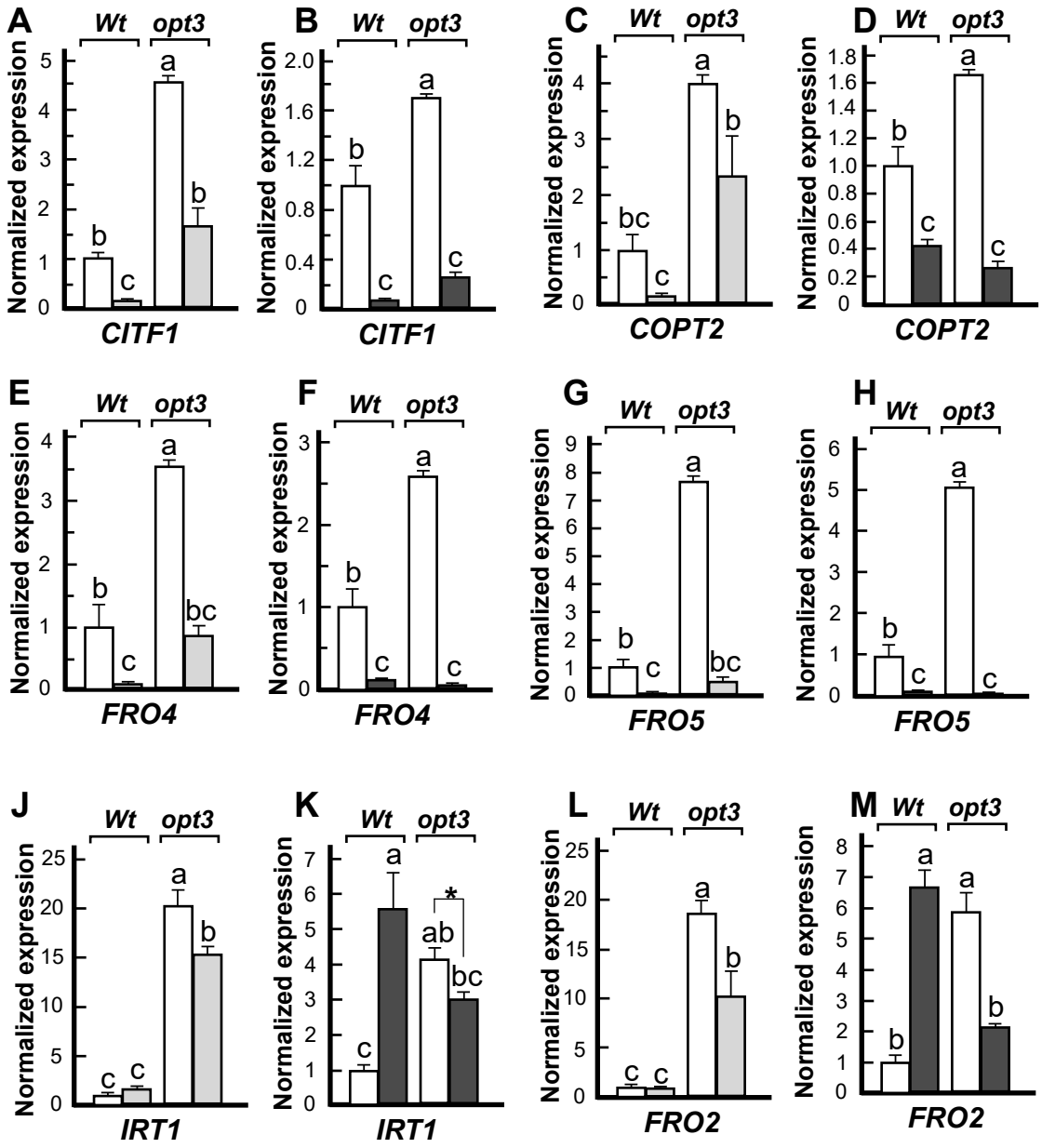

Figure 7. Copper supplementation partially rescues the molecular symptoms of copper deficiency in roots of the *opt3* mutant.

Plants were grown hydroponically under control conditions (**white bars**) until the late-vegetative stage before a subset of plants was transferred to a fresh medium with higher copper concentrations (250 nM $CuSO_4$, **light grey bars** in **A, B, E, F, J, K** or 500 nM $CuSO_4$, **dark grey bars** in **C, D, G, H, L, M**). Plants were grown for another week before tissue collection and RT-qPCR analysis. The transcript abundance of indicated genes was normalized to the wild type grown under control conditions. Data show mean values ± S.E. Levels not connected by the same letter are statistically different (Tukey HSD, JMP Pro 14 software package, n= 3 RT-qPCR experiments per genotype. In each experiment, roots were pooled from three plants grown in one container for RNA extraction. Data are normalized to the expression of *Actin2*; the expression of genes in wild type grown under 125 nM $CuSO_4$ (control conditions) was set to one.

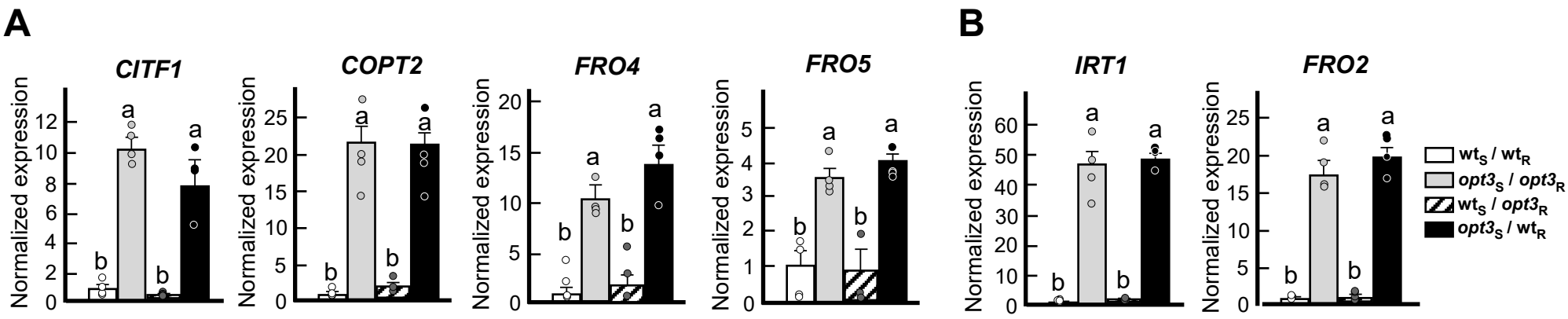

Figure 8. The OPT3 function in the shoot controls the expression of copper deficiency markers.

The transcript abundance of copper- (**A**) and iron-deficiency (**B**) markers in roots of grafted plants. Wild type and the *opt3* mutant were used for reciprocal grafting. **Wt*S*/Wt*R*,** wild type scion grafted to wild type rootstock (control); ***opt3S/opt3R***, *opt3* scion grafted to *opt3* rootstock; **Wt*S*/opt3*R***, wild type scion grafted to *opt3* rootstock; ***opt3S/WtR***, *opt3* scion grafted to wild type rootstock. Shown values represent means ± S.E. (n = 4 independent experiments [PCR runs, each representing an independent experimental setup]; roots were pooled from four plants per experimental set-up). Levels not connected by the same letter are statistically different ($p < 0.05$; Tukey HSD, JMP Pro 14 software package). Data are normalized to the expression of *Actin2*; the expression of genes in wild type was set to one.

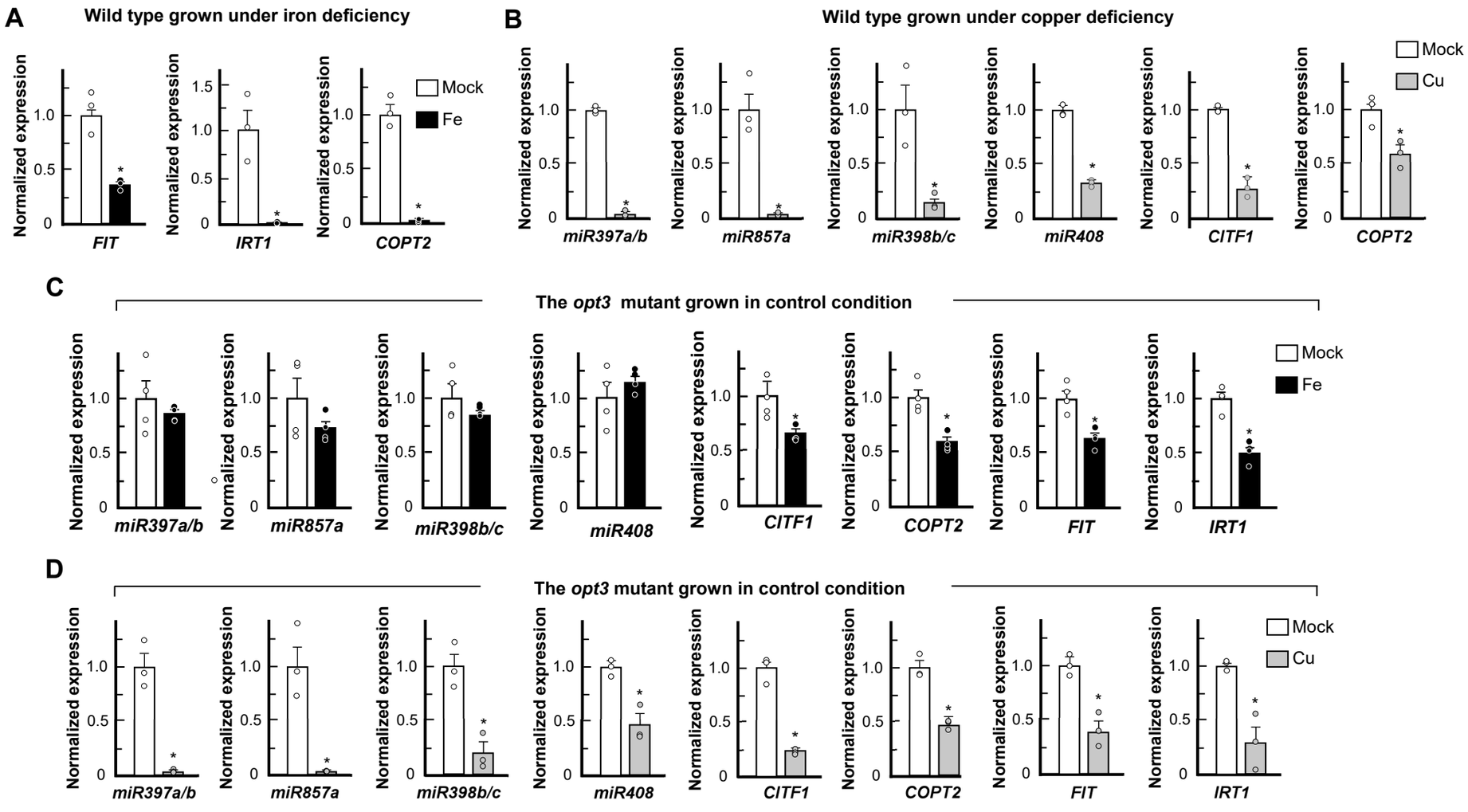

Figure 9. Copper or iron feeding *via* the phloem in the shoot represses the molecular symptoms of copper and iron deficiency in the root of the wild type and the *opt3* mutant.

RT-qPCR analysis of copper and iron deficiency molecular markers in roots of the 33-day-old wild type (**A, B**) or the *opt3* mutant (**C, D**). Wild type plants were grown hydroponically and subjected to either iron or copper deficiency (**A** and **B**, respectively). The *opt3* mutant was grown hydroponically in copper and iron sufficient conditions (**C**, **D**). Roots were collected after 24h of phloem feeding with iron (**Fe**, black bars) or copper (**Cu**, grey bars) or control feeding (**mock**, open bars). Mock treatment for copper feeding was MiliQ water, and mock treatment for iron feeding was citrate. Asterisks indicate statistically significant differences from the expression of genes in mock-fed plants, set to one ($p < 0.05$, Student-*t* test, n = 4 [PCR runs, each representing an independent experimental set up]; roots were pooled from four plants per each experimental set-up). Data are normalized to the expression of *Actin2*; the expression of genes in a mock-treated wild type (**A**, **B**) or a mock-treated *opt3* mutant (**C**, **D**) was set to one.

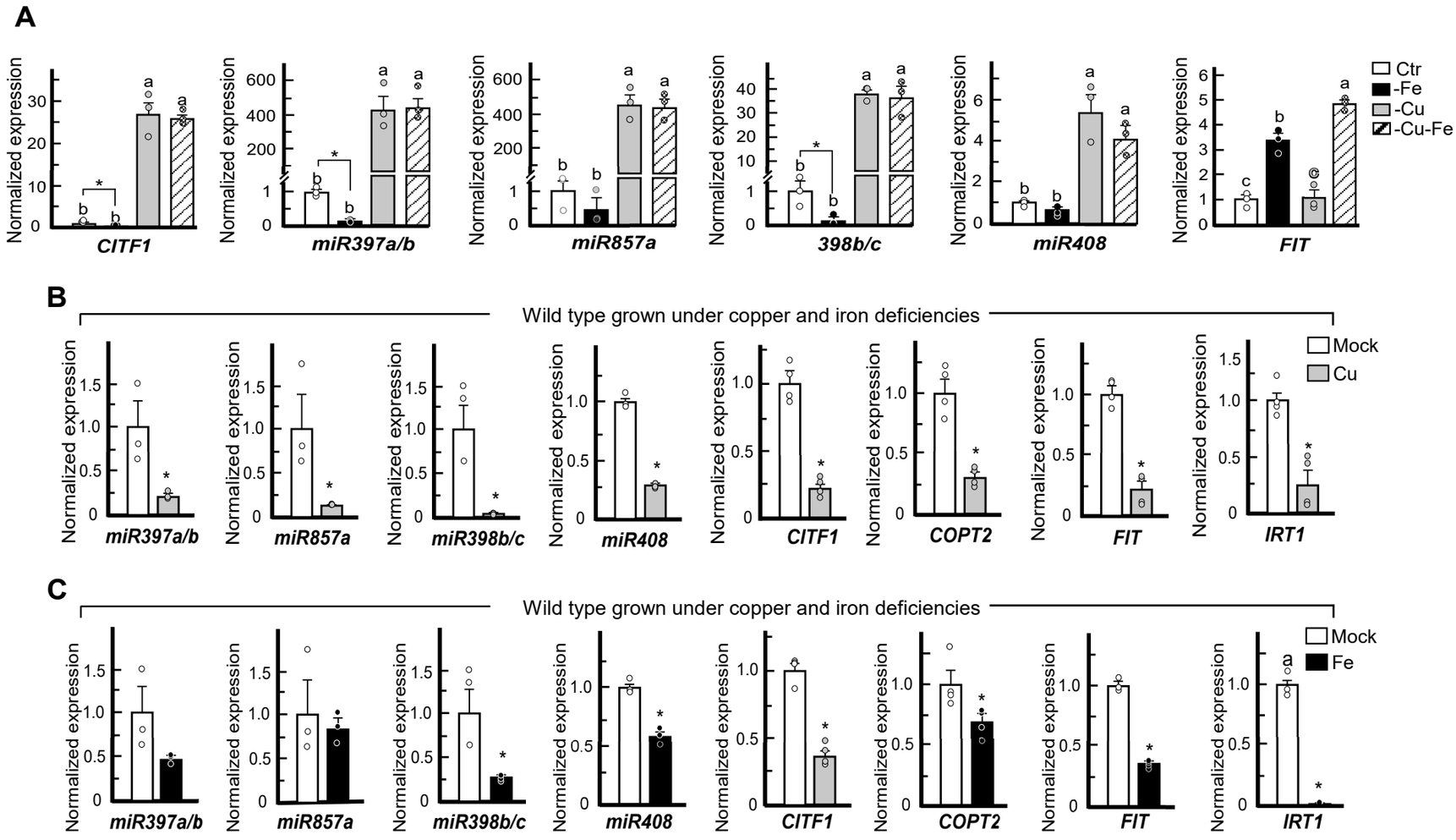

Figure 10. Copper and iron deficiency applied simultaneously increases the expression of *CITF1*, *copper miRNAs* and *FIT*.

(**A**) Transcript abundance of *CITF1* and indicated *copper miRNAs* and the *FIT* was analyzed in roots of plants grown under control conditions (**Ctr**) or without cooper but with iron (**–Cu**) for four weeks before tissue collection. To achieve iron deficiency, plants were grown under control conditions for three weeks, transferred to a solution without iron and grown for one additional week (**–Fe**). For the simultaneous iron and copper deficiency treatment, plants were grown without copper but with iron for three weeks and then transferred to a fresh hydroponic medium lacking both copper and iron. Tissues were collected and analyzed after an additional week of growth (**–Cu –Fe**). (**B**) Transcript abundance of indicated genes in roots of wild type grown under simultaneous copper and iron deficiency after phloem feeding with copper (**Cu**, grey bars) or control feeding (**mock**, open bars). (**C**) Transcript abundance of indicated genes in roots of wild type grown under simultaneous copper and iron deficiency after phloem feeding with iron (**Fe**, black bars or control feeding (**mock**, open bars). Mock treatment for copper feeding was MiliQ water, and mock treatment for iron feeding was citrate. In (**A**), (**B**) and (**C**), mean values ± S.E are shown. Levels not connected by the same letter are statistically different (Tukey HSD, JMP Pro 14 software package, n = 3 to 4 independent experiments (PCR runs, representing an independent experimental set-up where roots were pooled from three plants per experiment). Data are normalized to the expression of *Actin2*; the expression of genes in wild type grown under control conditions (**A**) or mock-treated wild type (**B, C**) was set to one.

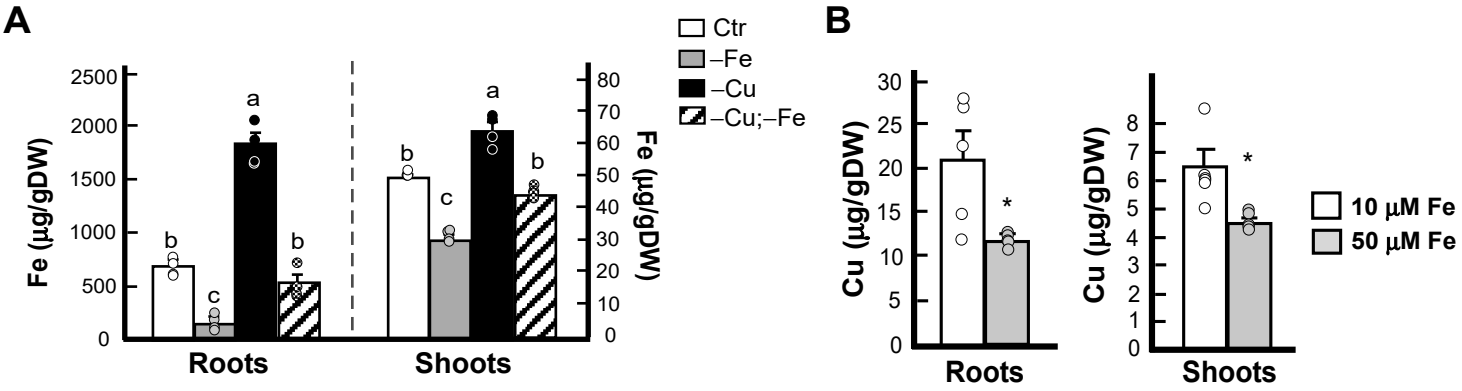

Figure 11. Copper and iron availability in the medium influence each other's uptake and accumulation in roots and shoot of *A. thaliana*.

(**A**) Iron concentration in roots and shoots of *A. thaliana* grown for five weeks in the control condition (**Ctr**), copper deficiency (**–Cu**), iron deficiency (**–Fe**), and simultaneous copper and iron deficiency (**–Cu –Fe**). Data are mean values ± S.E. Levels not connected by the same letter are statistically different (Tukey HSD, JMP Pro 14 software package, n = 3 to 5 independent ICP-MS measurements, each representing an independent experimental set-up; roots and shoots were pooled from four plants per each experimental set-up to obtain one measurement. (**B**) Copper concentration in roots and shoots of *A. thaliana,* grown for five weeks in the control condition (**10 µM Fe)** or with high iron (**50 µM Fe**). Mean values ± S.E is obtained with n = 5 ICP-MS measurements from two batches of independently grown plants per condition. Tissues from four plants were pooled for each measurement. Asterisks indicate statistically significant differences ($p < 0.05$, Student-*t* test).

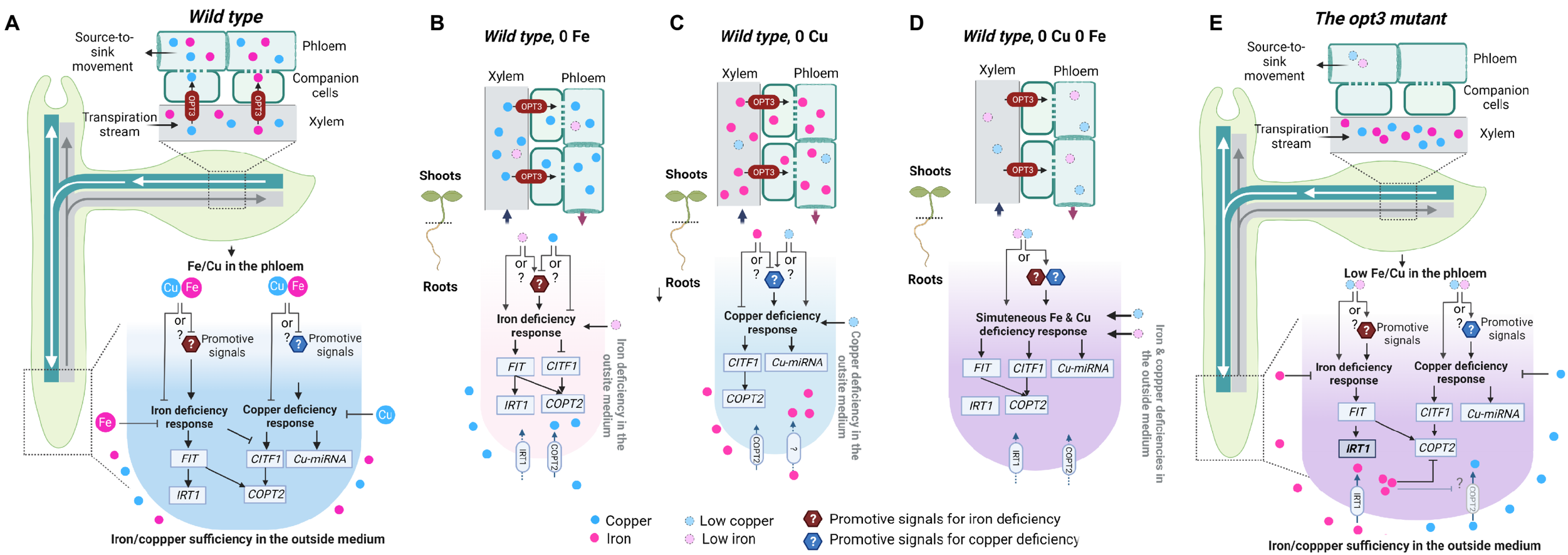

Figure 12. AtOPT3-facilitated Copper and Iron Transport to the Phloem Companion Cells Mediates Iron-Copper Crosstalk in Shoot-to-Root Signaling.

(**A**) AtOPT3 mediates iron and copper loading to the phloem companion cells for the distribution to sink organs, including roots. Phloem-mobile iron and/or copper represses the expression of iron and copper uptake systems, either acting directly as a repressor or indirectly by sequestering or inhibiting the synthesis of a promotive signal. (**B**) Iron deficiency in the outside medium stimulates copper accumulation in roots and leaves (Waters et al., 2012; Waters and Armbrust, 2013; Waters et al., 2014) and **Figure 11A.** Under these circumstances, AtOPT3 loads mainly copper to the phloem in the shoot. The concentration of iron in the phloem decreases, which causes the upregulation of the expression of the iron uptake system. Copper availability in the phloem, provided by the AtOPT3, fine tunes the expression of iron transport genes to avoid iron overload observed in the *opt3* mutant. The repressive role of copper on the expression of copper and iron uptake system can occur directly or indirectly *via* scavenging or inhibiting the production of a promotive signal. A similar scenario occurs under copper deficiency, where OPT3 mainly loads iron to fine-tune the expression of copper uptake genes (**C**). Simultaneous iron and copper deficiencies in the outside medium autonomously upregulate the expression of both copper and iron uptake genes as both elements are less available in the phloem sap (**D**). The scenario is different in the *opt3* mutant (**E**): although both iron and copper are available in the outside medium, the *opt3* mutant experiences simultaneous iron and copper deficiency in the phloem. Low iron accumulation in the phloem stimulates transcriptional iron deficiency response, overriding local iron sufficiency response. Since iron is available in the outside medium, iron accumulates in the *opt3* mutant. Copper deficiency in the phloem, roots and leaves also leads to iron accumulation and transcriptional copper deficiency response. Increased iron accumulation from both pathways, in turn, decreases copper uptake, as shown in (**Figure 11B**) and documented in animal species (Klevay, 2001; Ha et al., 2016), further altering Fe-Cu crosstalk. Figure created in Biorender.com

Parsed Citations

Agyeman-Budu DN, Choudhury S, Coulthard I, Gordon R, Hallin E, Woll AR (2016) Germanium Collimating micro-Channel Arrays For High Resolution, High Energy Confocal X-ray Fluorescence Microscopy. Icxom23: International Conference on X-Ray Optics and Microanalysis 1764
Google Scholar: Author Only Title Only Author and Title

Alexander SPH, Kelly E, Mathie A, Peters JA, Veale EL, Armstrong JF, Faccenda E, Harding SD, Pawson AJ, Sharman JL, et al. (2019) THE CONCISE GUIDE TO PHARMACOLOGY 2019/20: Transporters. British Journal of Pharmacology 176: S397-S493
Google Scholar: Author Only Title Only Author and Title

Araki R, Mermod M, Yamasaki H, Kamiya T, Fujiwara T, Shikanai T (2018) SPL7 locally regulates copper-homeostasis-related genes in Arabidopsis. J Plant Physiol 224-225: 137-143
Google Scholar: Author Only Title Only Author and Title

Bashir K, Ishimaru Y, Itai RN, Senoura T, Takahashi M, An G, Oikawa T, Ueda M, Sato A, Uozumi N, et al. (2015) Iron deficiency regulated OsOPT7 is essential for iron homeostasis in rice. Plant Molecular Biology 88: 165-176
Google Scholar: Author Only Title Only Author and Title

Baxter IR, Vitek O, Lahner B, Muthukumar B, Borghi M, Morrissey J, Guerinot ML, Salt DE (2008) The leaf ionome as a multivariable system to detect a plant's physiological status. Proceedings of the National Academy of Sciences 105: 12081-12086
Google Scholar: Author Only Title Only Author and Title

Benjamini Y, Hochberg Y (1995) Controlling the False Discovery Rate: A Practical and Powerful Approach to Multiple Testing. Journal of the Royal Statistical Society. Series B (Methodological) 57: 289-300
Google Scholar: Author Only Title Only Author and Title

Bernal M, Casero D, Singh V, Wilson GT, Grande A, Yang H, Dodani SC, Pellegrini M, Huijser P, Connolly EL, et al. (2012) Transcriptome Sequencing Identifies SPL7 -Regulated Copper Acquisition Genes FRO4 FRO5 and the Copper Dependence of Iron Homeostasis in Arabidopsis The Plant Cell 24: 738-761
Google Scholar: Author Only Title Only Author and Title

Bogs J, Bourbouloux A, Cagnac O, Wachter A, Rausch T, Delrot S (2003) Functional characterization and expression analysis of a glutathione transporter, BjGT1, from Brassica juncea: evidence for regulation by heavy metal exposure. Plant, Cell & Environment 26: 1703-1711
Google Scholar: Author Only Title Only Author and Title

Broadley M, Brown P, Cakmak I, Rengel Z, Zhao F (2012) Chapter 7 - Function of Nutrients: Micronutrients A2 - Marschner, Petra. In Marschner's Mineral Nutrition of Higher Plants (Third Edition). Academic Press, San Diego, pp 191-248
Google Scholar: Author Only Title Only Author and Title

Burkhead JL, Gogolin Reynolds KA, Abdel-Ghany SE, Cohu CM, Pilon M (2009) Copper homeostasis. New Phytologist 182: 799-816
Google Scholar: Author Only Title Only Author and Title

Cagnac O, Bourbouloux A, Chakrabarty D, Zhang MY, Delrot S (2004) AtOPT6 transports glutathione derivatives and is induced by primisulfuron. Plant Physiology 135: 1378-1387
Google Scholar: Author Only Title Only Author and Title

Chang CJ (2015) Searching for harmony in transition-metal signaling. Nat Chem Biol 11: 744-747
Google Scholar: Author Only Title Only Author and Title

Chao Z-F, Wang Y-L, Chen Y-Y, Zhang C-Y, Wang P-Y, Song T, Liu C-B, Lv Q-Y, Han M-L, Wang S-S, et al. (2021) NPF transporters in synaptic-like vesicles control delivery of iron and copper to seeds. Science advances 7: eabh2450-eabh2450
Google Scholar: Author Only Title Only Author and Title

Chen C, Galon Y, Rahmati Ishka M, Malihi S, Shimanovsky V, Twito S, Rath A, Vatamaniuk OK, Miller G (2020) ASCORBATE PEROXIDASE6 delays the onset of age-dependent leaf senescence. Plant Physiology
Google Scholar: Author Only Title Only Author and Title

Colangelo EP, Guerinot ML (2004) The essential basic helix-loop-helix protein FIT1 is required for the iron deficiency response. Plant Cell 16: 3400-3412
Google Scholar: Author Only Title Only Author and Title

Cui Y, Chen CL, Cui M, Zhou WJ, Wu HL, Ling HQ (2018) Four IVa bHLH Transcription Factors Are Novel Interactors of FIT and Mediate JA Inhibition of Iron Uptake in Arabidopsis. Mol Plant 11: 1166-1183
Google Scholar: Author Only Title Only Author and Title

Dancis A, Haile D, Yuan DS, Klausner RD (1994) The Saccharomyces cerevisiae copper transport protein (Ctr1p). Biochemical characterization, regulation by copper, and physiologic role in copper uptake. J Biol Chem 269: 25660-25667

Google Scholar: Author Only Title Only Author and Title

Emmerstorfer A, Wriessnegger T, Hirz M, Pichler H (2014) Overexpression of membrane proteins from higher eukaryotes in yeasts. Applied Microbiology and Biotechnology 98: 7671-7698
Google Scholar: Author Only Title Only Author and Title

Epstein E, Bloom A (2005) Mineral nutrition of plants: principles and perspectives, 2nd eds. Sunderland, Mass Sinaur: 292-305
Google Scholar: Author Only Title Only Author and Title

Gao F, Robe K, Bettembourg M, Navarro N, Rofidal V, Santoni V, Gaymard F, Vignols F, Roschzttardtz H, Izquierdo E, et al. (2020) The Transcription Factor bHLH121 Interacts with bHLH105 (ILR3) and Its Closest Homologs to Regulate Iron Homeostasis in Arabidopsis. Plant Cell 32: 508-524
Google Scholar: Author Only Title Only Author and Title

Garcia MJ, Romera FJ, Stacey MG, Stacey G, Villar E, Alcantara E, Perez-Vicente R (2013) Shoot to root communication is necessary to control the expression of iron-acquisition genes in Strategy I plants. Planta 237: 65-75
Google Scholar: Author Only Title Only Author and Title

Gayomba SR, Jung HI, Yan J, Danku J, Rutzke MA, Bernal M, Kramer U, Kochian LV, Salt DE, Vatamaniuk OK (2013) The CTR/COPT-dependent copper uptake and SPL7-dependent copper deficiency responses are required for basal cadmium tolerance in A. thaliana. Metallomics 5: 1262-1275
Google Scholar: Author Only Title Only Author and Title

Gayomba SR, Zhai Z, Jung HI, Vatamaniuk OK (2015) Local and systemic signaling of iron status and its interactions with homeostasis of other essential elements. Front Plant Sci 6: 716
Google Scholar: Author Only Title Only Author and Title

Green LS, Rogers EE (2004) FRD3 Controls Iron Localization in Arabidopsis. Plant Physiology 136: 2523-2531
Google Scholar: Author Only Title Only Author and Title

Grignon N, Touraine B, Durand M (1989) 6(5)Carboxyfluorescein as a tracer of phloem sap translocation. American Journal of Botany 76: 871-877
Google Scholar: Author Only Title Only Author and Title

Grillet L, Lan P, Li W, Mokkapati G, Schmidt W (2018) IRON MAN is a ubiquitous family of peptides that control iron transport in plants. Nat Plants 4: 953-963
Google Scholar: Author Only Title Only Author and Title

Grusak MA, Pezeshgi S (1996) Shoot-to-Root Signal Transmission Regulates Root Fe(III) Reductase Activity in the dgl Mutant of Pea. Plant Physiology 110: 329-334
Google Scholar: Author Only Title Only Author and Title

Ha JH, Doguer C, Wang X, Flores SR, Collins JF (2016) High-Iron Consumption Impairs Growth and Causes Copper-Deficiency Anemia in Weanling Sprague-Dawley Rats. PLoS One 11: e0161033
Google Scholar: Author Only Title Only Author and Title

Hirayama T, Lei GJ, Yamaji N, Nakagawa N, Ma JF (2018) The Putative Peptide Gene FEP1 Regulates Iron Deficiency Response in Arabidopsis. Plant Cell Physiol 59: 1739-1752
Google Scholar: Author Only Title Only Author and Title

Jain A, Wilson G, Connolly E (2014) The diverse roles of FRO family metalloreductases in iron and copper homeostasis. Frontiers in Plant Science 5
Google Scholar: Author Only Title Only Author and Title

Jeong J, Merkovich A, Clyne M, Connolly EL (2017) Directing iron transport in dicots: regulation of iron acquisition and translocation. Curr Opin Plant Biol 39: 106-113
Google Scholar: Author Only Title Only Author and Title

Jiang A, Guo Z, Pan J, Zhuang Y, Zuo D, Hao C, Gao Z, Xin P, Chu J, Zhong S, et al. (2020) The PIF1-MIR408-Plantacyanin Repression Cascade Regulates Light Dependent Seed Germination. bioRxiv: 2020.2007.2020.212340
Google Scholar: Author Only Title Only Author and Title

Joung J-G, Corbett AM, Fellman SM, Tieman DM, Klee HJ, Giovannoni JJ, Fei Z (2009) Plant MetGenMAP: An Integrative Analysis System for Plant Systems Biology. Plant Physiology 151: 1758-1768
Google Scholar: Author Only Title Only Author and Title

Jung HI, Gayomba SR, Rutzke MA, Craft E, Kochian LV, Vatamaniuk OK (2012) COPT6 is a plasma membrane transporter that functions in copper homeostasis in Arabidopsis and is a novel target of SQUAMOSA promoter-binding protein-like 7. J Biol Chem 287: 33252-33267
Google Scholar: Author Only Title Only Author and Title

Kastoori Ramamurthy R, Xiang Q, Hsieh EJ, Liu K, Zhang C, Waters BM (2018) New aspects of iron-copper crosstalk uncovered by transcriptomic characterization of Col-0 and the copper uptake mutant spl7 in Arabidopsis thaliana. Metallomics 10: 1824-1840
Google Scholar: Author Only Title Only Author and Title

Khan MA, Castro-Guerrero NA, McInturf SA, Nguyen NT, Dame AN, Wang J, Bindbeutel RK, Joshi T, Jurisson SS, Nusinow DA, et al. (2018) Changes in iron availability in Arabidopsis are rapidly sensed in the leaf vasculature and impaired sensing leads to opposite transcriptional programs in leaves and roots. Plant Cell Environ 41: 2263-2276
Google Scholar: Author Only Title Only Author and Title

Kim SA, LaCroix IS, Gerber SA, Guerinot ML (2019) The iron deficiency response in Arabidopsis thaliana requires the phosphorylated transcription factor URI. Proceedings of the National Academy of Sciences 116: 24933-24942
Google Scholar: Author Only Title Only Author and Title

Kim SA, Punshon T, Lanzirotti A, Li L, Alonso JM, Ecker JR, Kaplan J, Guerinot ML (2006) Localization of Iron in Arabidopsis Seed Requires the Vacuolar Membrane Transporter VIT1. Science 314: 1295-1298
Google Scholar: Author Only Title Only Author and Title

Klatte M, Schuler M, Wirtz M, Fink-Straube C, Hell R, Bauer P (2009) The analysis of Arabidopsis nicotianamine synthase mutants reveals functions for nicotianamine in seed iron loading and iron deficiency responses. Plant physiology 150: 257-271
Google Scholar: Author Only Title Only Author and Title

Klevay LM (2001) Iron overload can induce mild copper deficiency. J Trace Elem Med Biol 14: 237-240
Google Scholar: Author Only Title Only Author and Title

Knox K (2019) Measuring Phloem Transport Velocity in Arabidopsis Seedlings Using the Fluorescent Coumarin Glucoside, Esculin. In J Liesche, ed, Phloem: Methods and Protocols. Springer New York, New York, NY, pp 195-201
Google Scholar: Author Only Title Only Author and Title

Kobayashi T (2019) Understanding the Complexity of Iron Sensing and Signaling Cascades in Plants. Plant Cell Physiol 60: 1440-1446
Google Scholar: Author Only Title Only Author and Title

Kumar RK, Chu H-H, Abundis C, Vasques K, Rodriguez DC, Chia J-C, Huang R, Vatamaniuk OK, Walker EL (2017) Iron-Nicotianamine Transporters Are Required for Proper Long Distance Iron Signaling Plant Physiology 175: 1254-1268
Google Scholar: Author Only Title Only Author and Title

Kurt F (2021) An Insight into Oligopeptide Transporter 3 (OPT3) Family Proteins. Protein and Peptide Letters 28: 43-54
Google Scholar: Author Only Title Only Author and Title

Langmead B, Trapnell C, Pop M, Salzberg SL (2009) Ultrafast and memory-efficient alignment of short DNA sequences to the human genome. Genome Biology 10: R25
Google Scholar: Author Only Title Only Author and Title

Li WF, Lan P (2017) The Understanding of the Plant Iron Deficiency Responses in Strategy I Plants and the Role of Ethylene in This Process by Omic Approaches. Frontiers in Plant Science 8
Google Scholar: Author Only Title Only Author and Title

Long TA, Tsukagoshi H, Busch W, Lahner B, Salt DE, Benfey PN (2010) The bHLH transcription factor POPEYE regulates response to iron deficiency in Arabidopsis roots. Plant Cell 22: 2219-2236
Google Scholar: Author Only Title Only Author and Title

Love MI, Huber W, Anders S (2014) Moderated estimation of fold change and dispersion for RNA-seq data with DESeq2. Genome Biology 15: 550
Google Scholar: Author Only Title Only Author and Title

Lubkowitz M (2011) The Oligopeptide Transporters: A Small Gene Family with a Diverse Group of Substrates and Functions? Mol Plant 4: 407-415
Google Scholar: Author Only Title Only Author and Title

Mai HJ, Lindermayr C, von Toerne C, Fink-Straube C, Durner J, Bauer P (2015) Iron and FER-LIKE IRON DEFICIENCY-INDUCED TRANSCRIPTION FACTOR-dependent regulation of proteins and genes in Arabidopsis thaliana roots. Proteomics 15: 3030-3047
Google Scholar: Author Only Title Only Author and Title

Malzer W, Kanngießer B (2005) A Model for the Confocal Volume of 3D Micro X-ray Fluorescence Spectrometer. Spectrochimica Acta Part B: Atomic Spectroscopy 60: 1334-1341
Google Scholar: Author Only Title Only Author and Title

Mantouvalou I, Malzer W, Kanngiesser B (2012) Quantification for 3D micro X-ray fluorescence. Spectrochimica Acta Part B-Atomic Spectroscopy 77: 9-18
Google Scholar: Author Only Title Only Author and Title

Mendoza-Cózatl DG, Xie Q, Akmakjian GZ, Jobe TO, Patel A, Stacey MG, Song L, Demoin DW, Jurisson SS, Stacey G, et al. (2014) OPT3 is a component of the iron-signaling network between leaves and roots and misregulation of OPT3 leads to an over-accumulation of cadmium in seeds. Mol Plant 7: 1455-1469
Google Scholar: Author Only Title Only Author and Title

Morrissey J, Baxter IR, Lee J, Li L, Lahner B, Grotz N, Kaplan J, Salt DE, Guerinot ML (2009) The Ferroportin Metal Efflux Proteins Function in Iron and Cobalt Homeostasis in *Arabidopsis*. The Plant Cell 21: 3326-3338
Google Scholar: Author Only Title Only Author and Title

Mukherjee I, Campbell NH, Ash JS, Connolly EL (2006) Expression profiling of the Arabidopsis ferric chelate reductase (FRO) gene family reveals differential regulation by iron and copper. Planta 223: 1178-1190
Google Scholar: Author Only Title Only Author and Title

Mustroph A, Zanetti ME, Jang CJH, Holtan HE, Repetti PP, Galbraith DW, Girke T, Bailey-Serres J (2009) Profiling translatomes of discrete cell populations resolves altered cellular priorities during hypoxia in *Arabidopsis*. Proceedings of the National Academy of Sciences 106: 18843-18848
Google Scholar: Author Only Title Only Author and Title

Newville M (2013) Larch: An Analysis Package for XAFS and Related Spectroscopies. J. Phys.: Conf. Ser. 430
Google Scholar: Author Only Title Only Author and Title

Nguyen NT, Khan MA, Castro-Guerrero NA, Chia J-C, Vatamaniuk OK, Mari S, Jurisson SS, Mendoza-Cozatl DG (2022) Iron Availability Within the Leaf Vasculature Determines the Magnitude of Iron Deficiency Responses in Source and Sink Tissues in Arabidopsis. Plant and Cell Physiology
Google Scholar: Author Only Title Only Author and Title

Oparka KJ, Duckett CM, Prior DAM, Fisher DB (1994) Real-time imaging of phloem unloading in the root tip of Arabidopsis. The Plant Journal 6: 759-766
Google Scholar: Author Only Title Only Author and Title

Oparka KJ, Prior DAM, Wright KM (1995) Symplastic communication between primary and developing lateral roots of Arabidopsis thaliana. Journal of Experimental Botany 46: 187-197
Google Scholar: Author Only Title Only Author and Title

Osawa H, Stacey G, Gassmann W (2006) ScOPT1 and AtOPT4 function as proton-coupled oligopeptide transporters with broad but distinct substrate specificities. Biochemical Journal 393: 267-275
Google Scholar: Author Only Title Only Author and Title

Pilon M (2017) The copper microRNAs. New Phytologist 213: 1030-1035
Google Scholar: Author Only Title Only Author and Title

Pottier M, Dumont J, Masclaux-Daubresse C, Thomine S (2019) Autophagy is essential for optimal translocation of iron to seeds in Arabidopsis. Journal of experimental botany 70: 859-869
Google Scholar: Author Only Title Only Author and Title

Quast C, Pruesse E, Yilmaz P, Gerken J, Schweer T, Yarza P, Peplies J, Glöckner FO (2013) The SILVA ribosomal RNA gene database project: improved data processing and web-based tools. Nucleic Acids Research 41: 7
Google Scholar: Author Only Title Only Author and Title

Rahmati Ishka M, Chia J-C, Vatamaniuk OK (2022) Chapter 12 - Advances in understanding of copper function and transport in plants. In SK Upadhyay, ed, Cation Transporters in Plants. Academic Press, pp 205-226
Google Scholar: Author Only Title Only Author and Title

Rahmati Ishka M, Vatamaniuk OK (2020) Copper deficiency alters shoot architecture and reduces fertility of both gynoecium and androecium in Arabidopsis thaliana. Plant Direct 4: e00288
Google Scholar: Author Only Title Only Author and Title

Rai S, Singh PK, Mankotia S, Swain J, Satbhai SB (2021) Iron homeostasis in plants and its crosstalk with copper, zinc, and manganese. Plant Stress 1: 100008
Google Scholar: Author Only Title Only Author and Title

Ravet K, Pilon M (2013) Copper and Iron Homeostasis in Plants: The Challenges of Oxidative Stress. Antioxidants & Redox Signaling 19: 23
Google Scholar: Author Only Title Only Author and Title

Rees EM, Lee J, Thiele DJ (2004) Mobilization of Intracellular Copper Stores by the Ctr2 Vacuolar Copper Transporter. Journal of Biological Chemistry 279: 54221-54229
Google Scholar: Author Only Title Only Author and Title

Rellán-Álvarez R, Giner-Martínez-Sierra J, Orduna J, Orera I, Rodríguez-Castrillón JÁ, García-Alonso JI, Abadía J, Álvarez-

Fernández A (2009) Identification of a Tri-Iron(III), Tri-Citrate Complex in the Xylem Sap of Iron-Deficient Tomato Resupplied with Iron: New Insights into Plant Iron Long-Distance Transport. Plant and Cell Physiology 51: 91-102
Google Scholar: Author Only Title Only Author and Title

Rodríguez FI, Esch JJ, Hall AE, Binder BM, Schaller GE, Bleecker AB (1999) A Copper Cofactor for the Ethylene Receptor ETR1 from Arabidopsis. Science 283: 996-998
Google Scholar: Author Only Title Only Author and Title

Rogers EE, Guerinot ML (2002) FRD3, a Member of the Multidrug and Toxin Efflux Family, Controls Iron Deficiency Responses in Arabidopsis. The Plant Cell 14: 1787-1799
Google Scholar: Author Only Title Only Author and Title

Ross-Elliott TJ, Jensen KH, Haaning KS, Wager BM, Knoblauch J, Howell AH, Mullendore DL, Monteith AG, Paultre D, Yan D, et al. (2017) Phloem unloading in Arabidopsis roots is convective and regulated by the phloem-pole pericycle. eLife 6: e24125
Google Scholar: Author Only Title Only Author and Title

Schott-Verdugo S, Müller L, Classen E, Gohlke H, Groth G (2019) Structural Model of the ETR1 Ethylene Receptor Transmembrane Sensor Domain. Scientific Reports 9: 8869
Google Scholar: Author Only Title Only Author and Title

Schwarz B, Bauer P (2020) FIT, a regulatory hub for iron deficiency and stress signaling in roots, and FIT-dependent and -independent gene signatures. J Exp Bot 71: 1694-1705
Google Scholar: Author Only Title Only Author and Title

Selote D, Samira R, Matthiadis A, Gillikin JW, Long TA (2014) Iron-Binding E3 Ligase Mediates Iron Response in Plants by Targeting Basic Helix-Loop-Helix Transcription Factors Plant Physiology 167: 273-286
Google Scholar: Author Only Title Only Author and Title

Shaff JE, Schultz BA, Craft EJ, Clark RT, Kochian LV (2010) GEOCHEM-EZ: a chemical speciation program with greater power and flexibility. Plant and Soil 330: 207-214
Google Scholar: Author Only Title Only Author and Title

Sheng H, Jiang Y, Ishka MR, Chia JC, Dokuchayeva T, Kavulych Y, Zavodna TO, Mendoza PN, Huang R, Smieshka LM, et al. (2021) YSL3-mediated copper distribution is required for fertility, seed size and protein accumulation in Brachypodium. Plant Physiol 186: 655-676
Google Scholar: Author Only Title Only Author and Title

Solé VA, Papillon E, Cotte M, Walter P, Susini J (2007) A multiplatform code for the analysis of energy-dispersive X-ray fluorescence spectra. Spectrochimica Acta Part B: Atomic Spectroscopy 62: 63-68
Google Scholar: Author Only Title Only Author and Title

Spielmann J, Vert G (2020) The many facets of protein ubiquitination and degradation in plant root iron-deficiency responses. Journal of Experimental Botany 72: 2071-2082
Google Scholar: Author Only Title Only Author and Title

Stacey MG, Koh S, Becker J, Stacey G (2002) AtOPT3, a Member of the Oligopeptide Transporter Family, Is Essential for Embryo Development in Arabidopsis. The Plant Cell 14: 2799-2811
Google Scholar: Author Only Title Only Author and Title

Stacey MG, Patel A, McClain WE, Mathieu M, Remley M, Rogers EE, Gassmann W, Blevins DG, Stacey G (2008) The Arabidopsis AtOPT3 Protein Functions in Metal Homeostasis and Movement of Iron to Developing Seeds. Plant Physiology 146: 589-601
Google Scholar: Author Only Title Only Author and Title

Trapnell C, Pachter L, Salzberg SL (2009) TopHat: discovering splice junctions with RNA-Seq. Bioinformatics 25: 7
Google Scholar: Author Only Title Only Author and Title

Tsang T, Posimo JM, Gudiel AA, Cicchini M, Feldser DM, Brady DC (2020) Copper is an essential regulator of the autophagic kinases ULK1/2 to drive lung adenocarcinoma. Nature cell biology 22: 412-424
Google Scholar: Author Only Title Only Author and Title

Turski ML, Brady DC, Kim HJ, Kim BE, Nose Y, Counter CM, Winge DR, Thiele DJ (2012) A novel role for copper in Ras/mitogen-activated protein kinase signaling. Mol Cell Biol 32: 1284-1295
Google Scholar: Author Only Title Only Author and Title

Turski ML, Thiele DJ (2009) New roles for copper metabolism in cell proliferation, signaling, and disease. J Biol Chem 284: 717-721
Google Scholar: Author Only Title Only Author and Title

Vert GA, Briat J-F, Curie C (2003) Dual regulation of the Arabidopsis high-affinity root iron uptake system by local and long-distance signals. Plant physiology 132: 796-804

Google Scholar: Author Only Title Only Author and Title

Waters BM, Armbrust LC (2013) Optimal copper supply is required for normal plant iron deficiency responses. Plant Signal Behav 8: e26611
Google Scholar: Author Only Title Only Author and Title

Waters BM, McInturf SA, Amundsen K (2014) Transcriptomic and physiological characterization of the fefe mutant of melon (Cucumis melo) reveals new aspects of iron-copper crosstalk. New Phytol 203: 1128-1145
Google Scholar: Author Only Title Only Author and Title

Waters BM, McInturf SA, Stein RJ (2012) Rosette iron deficiency transcript and microRNA profiling reveals links between copper and iron homeostasis in Arabidopsis thaliana. J Exp Bot 63: 5903-5918
Google Scholar: Author Only Title Only Author and Title

Wongkaew A, Asayama K, Kitaiwa T, Nakamura SI, Kojima K, Stacey G, Sekimoto H, Yokoyama T, Ohkama-Ohtsu N (2018) AtOPT6 Protein Functions in Long-Distance Transport of Glutathione in Arabidopsis thaliana. Plant and Cell Physiology 59: 1443-1451
Google Scholar: Author Only Title Only Author and Title

Wu Y, Zhang D, Chu Jee Y, Boyle P, Wang Y, Brindle Ian D, De Luca V, Després C (2012) The Arabidopsis NPR1 Protein Is a Receptor for the Plant Defense Hormone Salicylic Acid. Cell Reports 1: 639-647
Google Scholar: Author Only Title Only Author and Title

Yamasaki H, Hayashi M, Fukazawa M, Kobayashi Y, Shikanai T (2009) SQUAMOSA Promoter Binding Protein-Like7 Is a Central Regulator for Copper Homeostasis in Arabidopsis. Plant Cell 21: 347-361
Google Scholar: Author Only Title Only Author and Title

Yan J, Chia J-C, Sheng H, Jung H-i, Zavodna T-O, Zhang L, Huang R, Jiao C, Craft EJ, Fei Z, et al. (2017) Arabidopsis Pollen Fertility Requires the Transcription Factors CITF1 and SPL7 That Regulate Copper Delivery to Anthers and Jasmonic Acid Synthesis. The Plant Cell 29: 3012-3029
Google Scholar: Author Only Title Only Author and Title

Zhai Z, Gayomba SR, Jung H-I, Vimalakumari NK, Piñeros M, Craft E, Rutzke MA, Danku J, Lahner B, Punshon T, et al. (2014) OPT3 Is a Phloem-Specific Iron Transporter That Is Essential for Systemic Iron Signaling and Redistribution of Iron and Cadmium in Arabidopsis. The Plant cell 26: 2249-2264
Google Scholar: Author Only Title Only Author and Title

Zhang Z, Xie Q, Jobe TO, Kau AR, Wang C, Li Y, Qiu B, Wang Q, Mendoza-Cózatl DG, Schroeder JI (2016) Identification of AtOPT4 as a Plant Glutathione Transporter. Mol Plant 9: 481-484
Google Scholar: Author Only Title Only Author and Title

Zhong S, Joung J-G, Zheng Y, Chen Y-r, Liu B, Shao Y, Xiang JZ, Fei Z, Giovannoni JJ (2011) High-Throughput Illumina Strand-Specific RNA Sequencing Library Preparation. Cold Spring Harbor Protocols 2011: pdb.prot5652
Google Scholar: Author Only Title Only Author and Title